JOINT TRANSPORTATION
RESEARCH PROGRAM
INDIANA DEPARTMENT OF TRANSPORTATION
AND PURDUE UNIVERSITY

Integration and Evaluation of Automated Pavement Distress Data in INDOT's Pavement Management System

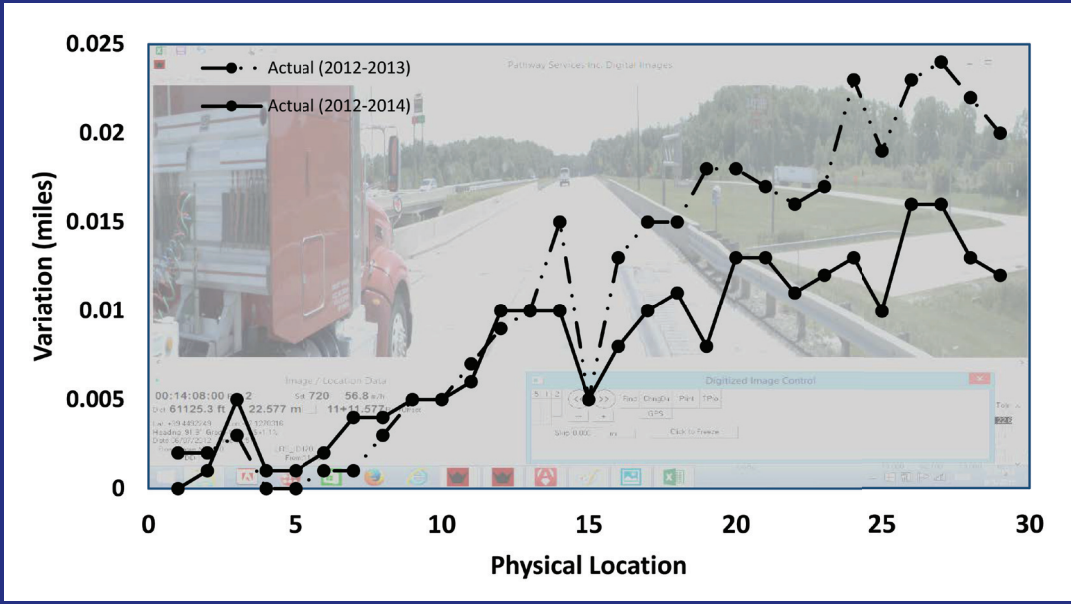

Majed Alinizzi, Julie Yu Qiao, Amr Kandil,
Hubo Cai, Samuel Labi

SPR-3803 • Report Number: FHWA/IN/JTRP-2017/07 • DOI: 10.5703/1288284316507

RECOMMENDED CITATION

Alinizzi, M., Qiao, J. Y., Kandil, A., Cai, H., & Labi, S. (2017). *Integration and evaluation of automated pavement distress data in INDOT's pavement management system* (Joint Transportation Research Program Publication No. FHWA/IN/JTRP-2017/07). West Lafayette, IN: Purdue University. https://doi.org/10.5703/1288284316507

AUTHORS

Majed Alinizzi
Graduate Research Assistant
Lyles School of Civil Engineering
Purdue University

Julie Yu Qiao
Graduate Research Assistant
Lyles School of Civil Engineering
Purdue University

Amr Kandil, PhD
Associate Professor of Civil Engineering
Lyles School of Civil Engineering
Purdue University
(765) 494-2246
akandil@purdue.edu
Corresponding Author

Hubo Cai, PhD
Professor of Civil Engineering
Lyles School of Civil Engineering
Purdue University
(765) 494-5028
hubocai@indot.in.gov
Corresponding Author

Samuel Labi, PhD
Professor of Civil Engineering
Lyles School of Civil Engineering
Purdue University

ACKNOWLEDGMENTS

The authors of this report acknowledge the valuable support and guidance provided by the members of the Study Advisory Committee.

JOINT TRANSPORTATION RESEARCH PROGRAM

The Joint Transportation Research Program serves as a vehicle for INDOT collaboration with higher education institutions and industry in Indiana to facilitate innovation that results in continuous improvement in the planning, design, construction, operation, management and economic efficiency of the Indiana transportation infrastructure. https://engineering.purdue.edu/JTRP/index_html

Published reports of the Joint Transportation Research Program are available at http://docs.lib.purdue.edu/jtrp/.

NOTICE

COPYRIGHT

Print ISBN: 978-1-62260-477-7

TECHNICAL REPORT STANDARD TITLE PAGE

1. Report No.	2. Government Accession No.	3. Recipient's Catalog No.
FHWA/IN/JTRP-2017/07		

4. Title and Subtitle	5. Report Date
Integration and Evaluation of Automated Pavement Distress Data in INDOT's Pavement Management System	May 2017
	6. Performing Organization Code

7. Author(s)	8. Performing Organization Report No.
Majed Alinizzi, Julie Yu Qiao, Amr Kandil, Hubo Cai, Samuel Labi	FHWA/IN/JTRP-2017/07

9. Performing Organization Name and Address	10. Work Unit No.
Joint Transportation Research Program Purdue University Mann Hall, 203 S. Martin Jischke Dr. West Lafayette, IN 47907	11. Contract or Grant No. SPR-3803

12. Sponsoring Agency Name and Address	13. Type of Report and Period Covered
Indiana Department of Transportation State Office Building 100 North Senate Avenue Indianapolis, IN 46204	Final Report
	14. Sponsoring Agency Code

15. Supplementary Notes
Prepared in cooperation with the Indiana Department of Transportation and Federal Highway Administration.

16. Abstract

This study was in two parts. The first part established and demonstrated a framework for pavement data integration. This is critical for fulfilling QC/QA needs of INDOT's pavement management system, because the precision of the physical location references is a prerequisite for the reliable collection and interpretation of pavement data. Such consistency is often jeopardized because the data are collected at different years, and are affected by changes in the vendor, inventory, or referencing system or reference points. This study therefore developed a "lining-up" methodology to address this issue. The applicability of the developed methodology was demonstrated using 2012-2014 data from Indiana's highway network. The results showed that the errors in the unlined up data are significant as they mischaracterize the true pavement condition. This could lead to the reporting of unreliable information of road network condition to the decision makers, ultimately leading to inappropriate condition assessments and prescriptions. Benefits of the methodology reverberate throughout the management functions and processes associated with highway pavements in Indiana, including pavement performance modeling, optimal timing of maintenance, rehabilitation, and reconstruction (MRR), and assessment of the effectiveness of MRR treatments and schedules.

The second part of the study developed correlations for the different types of pavement distresses using machine learning algorithms. That way, the severity of any one type of distress can be estimated based on known severity of other distresses at that location. The 2012-2014 data were from I-70, US-41, and US-52, and the distress types considered are cracking, rutting, faulting, and roughness. Models were developed to relate surface roughness (IRI) to pavement cracks, and between the different crack types, with resulting degrees of confidence that varied across the different crack types and road functional classes. In addition, for each functional class and for each crack type, models were built to relate crack depth to crack width. The concept can be applied to other distress types, such as spalling, bleeding, raveling, depression, shoving, stripping, potholes, and joint distresses, when appropriate data are available.

17. Key Words	18. Distribution Statement
data integration, data alignment, pavement distress, pavement management, distress type correlations, machine learning, crack types	No restrictions. This document is available to the public through the National Technical Information Service, Springfield, VA 22161.

19. Security Classif. (of this report)	20. Security Classif. (of this page)	21. No. of Pages	22. Price
Unclassified	Unclassified	66	

Form DOT F 1700.7 (8-69)

EXECUTIVE SUMMARY

INTEGRATION AND EVALUATION OF AUTOMATED PAVEMENT DISTRESS DATA IN INDOT'S PAVEMENT MANAGEMENT SYSTEM

Introduction

This study was conducted in two parts. The first part established and demonstrated a framework for pavement data integration. This is critical for fulfilling QC/QA needs of INDOT's pavement management system, because the precision of the physical location references is a prerequisite for the reliable collection and interpretation of pavement data. Such consistency is often jeopardized when the data are collected during different years, due to changes in the vendor, the inventory, or the referencing system or reference points. This study therefore developed a "lining-up" methodology to address this issue. The applicability of the developed methodology was demonstrated using 2012 to 2014 data from Indiana's highway network.

The second part of the study developed correlations and probability distributions for the different types of pavement distresses using machine learning algorithms. That way, the severity of any one type of distress can be estimated based on known severity of other distresses at that location. The 2012 to 2014 data are from I-70, US-41, and US-52, and the distress types considered are cracking, rutting, faulting, and roughness.

Findings

The results showed that the errors in the non-lined-up data are significant as they lead to mischaracterization of the true pavement condition. This could lead to the reporting of unreliable information regarding the road network condition to the decision makers, ultimately resulting in inappropriate condition assessments and prescriptions. Benefits of the methodology reverberate throughout the management functions and processes associated with highway pavements in Indiana, including pavement performance modeling; optimal timing of maintenance, rehabilitation, and reconstruction (MRR); assessing the effectiveness of MRR treatments and schedules; and, overall, responsible and cost-effective stewardship of the pavement infrastructure.

The second part of the study developed correlations for the different types of pavement distresses using machine learning algorithms. Models were developed to relate surface roughness (IRI) to pavement cracks, and between the different crack types, with varying degrees of confidence across the different crack types and road functional classes. In addition, for each functional class of highway and crack type, models were built to relate crack depth to crack width. This concept can also be applied to other distress types, such as spalling, bleeding, raveling, depression, shoving, stripping, potholes, and joint problems, when appropriate data are available.

Implementation

This study can be used by personnel at INDOT's Pavement Management Office to make more reliable assessments of the pavement condition of the state highway systems. Specifically, knowledge of true pavement condition can help facilitate the management functions and processes associated with highway pavements in Indiana.

A core group of pavement engineers and managers at INDOT under advisement of FHWA can further define and select implementation strategies relative to agency practices. The principal mission of this implementing panel could be to advance and institutionalize the most practicable methods outlined in this research report.

CONTENTS

PART I: DATA INTEGRATION (METHODOLOGY FOR ALIGNING THE DATA FROM AUTOMATED PAVEMENT CONDITION SURVEYS)

1. INTRODUCTION 1

2. METHODOLOGY 1
   2.1 Correction Method: Lined-Up Method. 1
   2.2 Estimating Positive and Negative Errors. 2
   2.3 Error Term 2
   2.4 Minimizing the Error Term 2
   2.5 Maximum Possible Error 3

3. APPLICATION OF THE METHODOLOGY 4
   3.1 Case Study of the State of Indiana. 4
   3.2 Correction Method. 5
   3.3 Error Term 9
   3.4 Minimizing the Error Term 10
   3.5 Maximum Possible Error 10

4. VALIDATION OF THE METHODOLOGY 10
   4.1 Case 1: I-70, Increasing Direction 11
   4.2 Case 2: I-70, Decreasing Direction 11

5. COMPARISON OF LINED-UP AND NON-LINED-UP PAVEMENT CONDITION DATA 13

6. SUMMARY, CONCLUSIONS, AND LIMITATIONS 14

LIST OF TABLES

Table	Page
Table 3.1 Sample Pavement Condition Data from I-70 in 2012	4
Table 3.2 RRs of the Identified Physical Locations on US-52 Taken at Different Times	6
Table 3.3 Reading References of the Starting and Ending Locations of a Selected Pavement Section on I-70	10
Table 4.1 Alignment of 2012 and 2014 Data for I-70 (Increasing Direction) and Error Terms Considering Two Locations	11
Table 4.2 Alignment of 2012 and 2014 Data for I-70 (Increasing Direction) and Error Terms Considering Five Locations	11
Table 4.3 Alignment of 2013 and 2014 Data for I-70 (Increasing Direction) and Error Terms Considering Two Locations	12
Table 4.4 Alignment of 2013 and 2014 Data for I-70 (Increasing Direction) and Error Terms Considering Five Locations	12
Table 4.5 Alignment of 2012 and 2013 Data for I-70 (Decreasing Direction) and Error Terms Considering Two Locations	12
Table 4.6 Alignment of 2012 and 2014 Data for I-70 (Decreasing Direction) and Error Terms Considering Two Locations	13
Table 4.7 Alignment of 2012 and 2013 Data for I-70 (Decreasing Direction) and Error Terms Considering Three Locations	13
Table 4.8 Alignment of 2012 and 2014 Data for I-70 (Decreasing Direction) and Error Terms Considering Three Locations	13

LIST OF FIGURES

Figure	Page
Figure 2.1 Illustration of the correction method	2
Figure 2.2 Illustration of the error term	2
Figure 2.3 Relationship between number of reference locations and error terms	3
Figure 2.4 Illustration of maximum possible error across different data sets	3
Figure 3.1 Screenshot of the video logs for a specific location on I-70 surveyed in 2012	5
Figure 3.2 Screenshot of the video logs for a specific location on I-70 surveyed in 2013	5
Figure 3.3 Screenshot of the video logs for a specific location on I-70 surveyed in 2014	6
Figure 3.4 Differences between the RRs of 29 identified physical locations on US-52 measured in 2012, 2013, and 2014	7
Figure 3.5 Screenshot of the starting location surveyed in 2012	7
Figure 3.6 Screenshot of the ending location surveyed in 2012	8
Figure 3.7 Screenshot of the starting location surveyed in 2013	8
Figure 3.8 Screenshot of the ending location surveyed in 2013	9
Figure 3.9 Screenshot of the starting location surveyed in 2014	9
Figure 3.10 Screenshot of the ending location surveyed in 2014	10
Figure 5.1 Cumulative percent passing versus IRI values (non-lined-up data)	14
Figure 5.2 Cumulative percent passing versus IRI values (lined-up data)	14

1. INTRODUCTION

Unreliable pavement condition data lead to errors in data analysis, which in turn results in inappropriate practices: misrepresentation of the causations and the correlations between pavement distresses, which leads to false understanding of pavement deterioration mechanisms; inaccurate pavement performance models; poor timing of pavement maintenance and repair activities; and incorrect evaluation and reporting of the effectiveness of pavement management programs. These inappropriate practices waste agencies' budgets and yield inadequate levels of service.

Manual collection of pavement condition data, particularly at the network-level, is resource intensive. Given the current shortages in resources, state highway agencies (SHAs) are seeking more cost-effective techniques to collect pavement performance data. McGhee (2004) reported that all SHAs in North America use some automated means. Fully automated pavement condition data collection techniques are becoming more popular due to advancements in computer technology, particularly digital image capturing and processing. Fully automated methods can be defined as those methods in which there is minimal human involvement in the data collection process. Typically, vehicles equipped with various sensors are driven over whole or part of a specific road to evaluate the road surface and report its condition at certain intervals (e.g., 0.005 miles). Identification codes are assigned to these short road segments as reference points of their physical locations on the road segment. Lanes are typically assessed separately. Given that truck traffic loads have the greatest impact on pavement performance and most trucks drive in the far-right lane, this lane is often the only one surveyed in practice. Pavement condition is usually reported through performance indicators (PIs), standard measurements that reflect pavement condition, e.g., cracking, rut depth, and roughness.

The techniques of automated pavement condition data collection and processing are generally cost-effective and help handle big data, reduce the hazards associated with data collection, and minimize subjectivity. However, quality control (QC) and quality assurance (QA) need to be performed regardless of the vendor or the method used to collect data. One of the benefits of QC/QA is the assurance of data accuracy. Collecting accurate data must be done consistently with high precision in terms of the physical location. That is, the collected data should be easily and accurately linked to specific locations, which is challenging when the data for the same pavement segment are collected at different times (e.g., in different years). This challenge is attributed to the following: (i) the starting point at which data is to be collected is not accurately identified; (ii) the frequency of vehicle movements, such as lane changes and traffic passing, varies depending on driver behavior and road conditions; and (iii) road geometry can change due to construction, rehabilitation and/or maintenance activities. Therefore, this report proposes an analytical methodology for "lining up" the collected pavement condition data in order to ensure the accuracy and reliability of pavement condition data.

2. METHODOLOGY

Automated pavement condition data are typically collected continuously (McGhee, 2004) using an instrumented vehicle driven over the whole or part of a specific road and are reported at uniform intervals, e.g., every 0.005 miles. An identification code referring to the location of the corresponding pavement segment is assigned to every reported data value. An example of such an identification code is the starting and ending mile readings that are used to determine pavement section length and location. However, these starting and ending mile readings, hereafter denoted as reading references (RRs), might vary for the same pavement section when data are collected and reported at different times (e.g., yearly). Therefore, to align pavement condition data collected at different times, a correction method based on linear stretching and proportioning is proposed in this chapter.

2.1 Correction Method: Lined-U Method

The correction method, called the lined-up method, maps the RRs taken at different times for the same pavement section. Figure 2.1 illustrates this concept, where the pavement section starts at location x and ends at location y, points A and D correspond to the starting and ending miles of the pavement section taken at time t_1, points B and E correspond to the starting and ending miles of the same pavement section taken at time t_2, and points C and F correspond to the starting and ending miles of the same pavement section taken at time t_3. Point k is included for the sake of geometrical representation. RR_A, RR_B, RR_C, RR_D, RR_E, RR_F, and RR_K are reading references corresponding to points A, B, C, D, E, F, and k, respectively.

The correction method works as follows:

- If the instrumented vehicle is driven from point x to point y, then the vehicle traveled a physical distance of $(y - x)$, which equals $(m + h)$.
- Assume that a straight line connects any two consecutive reading references taken at time t_i, such as the solid line between points (A, D), (B, E), and (C, F) in Figure 2.1.
- Determine the slopes (i.e., S_1, S_2, and S_3) between these points as follows:
  - $S_1 = (RR_D - RR_A) / (m + h)$
  - $S_2 = (RR_E - RR_B) / (m + h)$
  - $S_3 = (RR_F - RR_C) / (m + h)$
- Calculate RR for point k at time t_i using Equation 2.1:

$$RR_{k,i} = m * S_i + RR_{Beginning,i} \tag{2.1}$$

where $RR_{k,i}$ is the RR of point k at time t_i and $RR_{Beginning,i}$ (e.g., RR_A at time t_1, RR_B at time t_2, RR_C

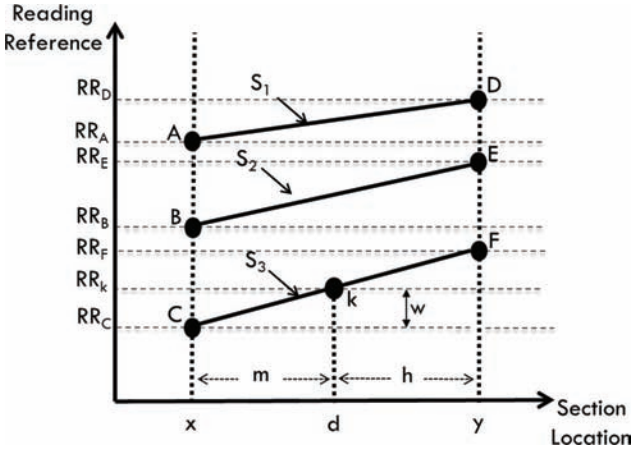

Figure 2.1 Illustration of the correction method.

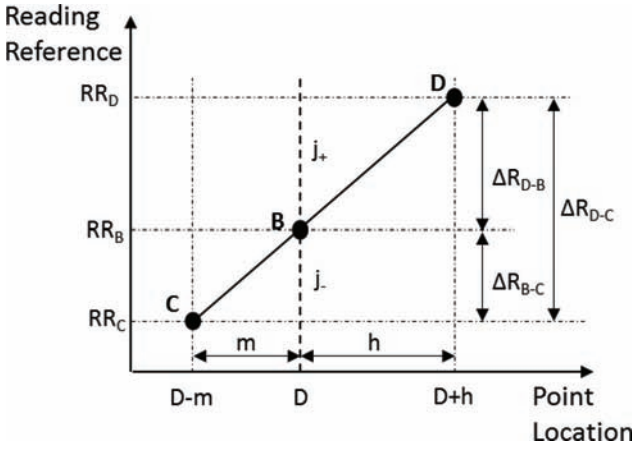

Figure 2.2 Illustration of the error term.

at time t_3) is the RR of the beginning point of the pavement section at time t_i.

- Because m represents the distance between the beginning point and the point of interest (i.e., k) on the same pavement section, its value is expected to persist regardless of when the measurements are taken. Therefore, given the estimated RR of point k at time t_i, the corresponding RR at time t_j is estimated using Equation 2.2.

$$RR_{k,j} = \left(RR_{k,i} - RR_{Beginning,I}\right) * \left(S_j/S_i\right) + RR_{Beginning,j} \quad (2.2)$$

Illustration Example: Point k taken at time t_3 has an RR of w. Its corresponding RR at time t_1 is $(w - RR_c) * (S_1/S_3) + RR_A$.

2.2 Estimating Positive and Negative Errors

In the correction method proposed in this study, a straight-line relationship is assumed between any two RRs representing two locations taken at time t_i. This assumption implies that a vehicle travels exactly along the lane with no lane changes. However, in practice this ideal driving path rarely occurs, and the relationship between the RRs of two locations on a pavement section is not linear. As a result, assuming a straight-line relationship might lead to cascading errors in the assignment of references to the collected pavement data. Therefore, to alert the pavement data manager of possible errors in the correction method, maximum and minimum possible errors associated with the RRs of the collected data are quantified using the error term (ET) measurement method discussed below.

2.3 Error Term

When driving on a pavement to measure its performance, the driver makes a conscious effort to minimize maneuvers and lane changes to reduce variations in the RRs of the collected data. This practice can be challenging where traffic is heavy. Therefore, the relationship between the distance traveled between two locations—calculated as the difference between the ending reference and the beginning reference—and the actual distance between two locations along the traffic lane is always associated with uncertainty.

In this study, an error term is introduced to quantify the aforementioned uncertainty in the location information. Figure 2.2 illustrates the error term. Note that points C and D are reference points only, not physical locations on the pavement section. Assuming increasing RRs, location B, in extreme cases, could have an RR comparable with the RR of either location D or C, which could result in an error term with a positive or negative magnitude (i.e., j_+ or j_-, respectively). The magnitude of the negative and positive error terms is denoted by $\Delta R_{D\text{-}B}$ and $\Delta R_{B\text{-}C}$, respectively, as illustrated in Figure 2.2. By assuming a straight-line relationship, the positive and negative error terms might have the highest possible values (i.e., $\Delta R_{D\text{-}C}$) at locations (D-m) and (D+h), respectively. If B is the middle point at an equal distance to locations C and D, the maximum magnitude of both the negative and positive errors for B is ½ $\Delta R_{D\text{-}C}$. This observation suggests that adding a calibration reference location in the middle of any two locations reduces the maximum error by half.

The error between any two locations can be as high as the difference between their RRs. Therefore, higher differences between these RRs indicate larger possible error magnitudes. This is because the longer the instrumented vehicle travels, the larger the differences between the RRs, decomposing the traveled distance to small sections could yield small error terms. The minimization of the error terms is explained in the following section.

2.4 Minimizing the Error Term

In cases where the error is large and not acceptable to the agency, the error should be minimized. The acceptance size of an error is mainly influenced by the

intended use of the data. For example, very localized data are useful for assessing small sections.

It is critical to develop a systematic way to minimize errors in the reported RRs of pavement condition data. Providing additional reference points leads to smaller maximum errors but requires additional effort. Simplified guidance is presented here to help Indiana Department of Transportation (INDOT) decision-makers evaluate the accuracy gained by the correction method against the method's required efforts. The accuracy criterion is measured by a defined maximum allowable error (MAE), while the criterion of measuring the required effort is represented by the number of locations at which users need to obtain RRs across different data sets (i.e., data collected at different times).

Figure 2.3 shows a straight-line relationship between consecutive locations surveyed at time t_i. Any location laid between locations C and D is assumed to lie on that straight line. This causes an error associated with the RR of that location, which can take a value up to J_{max+}. Adding a reference point, B, in the middle of the line between C and D reduces the error magnitude of any other locations by half, resulting in magnitudes of $J_{max+}/2$. As the number of locations surveyed increases, the error term decreases. The relationship between the number of locations and the error term is captured in Equation 2.3.

$$e = SL/(n-1) \tag{2.3}$$

where n is the number of needed locations, including the beginning and ending locations, to reach the required accuracy level; SL is the segment length between locations; and e is the maximum allowable error term defined by the users.

With Equation 2.3, a user can determine the achievable accuracy given the number of reference points and vice versa.

2.5 Maximum Possible Error

Typically, the accuracy of the collected data is reported relative to some benchmark. Consider data collected

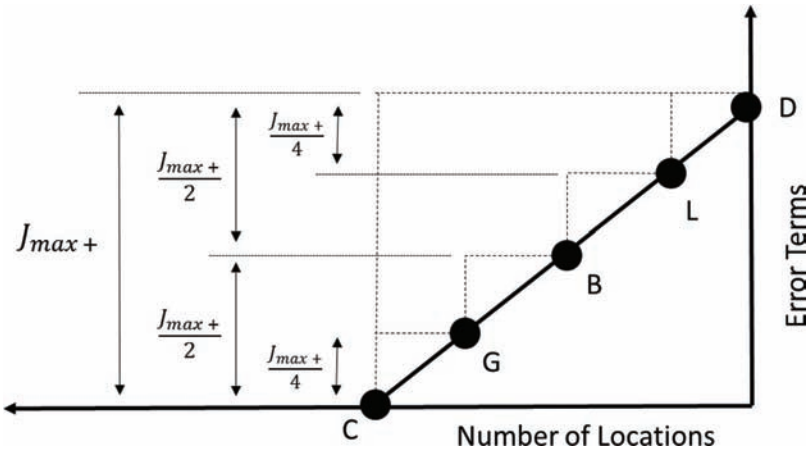

Figure 2.3 Relationship between number of reference locations and error terms.

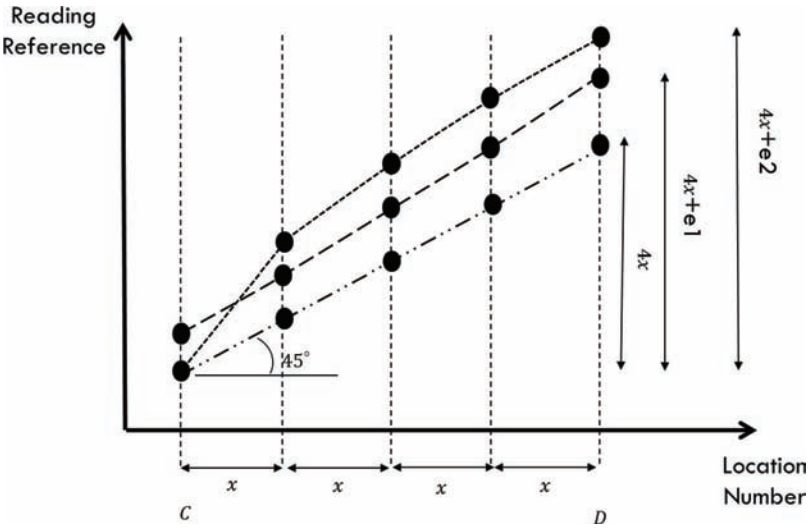

Figure 2.4 Illustration of maximum possible error across different data sets.

at two different time periods to represent the conditions of a particular pavement segment. Under the ideal situation, the instrumented vehicle remains in the traffic lane with no lane changes. The reference readings and the true distance yield a 45-degree line, as illustrated in Figure 2.4. If the RR of the beginning location of the same pavement section measured at different times has different values, then the 45-degree lines are parallel to each other. The shift, or e_1 in Figure 2.4, is a systematic error that should be corrected by aligning the beginning locations.

In reality, the driving distance is always greater than the true distance because of lane changes and even small deviations in the travel path from the traffic lane. Thus, any line connecting neighboring locations must have a slope that is no less than 45 degrees. For the ending location, the maximum error, e_2 in Figure 2.4, is attributed to deviations in the travel path from the traffic lane.

The two types of error (e_1 and e_2) are additive: the actual error is the sum of these two if the systematic error e_1 is not corrected. Figure 2.4 also illustrates that the error is cascading; the error of the preceding location carries over to the succeeding location. Therefore, adding more reference locations helps calibrate the RRs taken at different times and reduces the maximum possible error magnitude. This observation confirms the recommendation made in Section 2.4.

3. APPLICATION OF THE METHODOLOGY

3.1 Case Study of the State of Indiana

This section illustrates the implementation of the lined-up data correction method for Indiana's highway network. The pavement condition data used for the case study were collected during the years 2012 to 2014. Three roads—I-70, US-52, and US-41—were selected for the case study. The pavement condition data were collected by a vendor using an instrumented vehicle equipped with high-resolution cameras and sensors. The instrumented vehicle was driven on one lane at a time. The far-right lane was driven if the road had more than one lane because the far-right lane is likely to experience a higher volume of truck traffic than other lanes. In the data, pavement condition is reported in terms of distress type, such as cracking, rutting, and roughness, at regular pavement length intervals. The location of each interval is defined by a starting and ending mile reading (i.e., the RRs described in the previous chapter). Sample pavement condition data reported using the International Roughness Index (IRI) at 0.005-mile intervals are provided in Table 3.1.

Discussion of the misrepresentation of pavement segment locations

The pavement condition data used in the case study are reported at distance intervals that represent the condition of a particular pavement segment location at a specific time. For example, it can be seen in Table 3.1 that the pavement segment that starts from the RR 6.925 mile to the RR 6.93 mile had an average IRI of 142 (in/mile) in 2012. The same segment is surveyed annually to monitor its performance over time. As such, regardless of when the condition is assessed, the condition data should all represent the same pavement segment. Under the ideal situation, the RRs of every pavement segment would remain the same at different data collection times. To test whether this is the case for the condition data used in the case study, several physical structures (e.g., bridges and road intersections) were identified to compare the corresponding RRs taken at different times. These physical structures are expected to have the same physical locations irrespective of the year in which the pavement condition data were collected.

By examining the video logs provided by the vendor, physical locations were identified and the corresponding RRs obtained. Figures 3.1, 3.2, and 3.3 provide screenshots of video logs at the same location in 2012, 2013, and 2014. Note that the RR is 6.905 in 2012, 6.904 in 2013, and 6.901 in 2014.

Table 3.2 contains the RRs of 29 structures on US-52. Figure 3.4 illustrates the locational deviations as indicated by the RRs, with the 2012 RRs as the base. These variations (errors) indicate the locational errors in aligning the pavement condition data acquired at different times. These errors, if not controlled, lead to false

TABLE 3.1
Sample Pavement Condition Data from I-70 in 2012

Route	Direction	Starting Mile (mile)	Ending Mile (mile)	Date	Pavement type	IRI Left Wheel Path (in/mi)	IRI Right Wheel Path (in/mi)	IRI Average (in/mi)
I-70	I	6.9	6.905	7/6/2012	CON	215	185	200
I-70	I	6.905	6.91	7/6/2012	CON	278	141	209
I-70	I	6.91	6.915	7/6/2012	CON	577	510	543
I-70	I	6.915	6.92	7/6/2012	CON	477	419	448
I-70	I	6.92	6.925	7/6/2012	OVR	211	286	249
I-70	I	6.925	6.93	7/6/2012	OVR	116	169	142
I-70	I	6.93	6.935	7/6/2012	OVR	74	108	91
I-70	I	6.935	6.94	7/6/2012	OVR	146	359	252
I-70	I	6.94	6.945	7/6/2012	OVR	198	456	327

I: Increasing direction; CON: concrete pavement; OVR: overlay pavement.

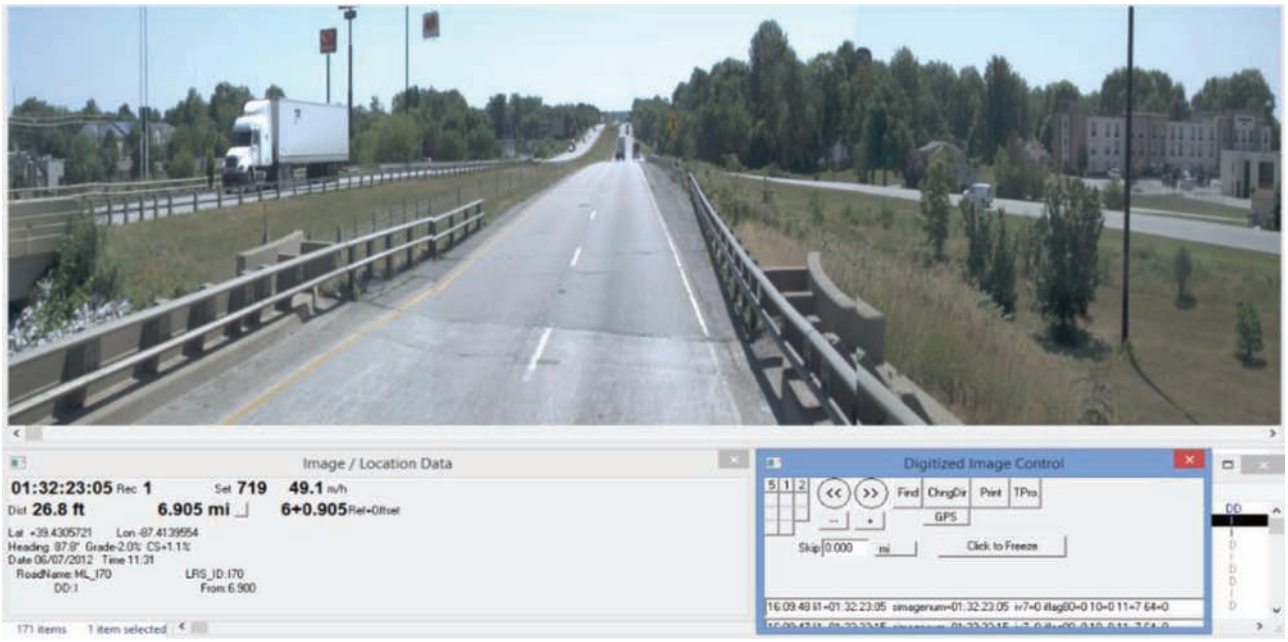

Figure 3.1 Screenshot of the video logs for a specific location on I-70 surveyed in 2012.

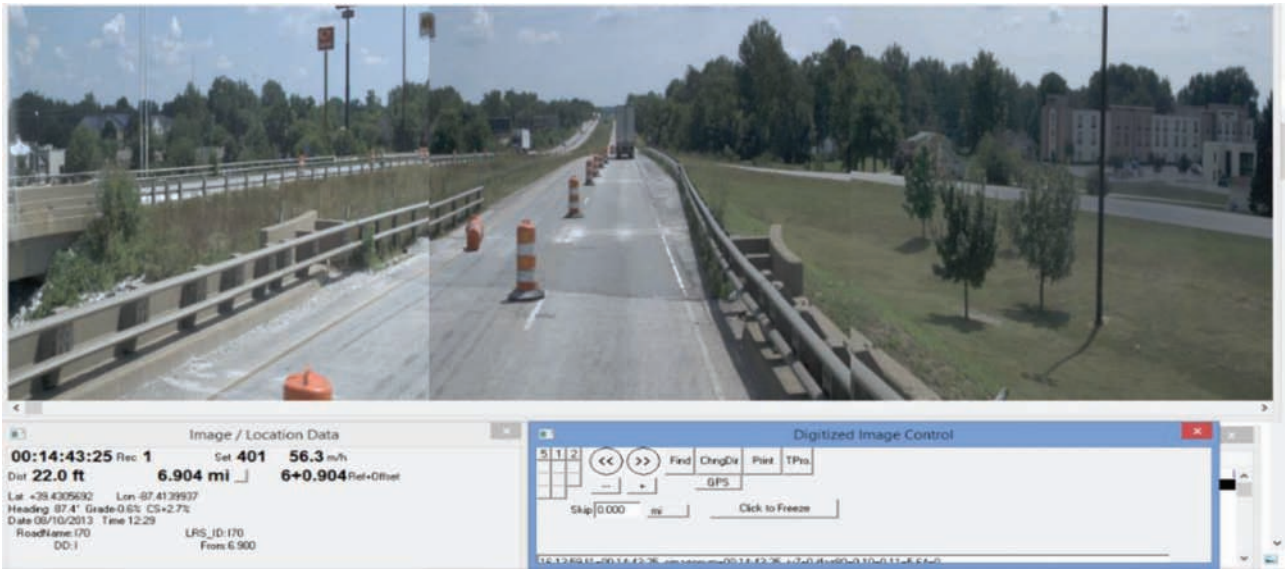

Figure 3.2 Screenshot of the video logs for a specific location on I-70 surveyed in 2013.

interpretations and erroneous assessments of pavement condition, which, in turn, lead to inappropriate decisions and actions in pavement management.

The problem of mismatching RRs representing the same location in different years exists on all routes on Indiana's road network. As such, a massive volume of pavement condition data are collected at great expense but plagued with inaccuracy, which represents is a serious lapse in pavement management accountability. To obtain accurate data, the differences (errors) between corresponding RRs need to be minimized and kept within an acceptable pre-defined range. Such error ranges should be defined by the highway agency.

3.2 Correction Method

This section illustrates the implementation of the correction method using the case study data. The aim of this step was to establish a correction mechanism that maps the RRs of any pavement segment to any other RRs representing the same pavement segment but collected at different times.

After determining the route (or part thereof) in question, the physical facilities (and their locations) on that route were identified. The data analyst accessed the video logs provided by the vendor to determine the locations of the facilities at different times. At least two

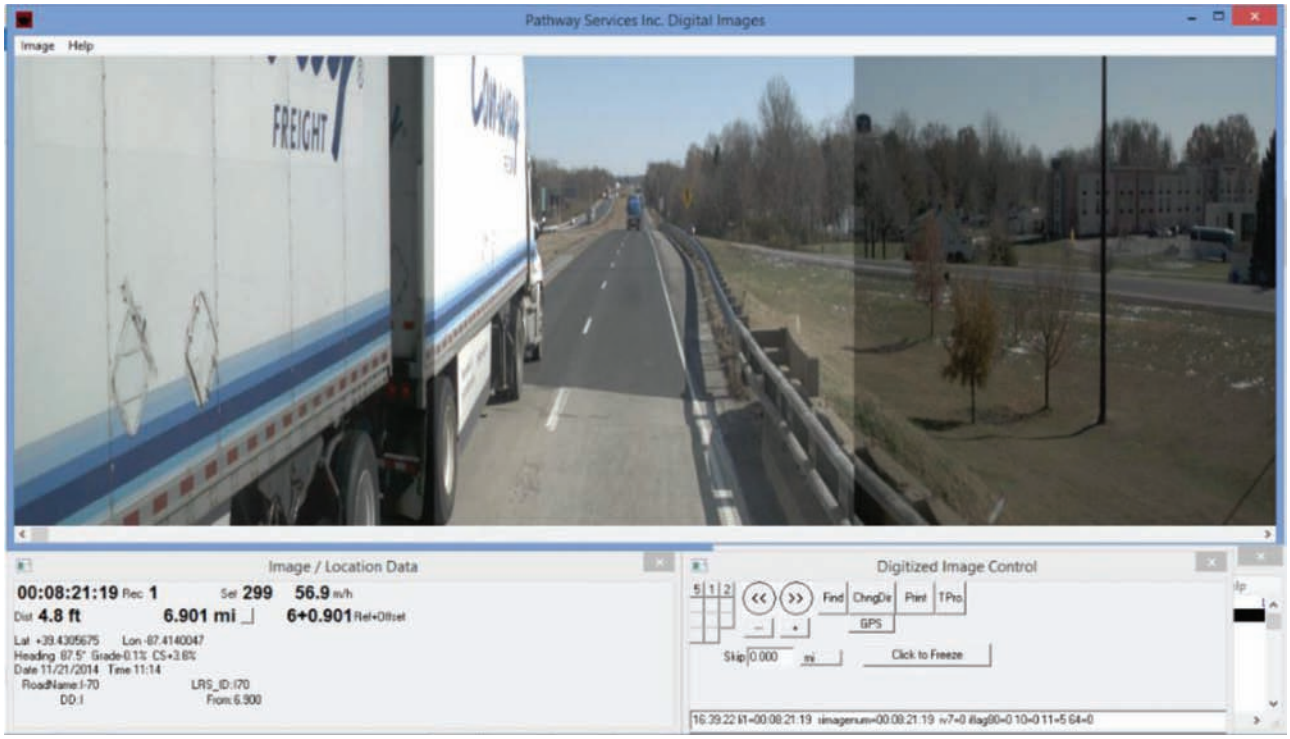

Figure 3.3 Screenshot of the video logs for a specific location on I-70 surveyed in 2014.

TABLE 3.2
RRs of the Identified Physical Locations on US-52 Taken at Different Times

Selected Physical Location	RRs (mile)			Selected Physical Location	RRs (mile)		
	2012 Y	2013 Y	2014 Y		2012 Y	2013 Y	2014 Y
L1	63.458	63.456	63.458	L16	70.836	70.849	70.844
L2	63.673	63.671	63.672	L17	71.27	71.285	71.28
L3	65.034	65.037	65.039	L18	71.274	71.289	71.285
L4	65.597	65.597	65.598	L19	72.027	72.045	72.035
L5	65.632	65.632	65.633	L20	72.042	72.06	72.055
L6	65.796	65.797	65.798	L21	72.102	72.119	72.115
L7	66.104	66.103	66.1	L22	73.234	73.25	73.245
L8	66.115	66.118	66.119	L23	73.343	73.36	73.355
L9	66.883	66.888	66.888	L24	73.922	73.945	73.935
L10	66.898	66.903	66.903	L25	74.006	74.025	74.016
L11	68.717	68.724	68.723	L26	76.269	76.292	76.285
L12	69.325	69.334	69.335	L27	78.079	78.103	78.095
L13	69.819	69.829	69.829	L28	78.651	78.673	78.664
L14	69.829	69.844	69.839	L29	78.797	78.817	78.809
L15	70.079	70.084	70.084	-	-	-	-

physical facilities (and their locations) were needed for each pavement segment, either for the entire route or a small part of it.

Figures 3.5, 3.6, 3.7, 3.8, 3.9, and 3.10 show screenshots of two facilities/locations selected on a section of I-70 that was surveyed in 2012, 2013, and 2014. One facility is a physical location (i.e., a bridge) near the beginning of the pavement section, and the other facility is near the end. Note that different RRs were reported at different times; Table 3.3 contains this location data. The assumed relationships in the case study were straight-line relationships. A straight line can be drawn to link the starting RR and the ending RR, and any identified location between these two locations is assumed to lie on that straight line. By knowing the RRs of the two locations and the slope of the connecting straight line, the RRs of intermediate locations can be estimated.

To estimate the slopes of the straight lines connecting the RRs of two locations, the difference between these RRs was estimated and then divided by the nominal distance. This nominal distance is the physical length

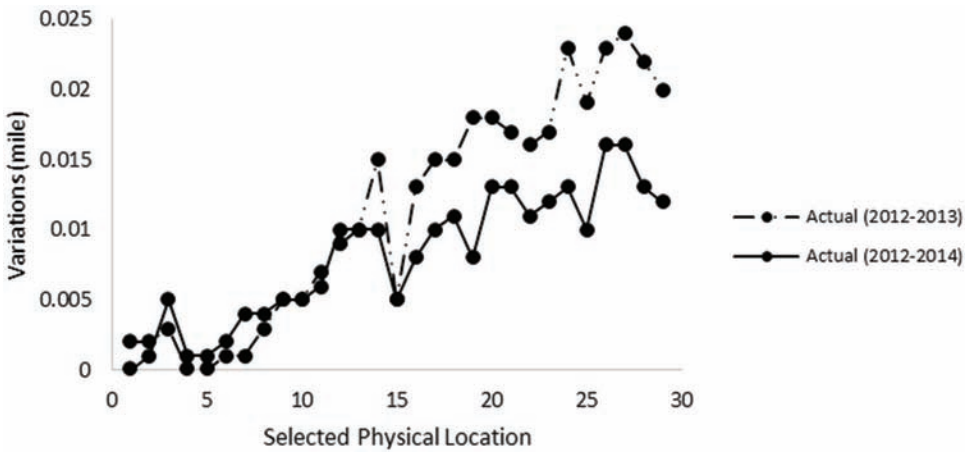

Figure 3.4 Differences between the RRs of 29 identified physical locations on US-52 measured in 2012, 2013, and 2014.

Figure 3.5 Screenshot of the starting location surveyed in 2012.

of the pavement section. The equations presented in Chapter 2 were then used to align the RRs of other years to the RRs of the benchmark year. An example is presented in the following section to illustrate this correction method.

Numerical example of correction and alignment

Table 3.3 shows the RRs representing the starting and ending locations of a pavement section on I-70 that was surveyed in 2012, 2013, and 2014. To obtain the slope of the line linking the beginning and ending RRs in each year, a true distance between the two locations is needed. The true distance was not available for this study, and the distance between the locations in each year was calculated from the pair of corresponding RRs, and the shortest distance was chosen to be the nominal distance to calculate the slopes. The rationale for choosing the shortest distance as the nominal distance is as follows: considering that all calculated distances are estimates of the true distance and are no less than the true distance, the shortest distance is the one that is the closest to the true distance. In this example, the 2012 data show the shortest distance as 15.672 miles. This distance was chosen to be the nominal distance. The slopes of the straight lines connecting the RRs in 2013

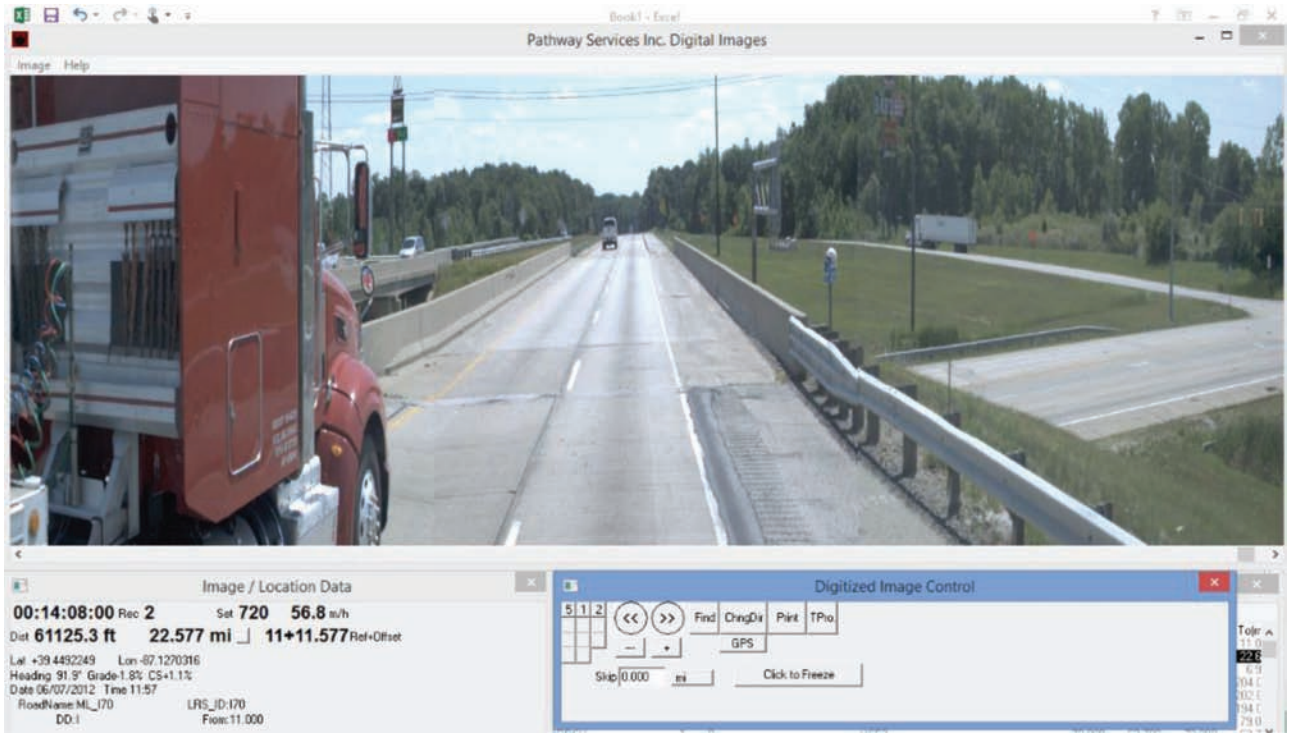

Figure 3.6 Screenshot of the ending location surveyed in 2012.

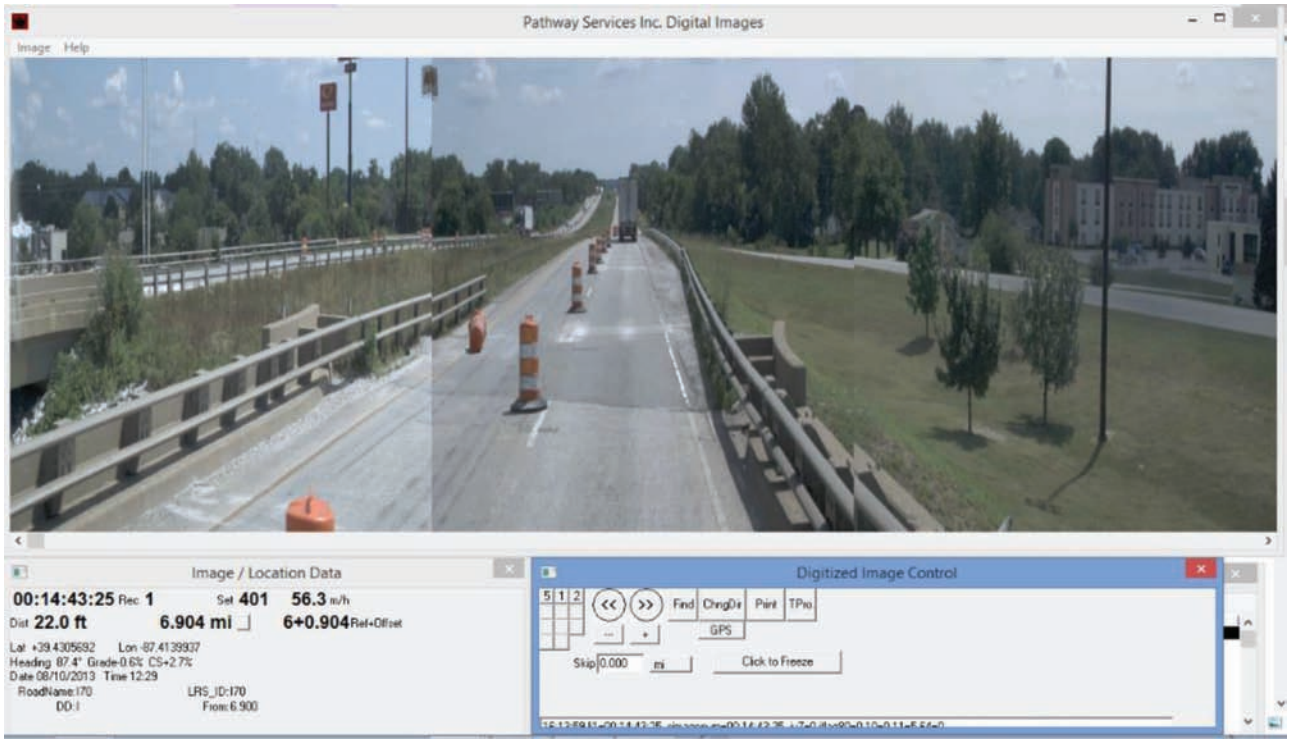

Figure 3.7 Screenshot of the starting location surveyed in 2013.

and 2014 were calculated as 1.00268 and 1.00013, respectively. Taking the middle point of the 2013 data as an example, its RR in 2013 is 14.761, and the corresponding RR in 2012 is 14.741. Following this process, the RRs of the 2013 and 2014 data can be aligned with that of the 2012 data.

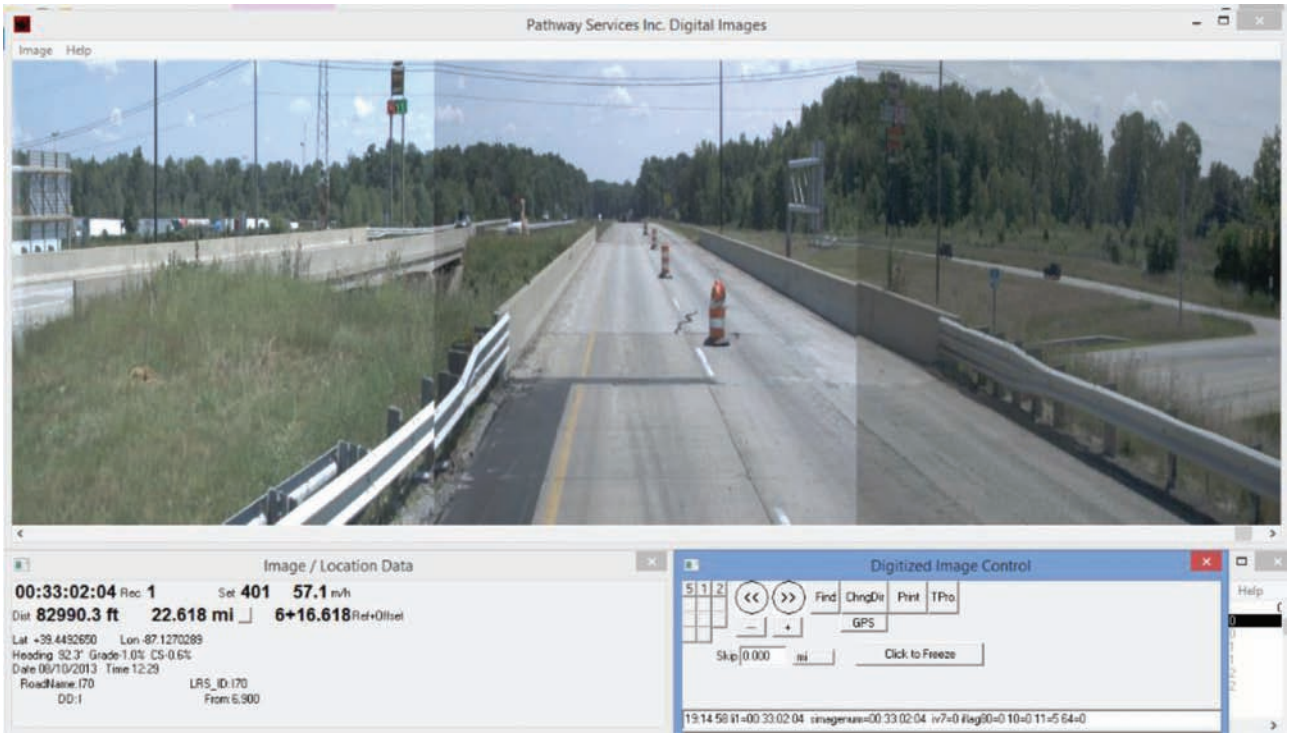

Figure 3.8 Screenshot of the ending location surveyed in 2013.

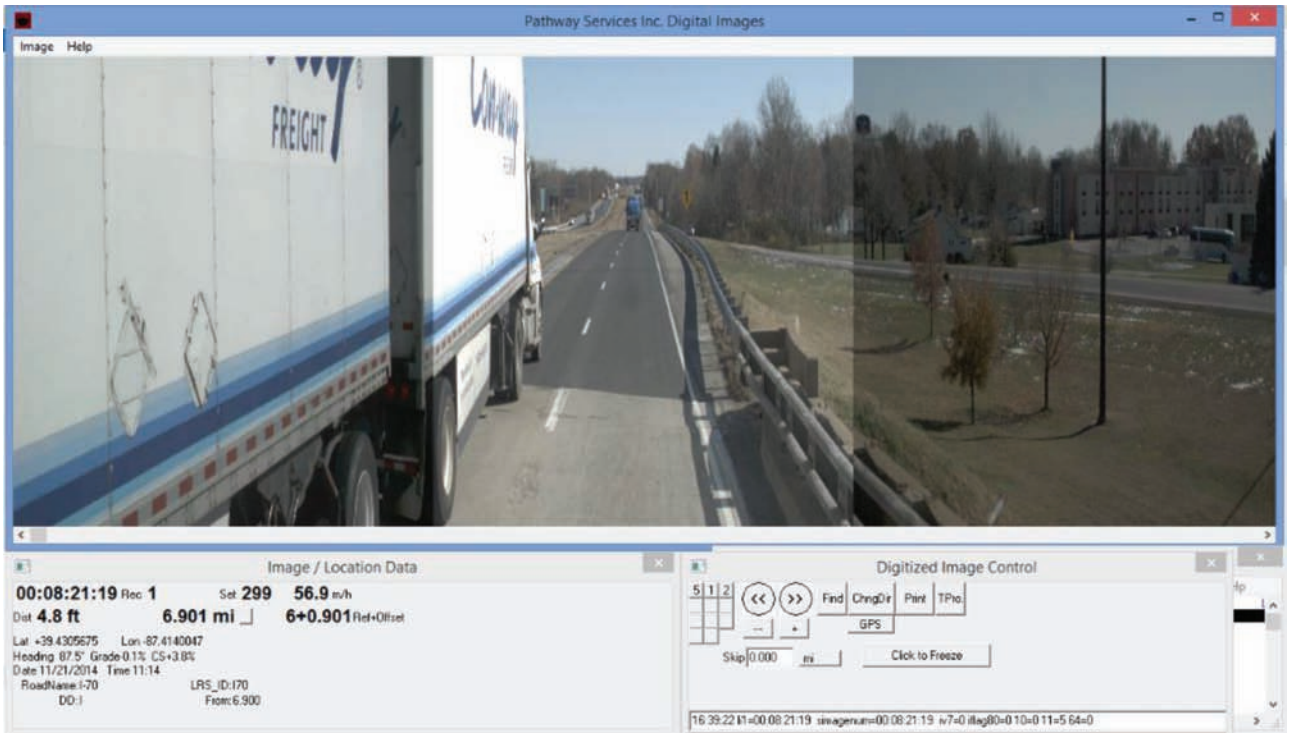

Figure 3.9 Screenshot of the starting location surveyed in 2014.

3.3 Error Term

An error is a deviation from correctness. In this study, a benchmark year was first selected and deemed to model correctness, meaning that the RRs collected in this specific year were assumed to be correct. Any deviation from the benchmark was considered to be an error, and the measured distance from the benchmark represented the magnitude of the error. For example, if a pavement section were surveyed in different years

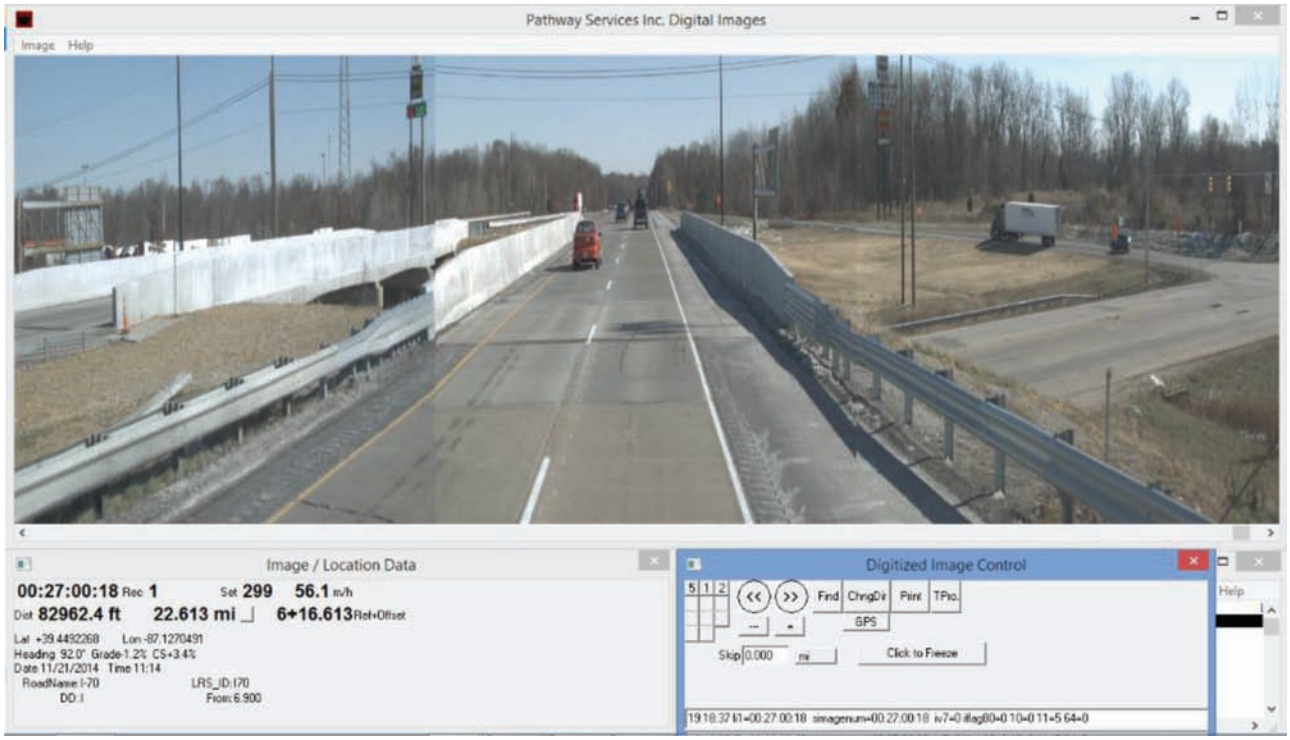

Figure 3.10 Screenshot of the ending location surveyed in 2014.

(e.g., 2012, 2013, and 2014) and 2012 were selected as the benchmark year, then the RRs obtained in 2012 would be considered to accurately represent the pavement segment locations. Accordingly, deviations in the RRs of years other than 2012 would be errors.

Using the data in Table 3.3, consider the data collected in 2012 to be the benchmark. After shifting the beginning RRs of 2013 and 2014 to the beginning RR of 2012 (to correct the systematic error), the maximum error in 2013 is calculated as (15.714 – 15.672), or 0.042 miles, and the maximum error in 2014 is calculated to be 0.04 miles. If these error magnitudes are acceptable to highway agencies, no further action is needed. If not, then further action (i.e., adding more intermediate reference points) is needed.

3.4 Minimizing the Error Term

As noted in Section 2.4, the error term due to the assumed linear relationship between any two locations with known data can be minimized by shortening the distance between these two locations. That is, the distance between these two locations can be broken down into smaller distances by adding new locations between the existing ones. To obtain the highest possible benefit from the newly added locations, the new locations need to be near the midpoint between any two existing locations. This would reduce the error terms by half. By adding more locations (creating shorter distances), the error terms can be further minimized. To achieve a specific error tolerance, the number of new locations to be added can be determined using Equation 2.3.

TABLE 3.3
Reading References of the Starting and Ending Locations of a Selected Pavement Section on I-70

	Years of Collecting the Data		
Reading References (RRs)	**2012**	**2013**	**2014**
Starting Location	6.905	6.904	6.901
Ending Location	22.577	22.618	22.613
Estimated Distance	15.672	15.714	15.712

3.5 Maximum Possible Error

According to Equation 2.4, the maximum possible error for the RRs collected in 2013 is about 0.042 miles. By using five locations with known RRs, the error term can be reduced to within 0.0105 miles. These locations need to be at approximately equal distances from each other.

4. VALIDATION OF THE METHODOLOGY

Data from three randomly selected pavement sections from three routes (one section per route) were used to test the validity of the proposed methodology. A route is surveyed at least once a year to assess its conditions in both traffic directions. One direction is considered to be increasing—the mile references increase along the survey direction—and is denoted as I, and the other direction is considered to be decreasing and is designated as D. The method is applicable for all sections, and the raw data are all in the same format.

Therefore, only the results for a pavement section on I-70 are presented in this chapter.

4.1 Case 1: I-70, Increasing Direction

The random pavement section selected on I-70 is from mileposts 6.9 to 22.6. Eleven physical structures (locations) in this range were identified, and their RRs in 2012, 2013, and 2014 were determined from video logs.

Table 4.1 contains the RRs of these 11 locations surveyed in 2012 and 2014. As expected, the largest difference is observed at the end location (location 11). The large deviations between these readings indicate significant misalignment in the RRs between 2012 and 2014. Using the 2014 data as the baseline/benchmark and following the correction method, the corresponding RRs in 2014 were used to estimate all RRs in 2012. Table 4.1 shows the results. The maximum error occurs at location 10, where the error magnitude is 0.0088 miles.

To further minimize the differences (error terms) between the actual and estimated RRs, three more locations (locations 4, 7, and 9) with known RRs were added between the existing ones. The results are shown in Table 4.2. The maximum error still occurs at location 10, though with a slight reduction in the magnitude. In this case, adding more locations does not reduce the error term, mainly because the linear assumption is invalid. Still, the maximum possible error between the RRs at two reference locations holds.

The RRs obtained in 2013 were similarly investigated, and the differences between these RRs and those obtained in 2014 are presented in Tables 4.3 and 4.4.

4.2 Case 2: I-70, Decreasing Direction

The validity of the proposed method when the RRs at non-increasing mileposts are reported was tested by applying the method to the decreasing direction of I-70. Nine physical signs (locations) in this direction were identified, and their corresponding RRs were obtained from video logs. Tables 4.5 and 4.6 show the results using two reference locations (the beginning and ending locations), and Tables 4.7 and 4.8 show the results using three reference locations (locations 1, 5, and 9).

TABLE 4.1
Alignment of 2012 and 2014 Data for I-70 (Increasing Direction) and Error Terms Considering Two Locations

	RRs (mile)			
Location Number	2012 Y	2014 Y	Estimates for 2012 Y	Error Terms (mile)
1	6.905	6.901	6.901	0.0000
2	7.44	7.435	7.435387483	0.0004
3	8.975	8.96	8.968630073	0.0086
4	10.22	10.206	10.21220468	0.0062
5	11.221	11.208	11.21205864	0.0041
6	13.267	13.257	13.25571619	-0.0013
7	14.831	14.817	14.81792558	0.0009
8	17.752	17.738	17.73558135	-0.0024
9	18.481	18.47	18.46374672	-0.0063
10	22.467	22.454	22.44518318	-0.0088
11	22.627	22.605	22.605	0.0000

TABLE 4.2
Alignment of 2012 and 2014 Data for I-70 (Increasing Direction) and Error Terms Considering Five Locations

	RRs (mile)			
Location Number	2012 Y	2014 Y	Estimates for 2012 Y	Error Terms (mile)
1	6.905	6.901	6.901	0.0000
2	7.44	7.435	7.434	-0.0006
3	8.975	8.96	8.965	0.0048
4	10.22	10.206	10.206	0.0000
5	11.221	11.208	11.207	-0.0010
6	13.267	13.257	13.253	-0.0040
7	14.831	14.817	14.817	0.0000
8	17.752	17.738	17.740	0.0024
9	18.481	18.47	18.470	0.0000
10	22.467	22.454	22.445	-0.0086
11	22.627	22.605	22.605	0.0000

TABLE 4.3
Alignment of 2013 and 2014 Data for I-70 (Increasing Direction) and Error Terms Considering Two Locations

	RRs (mile)			
Location Number	**2013 Y**	**2014 Y**	**Estimates for 2013 Y**	**Error Terms (mile)**
1	6.904	6.901	6.901	0.0000
2	7.437	7.435	7.434	-0.0014
3	8.967	8.96	8.963	0.0026
4	10.21	10.206	10.205	-0.0013
5	11.216	11.208	11.210	0.0020
6	13.26	13.257	13.253	-0.0044
7	14.824	14.817	14.815	-0.0015
8	17.739	17.738	17.728	-0.0096
9	18.472	18.47	18.461	-0.0091
10	22.458	22.454	22.444	-0.0099
11	22.619	22.605	22.605	0.0000

TABLE 4.4
Alignment of 2013 and 2014 Data for I-70 (Increasing Direction) and Error Terms Considering Five Locations

	RRs (mile)			
Location Number	**2013 Y**	**2014 Y**	**Estimates for 2013 Y**	**Error Terms (mile)**
1	6.904	6.901	6.901	0.0000
2	7.437	7.435	7.434	-0.0012
3	8.967	8.96	8.963	0.0034
4	10.21	10.206	10.206	0.0000
5	11.216	11.208	11.211	0.0033
6	13.26	13.257	13.254	-0.0030
7	14.824	14.817	14.817	0.0000
8	17.739	17.738	17.736	-0.0020
9	18.472	18.47	18.470	0.0000
10	22.458	22.454	22.444	-0.0095
11	22.619	22.605	22.605	0.0000

TABLE 4.5
Alignment of 2012 and 2013 Data for I-70 (Decreasing Direction) and Error Terms Considering Two Locations

	RRs (mile)			
Location Number	**2012 Y**	**2013 Y**	**Estimate of 2012 Y**	**Error Terms (mile)**
1	6.983	7.075	7.075	0.0000
2	7.387	7.474	7.477	0.0026
3	7.912	7.993	7.998	0.0054
4	10.282	10.356	10.354	-0.0019
5	11.182	11.248	11.249	0.0006
6	14.912	14.949	14.956	0.0071
7	17.787	17.815	17.814	-0.0013
8	18.377	18.399	18.400	0.0011
9	22.532	22.53	22.530	0.0000

TABLE 4.6
Alignment of 2012 and 2014 Data for I-70 (Decreasing Direction) and Error Terms Considering Two Locations

	RRs (mile)		Actual Differences in the RRs	
Location Number	2012 Y	2014 Y	Estimate for 2012 Y	Error Terms (mile)
1	6.983	7.067	7.067	0.0000
2	7.387	7.467	7.469	0.0018
3	7.912	7.99	7.991	0.0009
4	10.282	10.348	10.348	0.0000
5	11.182	11.24	11.243	0.0030
6	14.912	14.949	14.953	0.0037
7	17.787	17.811	17.812	0.0009
8	18.377	18.394	18.399	0.0047
9	22.532	22.531	22.531	0.0000

TABLE 4.7
Alignment of 2012 and 2013 Data for I-70 (Decreasing Direction) and Error Terms Considering Three Locations

	RRs (mile)			
Location Number	2012 Y	2013 Y	Estimate of 2012 Y	Error Terms (mile)
1	6.983	7.075	7.075	0.0000
2	7.387	7.474	7.476	0.0025
3	7.912	7.993	7.998	0.0052
4	10.282	10.356	10.354	-0.0024
5	11.182	11.248	11.248	0.0000
6	14.912	14.949	14.956	0.0067
7	17.787	17.815	17.813	-0.0016
8	18.377	18.399	18.400	0.0009
9	22.532	22.53	22.530	0.0000

TABLE 4.8
Alignment of 2012 and 2014 Data for I-70 (Decreasing Direction) and Error Terms Considering Three Locations

	RRs (mile)		Actual Differences in the RRs	
Location Number	2012 Y	2014 Y	Estimate for 2012 Y	Error Terms (mile)
1	6.983	7.067	7.067	0.0000
2	7.387	7.467	7.468	0.0015
3	7.912	7.99	7.990	0.0002
4	10.282	10.348	10.346	-0.0024
5	11.182	11.24	11.240	0.0000
6	14.912	14.949	14.951	0.0016
7	17.787	17.811	17.811	-0.0003
8	18.377	18.394	18.398	0.0036
9	22.532	22.531	22.531	0.0000

5. COMPARISON OF LINED-UP AND NON-LINED-UP PAVEMENT CONDITION DATA

This chapter aims to illustrate the difference between lined-up and non-lined up pavement condition data. Non-lined-up data are the original pavement condition data without RR correction, while lined-up data are the pavement condition data after the correction method has been implemented. Pavement condition is measured by IRI. Higher IRI values imply worse pavement condition.

A pavement section 0.25 miles long was randomly selected from I-70, and the corresponding IRI data in 2012, 2013, and 2014 were acquired. Following a procedure that is similar to sieve analysis, the percentage of pavement segments with IRI values below a certain value was determined. Figure 5.1 presents the cumulative percent passing versus IRI values for the non-lined-up data. Figure 5.2 presents the cumulative percent passing versus IRI values for the lined-up data.

Taking an IRI value of 100 in/mi as the threshold value, 44.7% of the non-lined-up data pass in 2012, 79.7% pass in 2013, and 99.5% pass in 2014; 51.6% of the lined-up data pass in 2012, 88.5% pass in 2013, and 100% pass in 2014. The performance curves are very different. The corrected data show much worse pavement

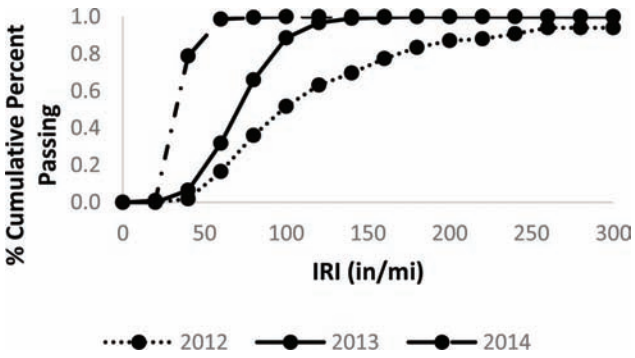

Figure 5.1 Cumulative percent passing versus IRI values (non-lined-up data).

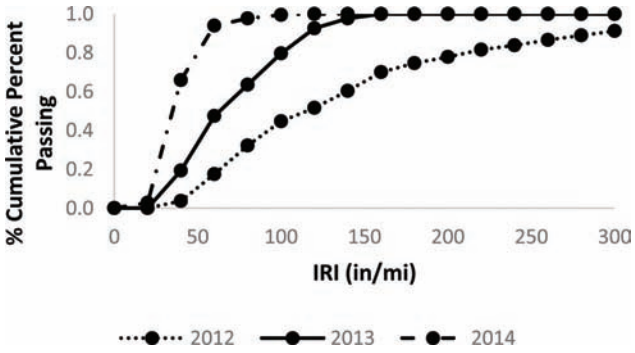

Figure 5.2 Cumulative percent passing versus IRI values (lined-up data).

conditions in all three years compared to the non-corrected data. In this case, the results seems to suggest that INDOT might have missed the optimal times to undertake the appropriate repair/rehabilitation actions at those highway sections.

6. SUMMARY, CONCLUSIONS, AND LIMITATIONS

A lined-up correction method with error control mechanisms was developed in this study to address misalignments in pavement condition data collected at different times. The method was tested and validated using INDOT's pavement condition survey data collected in 2012, 2013, and 2014. Lined-up and non-lined-up data were compared to illustrate the effect of correcting and aligning the location data, a process that is critical for developing accurate pavement performance curves and supporting decision-making in pavement management.

The results show that the correction method is successful in aligning the location information collected at different times, and the error control mechanism works as expected. INDOT can use the method not only to correct the reference readings and align pavement condition data collected at different times but also to control the maximum possible error so that it is within an acceptable range. The results also illustrate the effectiveness of correcting the location data; the correction method can help INDOT develop accurate pavement performance curves so that the appropriate actions can be taken at the optimal times based on accurate pavement condition assessments.

The main limitation of this proposed correction method is its reliance on the linear relationship assumption. The correction method and error control mechanism are both based on this assumption. In reality, however, this assumption does not always hold. To take full advantage of the method, practitioners should identify a number of permanent physical structures and use them to calibrate the pavement condition data.

CONTENTS

PART II: EMPIRICAL RELATIONSHIPS BETWEEN PERFORMANCE INDICATORS

1. INTRODUCTION 18

2. PAVEMENT DISTRESSES 18
2.1 Pavement Cracking 18
2.2 Rutting 18
2.3 Roughness 18
2.4 Faulting 18

3. PAVEMENT PERFORMANCE INDICATORS 20
3.1 International Roughness Index (IRI) 20
3.2 Pavement Surface Distress 20
3.3 Structural Condition 21
3.4 Combined Indicators of Overall Pavement Performance 21
3.5 Condition Criteria 21

4. ANALYSIS METHODS 23
4.1 Support Vector Machines (SVM) 23
4.2 Naïve Bayes 24
4.3 Logistic Regression 25

5. DATA DESCRIPTION 25
5.1 Data Summary 25
5.2 Data Statistics 25

6. ANALYSIS, RESULTS, AND DISCUSSION 31
6.1 Relationship between Crack Width and Cracking Depth 31
6.2 Correlation between Different Crack Types 36
6.3 Relationship between IRI and Pavement Cracking 46
6.4 Discussion and Conclusions 61

REFERENCES 61

LIST OF TABLES

Table	Page
Table 2.1 Summary of Pavement Crack Types	19
Table 2.2 Typical Pavement Condition Assessment based on Rutting	20
Table 3.1 FHWA 2001 Pavement Condition Criteria	22
Table 3.2 FHWA 2006 Pavement Condition Criteria	22
Table 3.3 INDOT Pavement Performance Standards for Two Indicators	22
Table 5.1 Summary of Pavement Condition-Related Variable Data	26
Table 5.2 Count of Pavement Distress Variables	26
Table 6.1 Regression Results of Linear Model Relating Crack Depth and Crack Width	31
Table 6.2 Regression Results between Non-Wheel Path Longitudinal Cracking and Non-Wheel Path Alligator Cracking	38
Table 6.3 Regression Results between Wheel Path Longitudinal Cracking and Wheel Path Alligator Cracking	39
Table 6.4 Regression Results between Edge Longitudinal Cracking and Edge Alligator Cracking	39
Table 6.5 Regression Results between Shoulder Longitudinal Cracking and Shoulder Alligator Cracking	40
Table 6.6 Correlation between Block Cracking and Transverse Cracking	41
Table 6.7 Correlation between Block Cracking, Non-Wheel Path Longitudinal/Alligator Cracking, and Wheel Path Alligator Cracking	41
Table 6.8 Regression Results for Transverse Cracking, Wheel Path Longitudinal Cracking, and Wheel Path Longitudinal/Alligator Cracking	44
Table 6.9 Regression Model Results	53
Table 6.10 Performance Comparison of Models with Different Training Data	56
Table 6.11 Performance Comparison of SVM Models with Different Kernels	57
Table 6.12 Performance Comparison of SVM Models with Different Models	60

LIST OF FIGURES

Figure	Page
Figure 3.1 IRI Roughness scale	20
Figure 3.2 Reproduction of an individual present serviceability rating form	22
Figure 4.1 Maximum-margin hyper-plane and margins for an SVM trained with samples from two classes	23
Figure 4.2 Form of the logistic function	25
Figure 5.1 Distribution of pavement distress	26
Figure 5.2 Histograms for all pavement distress variables in the data set	27
Figure 6.1 Actual observations versus preliminary fitted curve	32
Figure 6.2 Scatter plots relating non-wheel path longitudinal crack width and non-wheel path alligator crack width	37
Figure 6.3 Scatter plots relating non-wheel path longitudinal crack depth and non-wheel path alligator crack depth	38
Figure 6.4 Correlation between non-wheel path longitudinal cracking and non-wheel path alligator cracking	39
Figure 6.5 Correlation between wheel path longitudinal cracking and wheel path alligator cracking	39
Figure 6.6 Correlation between edge longitudinal cracking and edge alligator cracking	40
Figure 6.8 Correlation between block cracking and transverse cracking	41
Figure 6.9 Correlation between block cracking and non-wheel path longitudinal cracking	42
Figure 6.10 Correlation between block cracking and non-wheel path alligator cracking	43
Figure 6.11 Correlation between block cracking and wheel path alligator cracking	44
Figure 6.12 Correlation between transverse cracking and wheel path alligator cracking	45
Figure 6.13 Correlation between transverse cracking and non-wheel path alligator cracking	45
Figure 6.14 Correlation between transverse cracking and wheel path longitudinal cracking	46
Figure 6.15 Probability distribution of non-wheel path cracking under different IRI values	47
Figure 6.16 Probability distribution of pavement distresses for different IRI and curve fitting regression results	48
Figure 6.17 Testing results for Naïve Bayes classifier for 100 random observations	54
Figure 6.18 Testing results with aggregate data for 30 random observations	54
Figure 6.19 Histogram of average IRI values	55
Figure 6.20 Testing results for Naïve Bayes classifier using disaggregate data with IRI values smaller than 300 in/mi for 100 random observations	55
Figure 6.21 Testing results for Naïve Bayes classifier using aggregate data with IRI values smaller than 300 in/mi for 30 random observations	55
Figure 6.22 Performance comparison between models using different training data	56
Figure 6.23 Testing results for SVM models with different kernels	58
Figure 6.24 Performance comparison among SVM models with different kernels	59
Figure 6.25 Testing results for logistic regression model (30 random observations)	59
Figure 6.26 Model performance of logistic regression model for different error tolerances	60
Figure 6.27 Performance comparison between different methods (with aggregate data and extreme IRI values removed)	60

1. INTRODUCTION

Evaluating pavement condition is important in pavement management systems (Park, Thomas, & Wayne Lee, 2007). A successful pavement management system must accurately estimate or predict future pavement performance based on current pavement condition and maintenance and repair actions. Most studies have focused on developing pavement performance prediction or deterioration models to relate pavement condition to variables such as age, traffic, and climate. In contrast, this study focuses, among others, on correlating different types of pavement distresses so that the severity of one type of distress can be estimated based on other types of distresses. This is useful when only some types of distress data are available but other types of distress must be considered in decision-making.

INDOT's pavement condition data were used to establish relationships or correlations between pavement distresses. The data include pavement condition information for three roads—I-70, US-41, and US-52—in three consecutive years (2012 to 2014). The types of distresses considered include cracking, rutting, faulting, and roughness. The model developed in this study can be applied to other distress types, such as spalling, bleeding, raveling, depression, shoving, stripping, potholes, and joint problems, when appropriate data are available. The statistical analysis involves three tasks: (1) building a statistical regression model to relate crack depth to crack width for each type of pavement cracking on different road functional classes, (2) determining the relationships among different types of cracking in terms of crack depth and crack width, and (3) relating IRI to pavement cracking.

2. PAVEMENT DISTRESSES

The common forms of distress for flexible pavement include different types of cracking, bleeding, corrugation and shoving, depression, patching, aggregate polishing, potholes, raveling rutting, slippage cracking, stripping, water bleeding, and pumping. For rigid pavements, the common distresses include different types of cracking, spalling, faulting, aggregate polishing, shrinkage cracking, pumping, punchout, corner breaking, blowups, pop-outs, and reactive aggregate distress. Due to the limited availability of data, only the most common distresses are analyzed in this study: various types of cracking, rutting, faulting, and roughness. Therefore, this chapter focuses on descriptions of these distresses only.

2.1 Pavement Cracking

Cracks are common surface defect in rigid (concrete) and flexible (asphalt) pavements. They are often commonly caused by any combination of multiple degradation agents or processes that include traffic overloading, material weathering, differential settlement of the subgrade, and shrinkage. A summary of these crack types is provided in Table 2.1.

2.2 Rutting

Rutting refers to longitudinal depressions in the wheel paths, typically due to consolidation or movement of the material in the subgrade, subbase, base, or surface asphalt (Khurshid, 2010). This may be due to excessive traffic loads, poor asphalt mix design leading instability of the surface asphalt, or low load-bearing strength of the pavement layers. The middle of the rut is a grove and the side lines of the rut may be slightly lifted pavement material. During rain, ruts become filled with water and may cause hydroplaning. Rutting may be confined to the surface layers only or may be caused by subgrade failure. Table 2.2 shows a typical way to assess the severity of a rutted pavement.

2.3 Roughness

Pavement roughness is generally a representation of irregularities on the pavement surface that impair the vehicle ride quality and therefore affects the occupants adversely. Roughness directly influences the road user costs and is a universally used indicator of road condition (UMTRI, 1998). This is often measured using the International Roughness Index (IRI) which is measured along a specified distance (for example, mm/m or in/mi).

2.4 Faulting

Faulting is defined as height difference across a rigid pavement slab crack or joint: the height of the approach slab typically exceeds that of the leave slab. Faulting can be caused by pumping, slab settlement, or warping. It is possible to visually discern faulting when the height differential exceeds 2.5 mm (0.1 inches).

TABLE 2.1
Summary of Pavement Crack Types

Distress Types	Severity	Distresses for pavements with asphalt concrete surfaces	Distresses for pavements with jointed portland cement concrete surfaces
Longitudinal/ Transverse Cracking	Low	A crack with a mean width ≤6 mm; or a sealed crack with sealant material in good condition and with a width that cannot be determined.	Longitudinal: Crack widths <3 mm, no spalling and no measurable faulting; or well-sealed and with a width that cannot be determined. Transverse: Crack widths <3 mm, no spalling and no measurable faulting; or well-sealed and the width cannot be determined.
	Med	Any crack with a mean width >6 mm and ≤19 mm; or any crack with a mean width ≤19 mm and adjacent low severity random cracking.	Longitudinal: Crack widths ≥3 mm and <13 mm; or with spalling <75 mm; or faulting up to 13 mm. Transverse: Crack widths ≥3 mm and <6 mm; or with spalling <75 mm; or faulting up to 6 mm.
	High	Any crack with a mean width >19 mm; or any crack with a mean width ≤19 mm and adjacent moderate to high severity random cracking.	Longitudinal: Crack widths ≥13 mm; or with spalling ≥75 mm; or faulting ≥13 mm. Transverse: Crack widths ≥6 mm; or with spalling ≥75 mm; or faulting ≥6 mm.
Corner Cracking	Low	Crack is not spalled for more than 10 percent of the length of the crack; there is no measurable faulting; and the corner piece is not broken into two or more pieces and has no loss of material and no patching.	
	Med	Crack is spalled at low severity for more than 10 percent of its total length; or faulting of crack or joint is <13 mm; and the corner piece is not broken into two or more pieces.	
	High	Crack is spalled at moderate to high severity for more than 10 percent of its total length; or faulting of the crack or joint is ≥13 mm; or the corner piece is broken into two or more pieces or contains patch material.	
Block Cracking	Low	Cracks with mean width ≤6 millimeters (mm); or sealed cracks with sealant material in good condition and with a width that cannot be determined.	Not Applicable
	Med	Cracks with mean width >6 mm and ≤19 mm; or any crack with a mean width ≤19 mm and adjacent low severity random cracking.	Not Applicable
	High	Cracks with mean width >19 mm; or any crack with a mean width ≤19 mm and adjacent moderate to high severity random cracking.	Not Applicable
Edge Cracking	Low	Cracks with no breakup or loss of material.	Not Applicable
	Med	Cracks with some breakup and loss of material for up to 10 percent of the length of the affected portion of the pavement.	Not Applicable
	High	Cracks with considerable breakup and loss of material for more than 10 percent of the length of the affected portion of the pavement.	Not Applicable
Spalling (Longitudinal/ Transverse)	Low	Not Applicable	Spalls <75 mm wide
	Med	Not Applicable	Spalls 75 mm to 150 mm wide
	High	Not Applicable	Spalls >150 mm wide

Source: Distress Identification Manual for the Long-Term Pavement Performance Program (Miller & Bellinger, 2003).

TABLE 2.2
Typical Pavement Condition Assessment based on Rutting (Teede Tehnokeskus, 2016)

Pavement condition	Characteristics (traffic safety and impact on the road user)	Rut depth limits (mm)
Very good	Pavement has no ruts.	<5
Good	No ruts can be observed in the pavement and there is no impact on road users.	5–10
Fair	Ruts in the pavement can be observed. When it rains, water accumulates in the ruts. Road users start to search for best trajectory. Ruts should be eliminated within 1 to 3 years.	10–20
Poor	Ruts can clearly be seen in the pavement, driving speed as well as trajectory are influenced. When it rains, a lot of water accumulates in ruts and aquaplaning may occur. Ruts should be eliminated.	20–30
Very poor	Ruts can clearly be seen in the pavement, driving speed as well as trajectory and traffic safety are influenced. Ruts affect traffic safety both in rain and in dry conditions. Ruts should be eliminated immediately.	>30

3. PAVEMENT PERFORMANCE INDICATORS

Several decades ago, a pavement's ability to serve traffic was determined in a subjective manner based on visual inspection by experienced pavement engineers. In the current era, pavement performance is often measured as a function of a pavement's ability to serve traffic over a given period. Therefore, a performance indicator represents, in quantitative or qualitative terms, the extent to which a specific function of the pavement is carried out (Sinha & Labi, 2007). Generally, pavement performance can be categorized into surface roughness, surface distress, and structural condition depending on the pavement attribute in question (Haas, Hudson, & Zaniewski, 1994).

3.1 International Roughness Index (IRI)

Pavement roughness is a summary statement of a pavement surface's distortion along a linear plane, and describes the severity of pavement surface irregularities that impair the vehicle's ride quality. Roughness impacts vehicle dynamics and therefore significantly impacts vehicle operating costs, safety, and the travel comfort (Patterson et al., 1986). It also increases the dynamic loadings imposed on the pavement surface by the vehicle; this accelerates the deterioration of the pavement structure. Roughness is a primary criterion by which road users judge the quality of a pavement. As such, this is one of the key criteria for pavement investment decisions at most agencies. Roughness is usually reported using IRI. The open-ended IRI scale is shown in Figure 3.1.

The use of IRI has increased over the years, and IRI is now a dominant criterion of pavement performance. Research has established that IRI reflects pavement performance and is directly related to the vehicle operation cost (Chesher & Harrison, 1987; Archondo-Callao & Faiz, 1994).

3.2 Pavement Surface Distress

Surface distress can be defined as a manifestation of pavement surface damage, and the modes of surface distress can be placed categorized as follows (Paterson, 1987):

- *Fracture.* This group contains all types of cracking (in rigid and flexible pavements) and spalling caused by excessive loading, thermal changes, fatigue, slippage, moisture damage, or contraction.
- *Distortion.* This group contains all forms of deformation, which results from such factors as rutting, corrugation, and shoving. For rigid pavements, the rut shape distortion is referred to as wheel path wear.

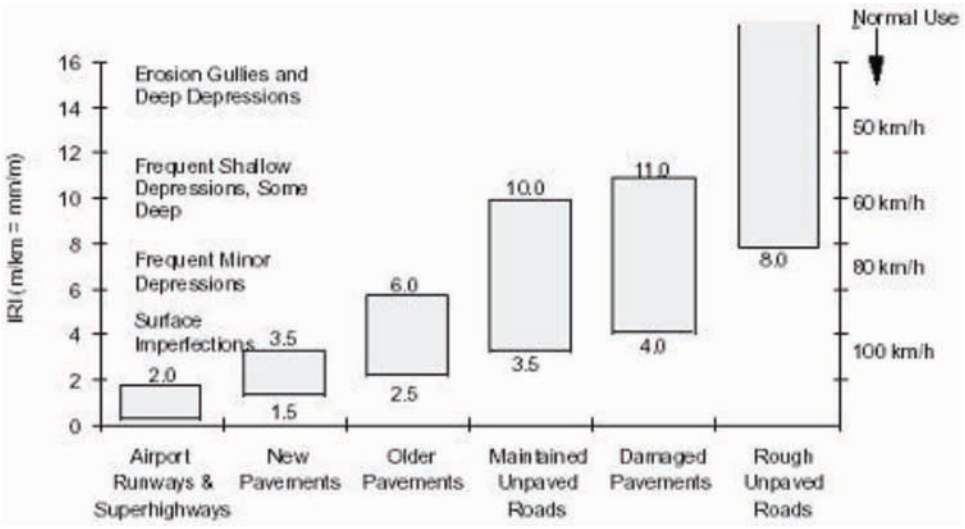

Figure 3.1 Conceptual scale for IRI (adapted from Sayers et al., 1986).

- *Disintegration.* This group contains raveling, stripping, and spalling, which are caused by a variety of factors including poor consolidation/compaction, traffic abrasion, aggregate degradation, loss of bonding, chemical reactivity, and binder aging.

Surface distress bears some relationship with surface roughness (inter alia, greater frequency and intensity of surface material distortion, disintegration, or cracking is associated with increased pavement roughness) and pavement structural capability (inter alia, surface distress could indicate some structural deficiency). Each distress type within the above-named categories of surface distresses can constitute a performance indicator for purposes of pavement condition evaluation. For example, rutting is a common performance indicator that has been used to evaluate pavement condition in a significant number of studies (Hall, Correa, & Simpson, 2003; Irfan, Khurshid, & Labi, 2009; Labi, Lamptey, Konduri, & Sinha, 2005). However, given all the different types of distresses, choosing one type of distress to evaluate overall pavement condition may not be appropriate for making rehabilitation decisions. It should be noted that pavement maintenance is a different situation; different types of maintenance are appropriate for different levels of each type of distress (Paterson, 1987). Pavement condition rating (PCR) is another common pavement performance indicator for surface distress. PCR characterizes pavement distress in terms of extent and severity on a condition evaluation scale that ranges from 0 (very poor) to 100 (excellent).

3.3 Structural Condition

To evaluate a pavement's structural integrity (and the load transfer of rigid pavement slabs), agencies typically use surface deflection measurements. The surface deflection measures the vertical movement of the pavement surface in response to an applied load. The shape and magnitude of pavement deflection can be modeled as a function of traffic (type and volume) and the soil temperature and moisture (Pavement Interactive, 2016). Surface deflection is the most commonly used measurement of pavement structural condition because it costs relatively little, minimally interrupts traffic, and causes little damage to the existing pavement (Haas et al., 1994).

3.4 Combined Indicators of Overall Pavement Performance

A number of highway agencies have established a distress index for each individual distress type, such as transverse crack index, while others have an index representing various combinations of distress type, extent, and severity. Similar to the calculation of PCR, the calculation of combined indices requires the establishment of weights or priority factors for the various distress types. A pavement can have an overall score based on its deflection, roughness, skid resistance, and other surface distresses. This score quantifies a pavement's overall performance and could, in certain cases, be used to help determine the type of maintenance and rehabilitation needs during the decision-making process and help pavement managers prioritize projects by allowing a comparison of different pavements.

3.4.1 Present Serviceability Rating (PSR)

PSR is described as the judgment of a pavement to serve the traffic it is intended to serve. This subjective scale ranges from 0 (impassable) to 5 (excellent). PSR is based on the passenger's assessment of ride quality and is therefore a reflection of the road roughness.

Two correlations developed to link IRI and PSR are herein presented (Paterson, 1987; Al-Omari & Darter, 1992):

$$PSR = 5\ e^{-9.18\ (IRI)} \tag{3.1}$$

$$PSR = 5\ e^{-0.26\ (IRI)} \tag{3.2}$$

3.4.2 Present Serviceability Index (PSI)

PSI is based on the PSR measure developed in the original AASHO Road Test. To migrate from the PSR concept (panel required) to the PSI measure (no panel required), a rating panel, in 1959, rated the PSR of various roads in three Midwest states. This was then correlated to pavement attributes including the slope variance (profile) and cracking to yield the PSI equations. Subsequently, the following relationships were developed:

Flexible pavements:

$$PSI = 5.41 - 1.80\log(1+SV) - 0.09(C+P)^{0.5} \tag{3.3}$$

Rigid pavements:

$$PSI = 5.03 - 1.91\log(1+SV) - 1.38RD^2 - 0.01(C+P)^{0.5} \tag{3.4}$$

where PSI is the present serviceability index.

Figure 3.2 illustrates the PSI concept.

3.5 Condition Criteria

Based on the performance indicators described above, pavement condition can be categorized into ordered discrete classes, such as good condition, fair condition, and poor condition, using a variety of standards. Among all the performance measurements, IRI, PSR, and PCR are the most commonly used as condition criteria in the standards of state agencies. Tables 3.1 and 3.2 present the Federal Highway Administration (FHWA, 2002, 2007) pavement condition criteria as of 2002 and 2006. Table 3.3 presents pavement performance standards that were used by INDOT as possible application triggers, in terms of IRI and PCR, for different treatment types (INDOT, 2001).

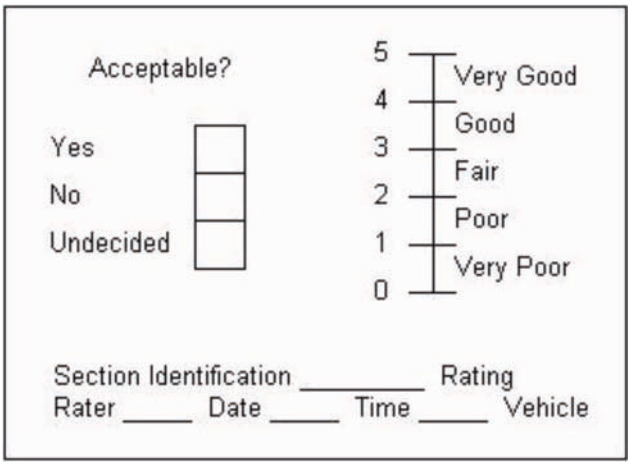

Figure 3.2 Reproduction of an individual present serviceability rating form (Pavement Interactive, 2016).

TABLE 3.1
FHWA 2001 Pavement Condition Criteria (FHWA, 2002)

	IRI Rating		PSR Rating	
Condition Term Categories	**Interstate**	**Other**	**Interstate**	**Other**
Very Good	<60	<60	>4.0	>4.0
Good	60 to 94	60 to 94	3.5 to 3.9	3.5 to 3.9
Fair	95 to 119	95 to 170	3.1 to 3.4	2.6 to 3.4
Mediocre	120 to 170	171 to 220	2.6 to 3.0	2.1 to 2.5
Poor	>170	>220	<2.5	<2.0

TABLE 3.2
FHWA 2006 Pavement Condition Criteria (FHWA, 2007)

	All Functional Classifications	
Ride Quality Terms	**IRI Rating**	**PSR Rating**
Good	<95	≥3.5
Acceptable	≤170	≥2.5
Not Acceptable	>170	<2.5

TABLE 3.3
INDOT Pavement Performance Standards for Two Indicators

	Performance Indicator Value (INDOT Standards)		
Performance Indicator	**(m/km)**	**(in/mi)**	**Performance**
International Roughness Index (IRI)	<1.6	<100	Excellent
	1.6–2.37	100–150	Good
	2.37–3.15	150–200	Fair
	>3.15	>200	Poor
PCR	>90		Excellent
	90–80		Good
	80–70		Fair
	<70		Poor

4. ANALYSIS METHODS

In this study, both regression analysis and machine learning techniques (Naïve Bayes, and logistic regression, and support vector machines) were adopted to analyze the relationship between IRI and other pavement distresses. This section provides background information on the three machine learning methods. The section represents a synthesis of literature on the subject of machine learning techniques taken from various sources in the literature (Caruana & Niculescu-Mizil, 2006; Chand, Aruna, Masqood, & Rao, 2005; Murty & Devi, 2011; Niculescu-Mizil & Caruana, 2005; Nigam, McCallum, Thrun, & Mitchell, 2000; Russell & Norvig, 2003; Zhang, Oussena, Clark, & Hyensook, 2010; Zhefu & Chuanying, 2008).

4.1 Support Vector Machines (SVM)

SVM, which takes roots from the theory of statistical learning, is an algorithm for machine learning (Cortes & Vapnik, 1995). SVM uses a transformation that is described by an inner product function to transform the input space into a high-dimensional space, creates an optimal hyper-plane to place the data in two classes—negative and positive—and then maximizes the distance between the hyper-plane separating the negative and positive classes and the data points closest to the hyper-plane. Figure 4.1 presents an example.

The SVM computation involves optimization of a convex quadratic nature, to ensure that the solution is optimal. SVM is advantageous compared to conventional algorithms for statistical learning because it exhibits high generalization performance even with feature vectors that have high dimensions. In addition, it is able to manage kernel functions that carry out mapping of the input data to a higher dimensional space while keeping computational complexity to low levels.

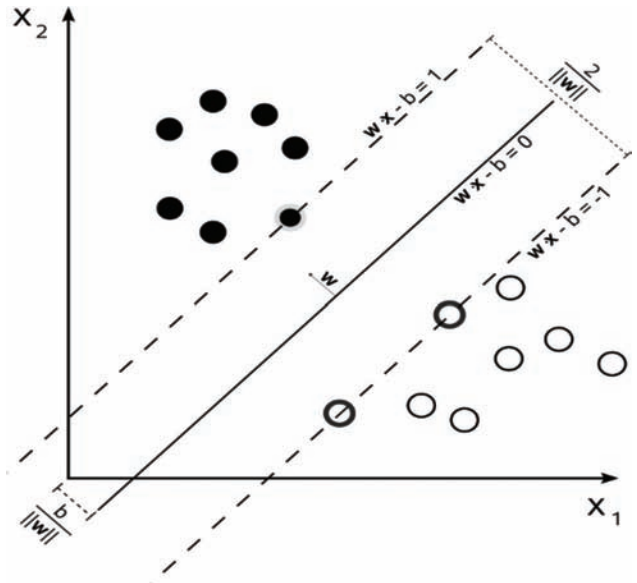

Figure 4.1 Illustration of Maximum-margin hyperplane and margins for an SVM trained with samples from two classes (Prakash, 2014).

Yang et al. (2007) presented the formulation for this problem as follows: starting with a training dataset (x_i,y_i, where i = 1,2 ... ..., l, x ∈ R is a vector in n-dimensions, and $y_i \in \{-1, +1\}$ represents the class label of ith data. The optimal hyper-plane separates the training data into two classes. SVM maximizes the margin between the negative and positive classes. Figure 4.1 shows training examples placed linearly into two separate classes. Yang et al. (2007) stated that it is generally not required to separate the training examples into each class. The variable $\delta_i \geq 0$, introduced to account for errors of misclassification, is a constant. Therefore, the resulting optimization problem formulation is:

$$\min_w \varnothing(w) = ||w||^2 + C \sum_{i=1}^{l} \delta_i \tag{4.1}$$

$$s.t.: y_i[(w * x_i) + b] \geq 1 - \delta_i,\ i = 1,2 \ldots \ \ldots, l \tag{4.2}$$

In Equation 4.1, the term $||w||^2$ is the margin size, and C is the misclassification cost.

$f(x)$, the decision function, may be written as:

$$f(x) = sgn(g(x)) \tag{4.3}$$

$$g(x) = \sum_i \alpha_i y_i (x_i \cdot x) + b \tag{4.4}$$

where $a_i \geq 0$ represent the Lagrange multipliers. When the maximal margin hyper-plane is located in the feature space, $a_i \geq 0$ holds for the support vectors only, that is, those points that lie closest to the hyper-plane. $a_i = 0$ for all the other points. The support vectors exhibit the most informative patterns in the data (Yang et al., 2007).

As defined in the literature, the kernel function is expressed as:

$\varnothing(u) \cdot \varnothing(v) = K(u \cdot v)$ for a nonlinear SVM classifier.

Using a kernel function, Equation 4.4 can be re-written as:

$$g(x) = \sum_i \alpha_i y_i K(x_i \cdot x) + b \tag{4.5}$$

In this study, a linear kernel function, radial basis function (RBF), and polynomial kernel function (Equations 4.6 to 4.8) were used. These have the following forms:

$$\text{Linear: } K(x,x') = x^T \cdot x' \tag{4.6}$$

$$\text{RBF: } K(x,x') = exp(-\gamma||x - x'||^2) \tag{4.7}$$

$$\text{Polynomial: } K(x,x') = (x^T \cdot x' + 1)^d \tag{4.8}$$

Classical SVM places the data into two classes (in practical applications, however, multiple classes are commonly used). The methods to solve multi-classification include one-against-all and one-against-one. In this

study, each distinct IRI value is treated as a class. SVM with multi-classification is applied using the one-against-one method. The algorithm was implemented in Python.

4.2 Naïve Bayes

A classifier is model that assigns class labels drawn from a given, finite set to problem instances, represented as vectors of feature values (John & Langley, 1995; McCallum & Nigam, 1998; Metsis, Androutsopoulos, & Paliouras, 2006; Rennie et al., 2003; Zhang, 2004). Naïve Bayes is a collection of algorithms that are based on the notion that all Naïve Bayes classifiers are based on the assumption that given the class variable, any particular feature's value is not dependent on that of any other feature. It is possible to train Naïve Bayes classifiers, for certain types of probability models, in a supervised-learning environment. The Naïve Bayes technique is advantageous because it needs a rather small set of training data in order to estimate the parameters needed for the classification. The parameters are estimated using the maximum likelihood technique. Therefore, in order to use the Naïve Bayes model, one does not need to adopt the concept of Bayesian probability or use Bayesian methods. Naïve Bayesian models are useful for analyzing large data sets because they are relatively easy to build and are unencumbered by iterative estimation of the model parameters.

Using Bayes' theorem, it is possible to calculate the posterior probability, $P(c|x)$, from $P(c)$, $P(x)$, and $P(x|c)$. An assumption associated with Naïve Bayes classifiers is the "class conditional independence assumption", that is, the impact of a predictor value on a given class (c) is independent of the values of other predictors. For example, consider a problem that is to be classified, represented by vector $x = (x_1, x_2, \ldots \ldots x_n)$ representing some n features (that is, independent variables); this instance is assigned the probabilities for each of k possible outcomes of classes C_k:

$$P(C_k|x_1, \ldots, x_n) \tag{4.9}$$

However, if the features is too many or if a feature can take on too many values, it becomes infeasible to base such a model on probability tables. To make the model more tractable to analysis, it may be formulated using Bayes' theorem. It is possible to decompose the conditional probability as follows:

$$P(c_k|x) = \frac{P(x|c_k)P(c_k)}{P(x)} \tag{4.10}$$

$P(c_k|x)$ and $P(c)$ represent the posterior and prior probabilities of a class,

$P(x|c_k)$ refers to the likelihood of the probability of the predictor, and $P(x)$ is the prior probability of the predictor.

Using the following naïve independence assumption:

$$P(x_i,|C_k,x_1,\ldots x_{i-1},x_{i-2}\ldots \ \ldots x_n) = P(x_i,C_k) \tag{4.11}$$

This relationship is simplified to obtain Equation 4.12.

$$P(c_k|x_1,\ldots..,\ x_n) = P(C_k)\prod_{i=1}^{n} P(x_i|c_k) \tag{4.12}$$

The Naïve Bayes classifier represents a combination of the Naïve Bayes probability model and a decision rule. An example of a decision rule is the "maximum a-posteriori decision rule": adopt the most probable hypothesis. The corresponding Bayes classifier assigns a class label (Equation 4.13).

$$\hat{y} = argmax_{k\in\{1,\ldots,k\}} P(C_k)\prod_{i=1}^{n} p(x_i|C_k) \tag{4.13}$$

Critics contend that Naïve Bayes classifiers are rather simple in their methodology and are based on simple assumption. However, these classifiers are used widely because they perform surprisingly well—they often outperform more sophisticated classification methods (Rish, 2001; Zhang, 2004). The assumptions regarding the distribution of features are referred to as the Naïve Bayes classifier's "event model." The Bernoulli and multinomial distributions are often used in the case of discrete features such as associated with internet spam identification. In the current study, the feature set mainly consists of continuous data, and Gaussian distribution is therefore assumed.

We assume that the Gaussian function governs the distribution of continuous values associated with each class in our problem. Consider that our data has a continuous attribute that is denoted by x. We herein follow the steps outlined in Hand and Yu (2001): first, the data is segmented by class and then in each class, the mean and variance of is calculated. We denote the mean of the values of x associated with class c as μ_c; and the variance of the values of x associated with class c as σ_c^2. Consider that some value v as been observed. The probability distribution of v given class c, $p(x = v|c)$, can be determined by substituting v into the normal distribution equation (with parameters μ_c, σ_c^2) as shown in Equation 4.14 (Hand & Yu, 2001):

$$P(x = v|c) = \frac{1}{\sqrt{2\pi\sigma_c^2}} e^{-\frac{(v-\mu_c)^2}{2\sigma_c^2}} \tag{4.14}$$

4.3 Logistic Regression

Logistic regression, a statistical technique, is a technique that uses learning functions that have the form:

$f: X \rightarrow Y$, or $P(Y|X)$ in the case where Y is a discrete value, and $X = < X_1 \ldots X_n >$ is a vector containing continuous or discrete variables.

Although the predicted variable (IRI) is a continuous variable, it can be treated as a discrete value and then logistic regression can be applied.

In this section, we consider the case where Y is a 0-1 variable in order to simplify the notation (in a real application, this can be extended to cases where Y takes on any finite number of discrete values). This regression technique assumes that the distribution $P(Y|X)$ has a parametric form and estimates its parameters from the

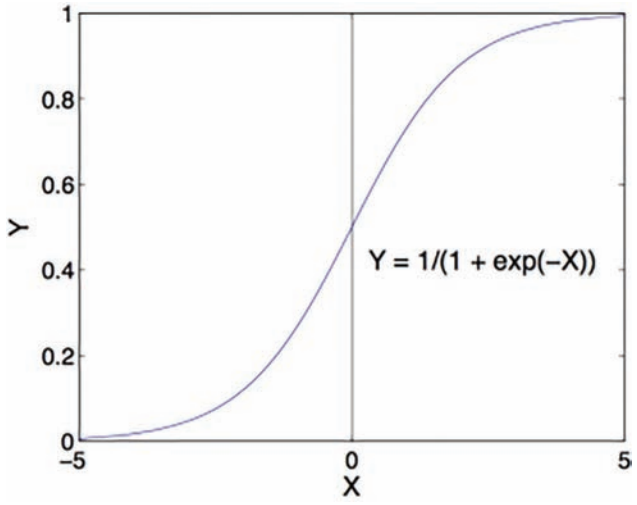

Figure 4.2 Form of the logistic function.

training dataset (Xing & Bar-Joseph, 2015). Equation 4.15 represents the parametric model that the logistic regression assumes in cases where Y is a 0-1 variable. Equation 4.1 represents the case where Y has more than 2 outcomes.

$$P(Y=1|X)=\frac{1}{1+\exp(w_0+\sum_{i=1}^{n} w_i x_i)} \quad (4.15)$$

$$P(Y=0|X)=\frac{\exp(w_0+\sum_{i=1}^{n} w_i x_i)}{1+\exp(w_0+\sum_{i=1}^{n} w_i x_i)} \quad (4.16)$$

The logistic function is S shaped (Figure 4.2).

5. DATA DESCRIPTION

5.1 Data Summary

The data used in this study are provided by the Indiana Department of Transportation (INDOT), including detailed condition data for pavements on three roads (I-70, US-41 and US-52) for three consecutive years (2012, 2013, and 2014). Although the data only include pavements on three road corridors, the number of observations is large (50,400 sections) because the data are reported at 0.005-mile intervals. The condition data include IRI, rutting, faulting, texture, spalling, and many different types of cracking, as summarized in Table 5.1.

5.2 Data Statistics

This section provides the summary statistics for all of the pavement distress variables in the data set. IRI and rutting are continuous variables with all entries larger than 0. For cracking, spalling, and faulting, many or most of the data entries are zero, indicating that this type of distress does not exist on those pavement segments. Table 5.2 summarizes the number of non-zero entries for each type of pavement distress under the different severity levels. Figure 5.1 shows the proportion of each distress type in the dataset. The most common distresses in the data set were non-wheel path longitudinal cracks, transverse crack, edge longitudinal cracks, and wheel path longitudinal cracks.

Figure 5.2 (i) – (xv) present the distributions of all the distress variables after removing nonzero entries. The histograms show that most of the crack widths and crack depths are typically somewhat skewed normally distributed. It was also found that, in most cases, the crack widths/depths at a high severity level have the highest mean, followed by crack widths/depths at a medium severity level and the crack widths/depths at a low severity level. This is expected because the level of severity of pavement distress is determined by crack width, as discussed in Section 2.1. Additionally, crack depth is highly correlated with crack width, which is explained in Section 6.1.

TABLE 5.1
Summary of Pavement Condition-Related Variable Data

Distress	Type	Variables	Severity Level
Non-Wheel Path	Longitudinal	Length(ft), Width(in), Depth(in)	Low Med High
	Alligator	Percentage (%), Width(in), Depth(in)	Low Med High
Wheel Path	Longitudinal	Length(ft), Width(in), Depth(in)	Low Med High
	Alligator	Percentage (%), Width(in), Depth(in)	Low Med High
Edge Shoulder	Longitudinal	Length(ft), Width(in), Depth(in)	Low Med High
	Alligator	Percentage (%), Width(in), Depth(in)	Low Med High
Transverse	-	Number(num), Width(in), Depth(in)	Low Med High
Block	-	Percentage (%), Width(in), Depth(in)	Low Med High
Spall	Longitudinal	Number(num), Width(in), Depth(in)	Low Med High
	Transverse	Number(num), Width(in), Depth(in)	Low Med High
Shoulder	Longitudinal	Length(ft), Width(in), Depth(in)	Low Med High
	Transverse	Percentage (%), Width(in), Depth(in)	Low Med High
Corner	-	Number(num), Width(in), Depth(in)	Low Med High
Roughness	-	IRI_LWP(in/mi), IRI_RWP(in/mi), IRI_Avg(in/mi)	-

TABLE 5.2
Count of Pavement Distress Variables

	Low	Med	High	Total	Percentage
Non-Wheel Path Longitudinal Crack	7726	8228	3709	19663	23.6%
Wheel Path Longitudinal Crack	4456	3039	848	8343	10.0%
Non-Wheel Path Alligator Crack	433	534	325	1292	1.5%
Wheel Path Alligator Crack	809	2899	975	4683	5.6%
Edge Longitudinal Crack	4306	6112	2932	13350	16.0%
Edge Alligator Crack	2922	3052	1081	7055	8.5%
Shoulder Longitudinal Crack	1080	1345	809	3234	3.9%
Shoulder Alligator Crack	37	16	38	91	0.1%
Transverse Crack	7758	3330	2687	13775	16.5%
Block Crack	747	2497	736	3980	4.8%
Longitudinal Spall	1342	389	296	2027	2.4%
Transverse Spall	1759	1122	311	3192	3.8%
Corner Crack	7	3	2	12	0.0%
Faulting				2705	3.2%

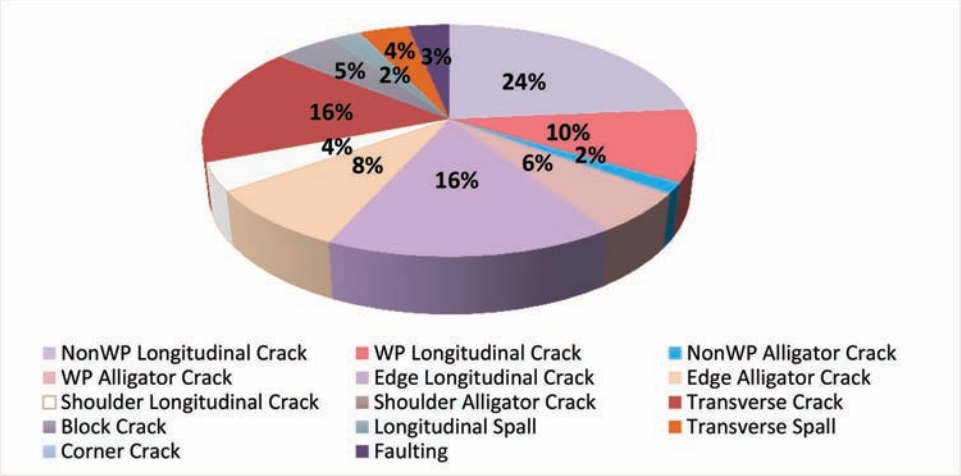

Figure 5.1 Distribution of pavement distress.

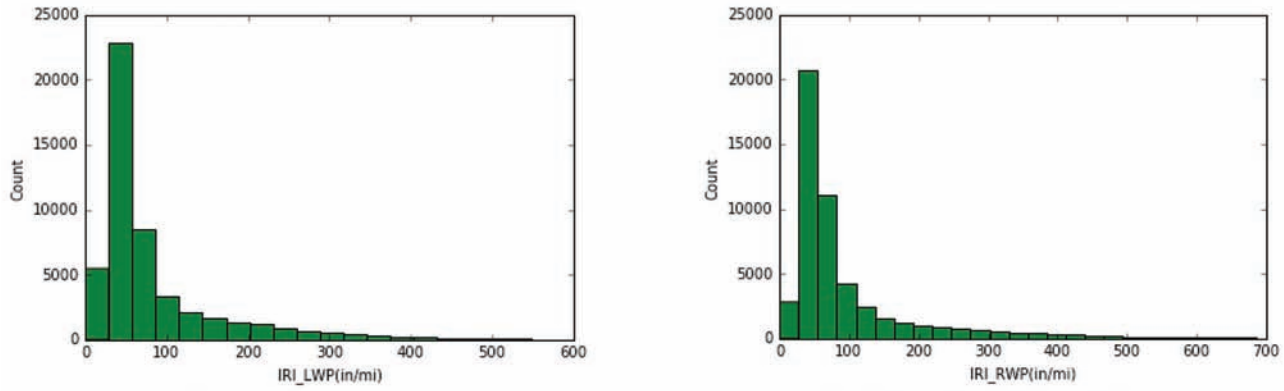

(a) IRI on Left Wheel Path (in./mi) (b) IRI on Right Wheel Path (in./mi)

i. IRI

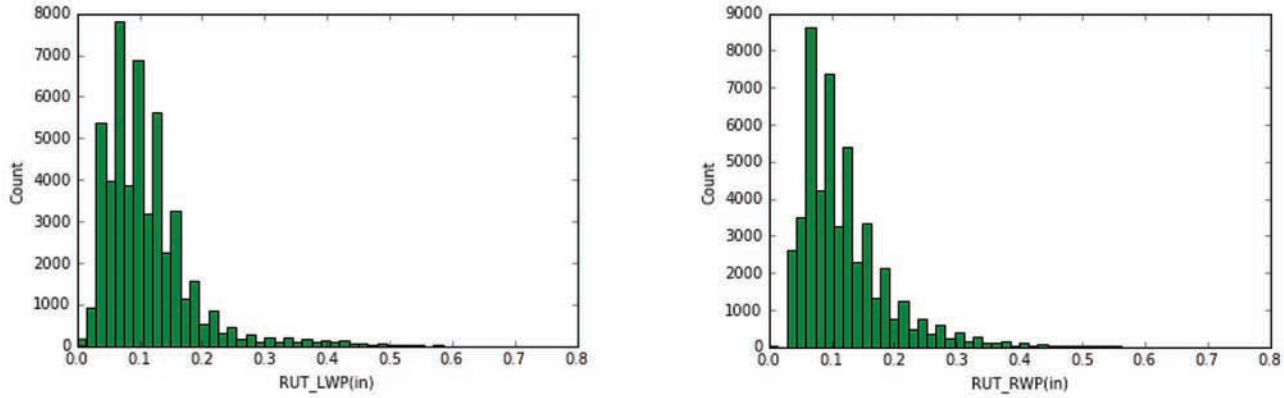

(a) Rut on Left Wheel Path (in.) (b) Rut on Right Wheel Path (in.)

ii. Rutting

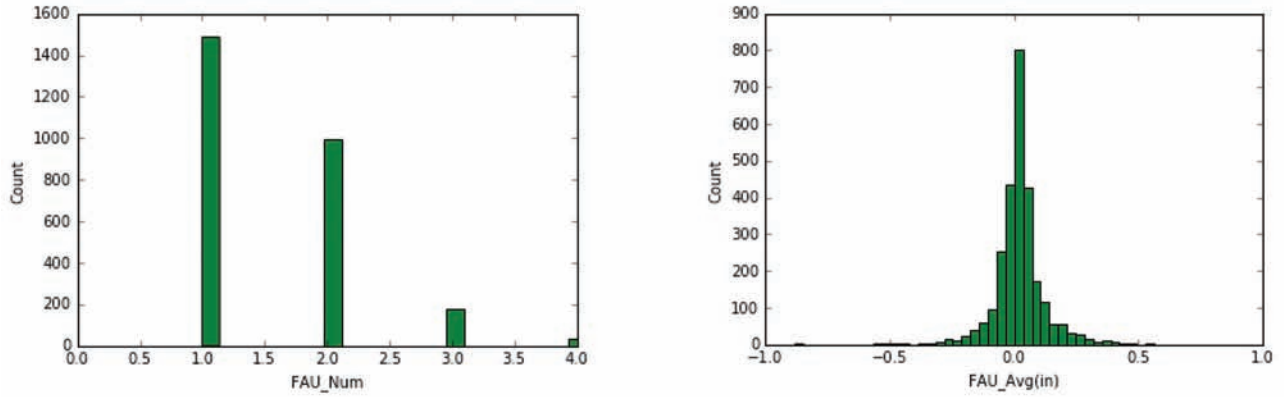

(a) Faulting Number (Num) (b) Faulting Average (in.)

iii. Faulting

Figure 5.2 Histograms for all pavement distress variables in the data set. (*Figure continued on next page*)

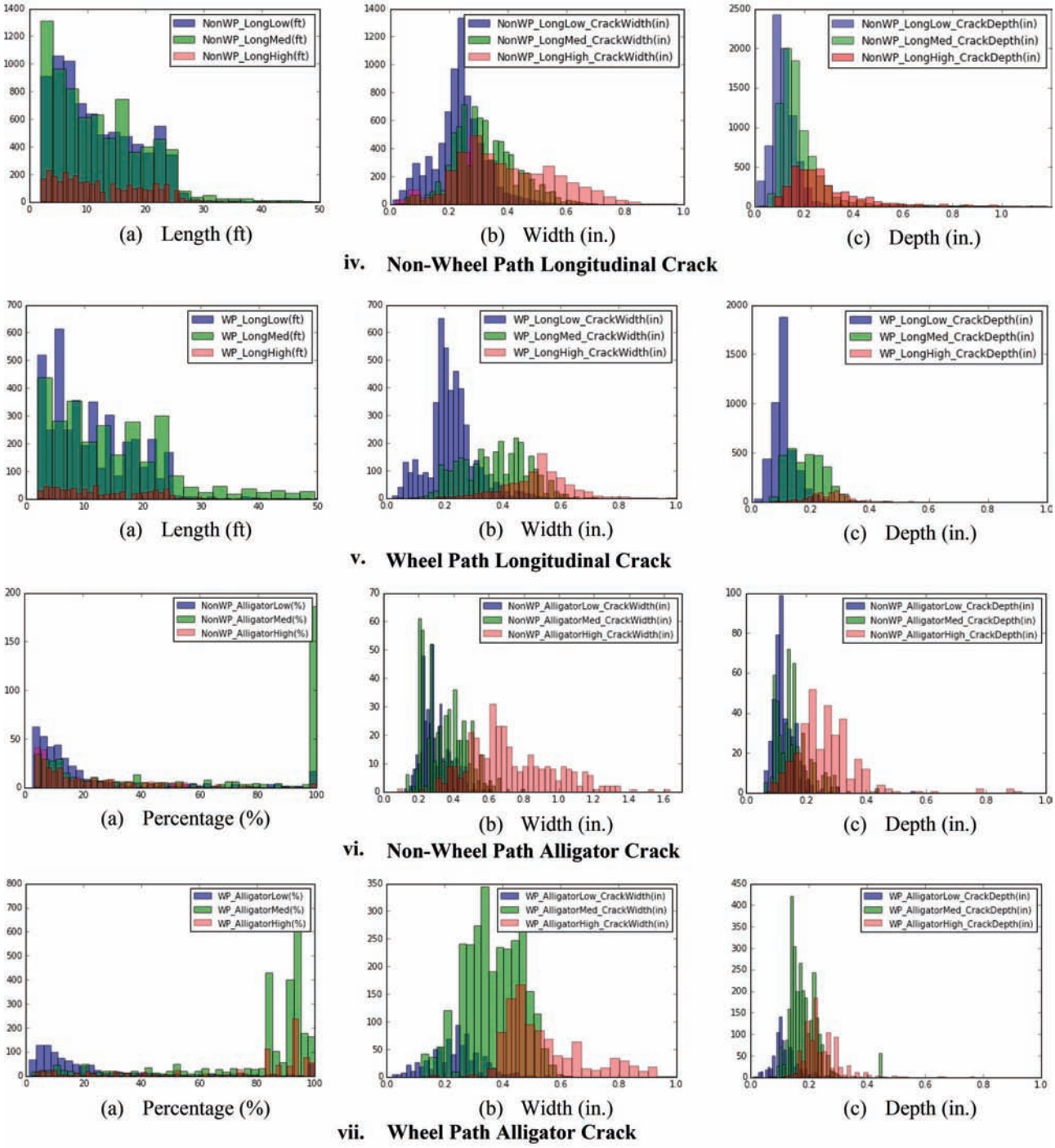

Figure 5.2 (Continued)

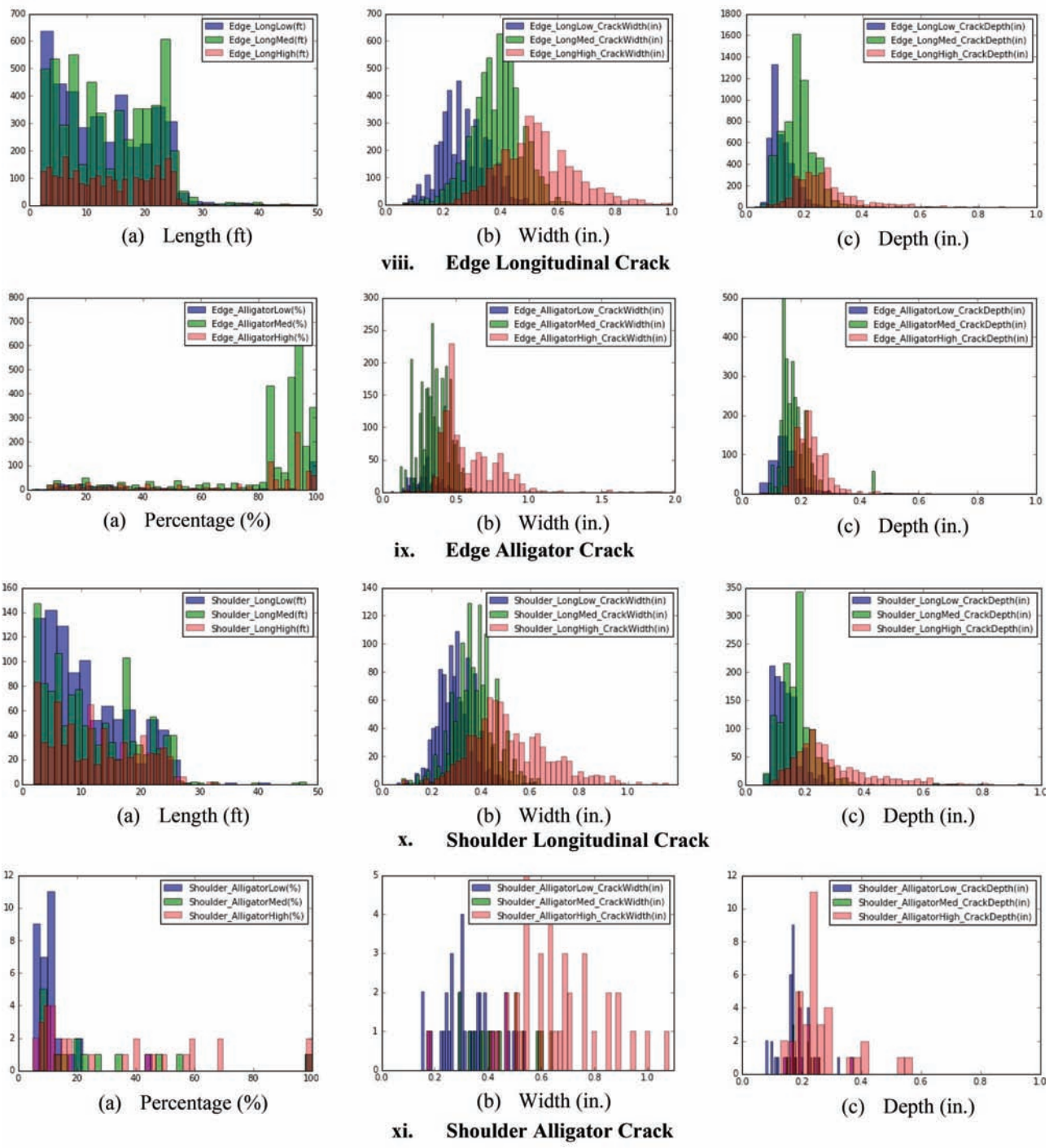

Figure 5.2 (Continued)

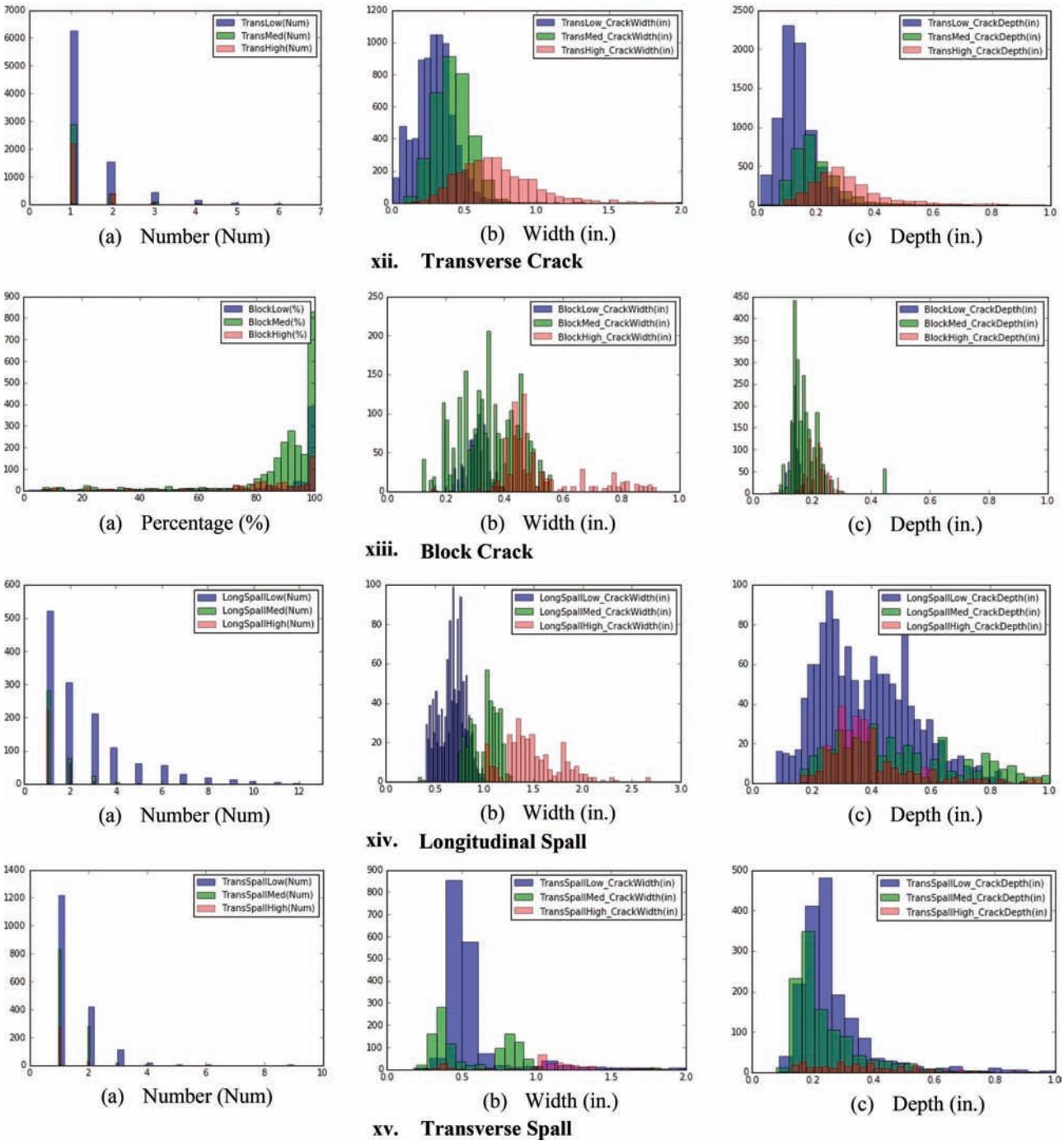

Figure 5.2 (Continued)

6. ANALYSIS, RESULTS, AND DISCUSSION

6.1 Relationship between Crack Width and Cracking Depth

Pavement cracking can be measured in terms of percentage, length, width, and depth. When a wide, deep crack occurs, road safety may be more or less degraded and user costs may increase significantly. Therefore, it is necessary to inspect pavements periodically for cracking to control the progress of crack development. Crack widths and lengths can be measured using state-of-the-art sensors with a good degree of accuracy, there is no documented evidence that this has been done for crack depths (Amarasiri, Gunaratne, & Sarkar, 2010). If crack depth can be estimated on the basis of available measurements of conditions such as crack width, then the crack depth would be useful for evaluating structural performance (Furuya, Yokota, Komatsu, Hashimoto, & Kato, 2014). An almost linear relationship between crack depth and width was determined in the literature (with a correlation coefficient (R) of 0.679). However, no existing studies provide relationship models in detail for each type of cracking at different levels of severity.

In the current study, we developed linear regression models for 12 types of cracking at low, medium, and high severity levels separately, and we developed models for cracks at Interstate and non-Interstate roads separately. The functional from is given in Equation 6.1. The regression results are summarized in Table 6.1. Figure 6.1 roughly shows how the developed models fit the actual observations. The R^2 values for most of the

TABLE 6.1
Regression Results of Linear Model Relating Crack Depth and Crack Width

		Interstate				Non-Interstate			
Cracking Type	**Level of Distress**	**Obs**	**a**	**b**	**R^2**	**Obs**	**a**	**b**	**R^2**
Longitudinal Cracking Non-Wheel Path	Low	2837	0.032	0.305	0.631	4795	0.035	0.383	0.665
	Med	2156	0.024	0.367	0.677	5656	0.111	0.198	0.328
	High	479	0.088	0.267	0.575	2495	0.172	0.149	0.297
Alligator Cracking Non-Wheel Path	Low	218	0.034	0.277	0.742	214	0.043	0.295	0.587
	Med	132	0.062	0.219	0.685	400	0.018	0.41	0.821
	High	192	0.065	0.238	0.786	105	-0.009	0.438	0.797
Longitudinal Cracking Wheel Path	Low	2371	0.046	0.289	0.67	2083	0.015	0.432	0.879
	Med	1352	0.038	0.345	0.796	1678	0.01	0.476	0.804
	High	241	0.069	0.306	0.647	568	0.082	0.353	0.638
Alligator Cracking Wheel Path	Low	443	0.036	0.314	0.726	368	0.029	0.393	0.785
	Med	336	0.054	0.293	0.643	2506	0.044	0.364	0.847
	High	305	0.078	0.239	0.815	641	0.022	0.434	0.797
Edge Alligator Cracking	Low	267	0.059	0.264	0.697	174	0.034	0.396	0.488
	Med	570	0.059	0.289	0.672	2425	0.056	0.329	0.828
	High	508	0.079	0.246	0.837	544	0.088	0.275	0.723
Edge Alligator Cracking	Low	1818	0.841	0.026	0.377	2478	0.03	0.305	0.632
	Med	3765	0.008	0.437	0.75	2305	0.001	0.444	0.729
	High	1299	0.015	0.436	0.773	1302	0.059	0.379	0.697
Transverse Cracking	Low	13	-0.296	1.273	0.895	734	0.053	0.281	0.725
	Med	89	0.064	0.24	0.799	2351	0.056	0.328	0.835
	High	263	0.068	0.246	0.927	473	0.015	0.5	0.832
Block Cracking	Low	3	0.296	1.273	0.895	734	0.053	0.281	0.725
	Med	89	0.064	0.24	0.799	2351	0.056	0.328	0.835
	High	263	0.068	0.246	0.927	473	-0.015	0.5	0.832
Shoulder Longitudinal Cracking	Low	239	0.03	0.372	0.683	840	0.024	0.355	0.582
	Med	538	0.032	0.395	0.729	797	-0.001	0.446	0.644
	High	256	0.056	0.369	0.622	408	0.072	0.361	0.685
Shoulder Alligator Cracking	Low	5	0.039	0.282	0.99	32	0.098	0.264	0.44
	Med	9	0.113	0.189	0.734	7	0.087	0.233	0.816
	High	17	0.087	0.254	0.823	15	0.078	0.238	0.766
Transverse Spall Cracking	Low	180	0.14	0.154	0.508	1380	0.099	0.265	0.358
	Med	46	0.133	0.154	0.361	955	0.104	0.2	0.748
	High	26	0.166	0.11	0.457	161	0.103	0.168	0.787

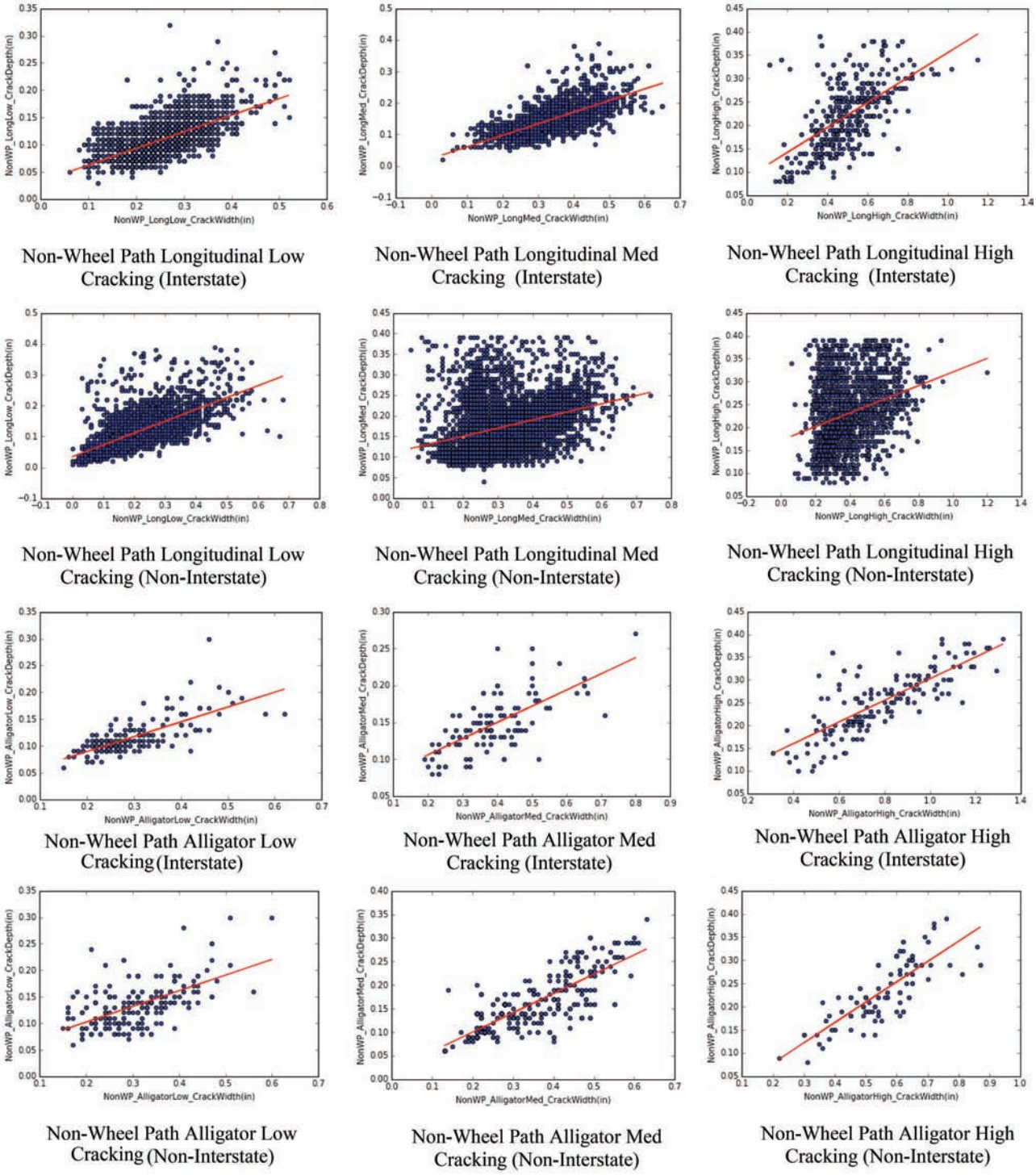

Figure 6.1 Actual observations versus preliminary fitted curve. (*Figure continued on next page*)

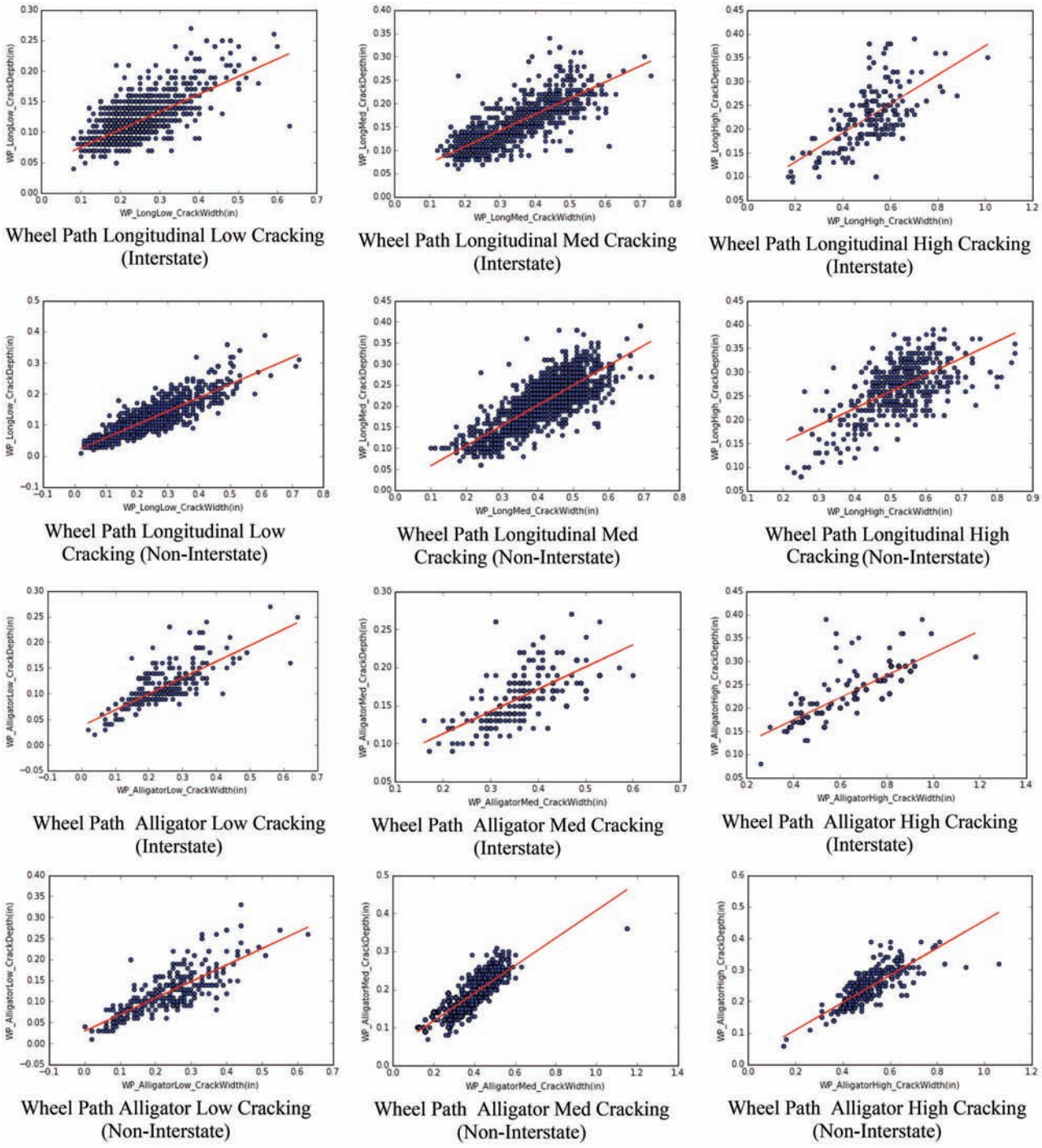

Figure 6.1 (Continued)

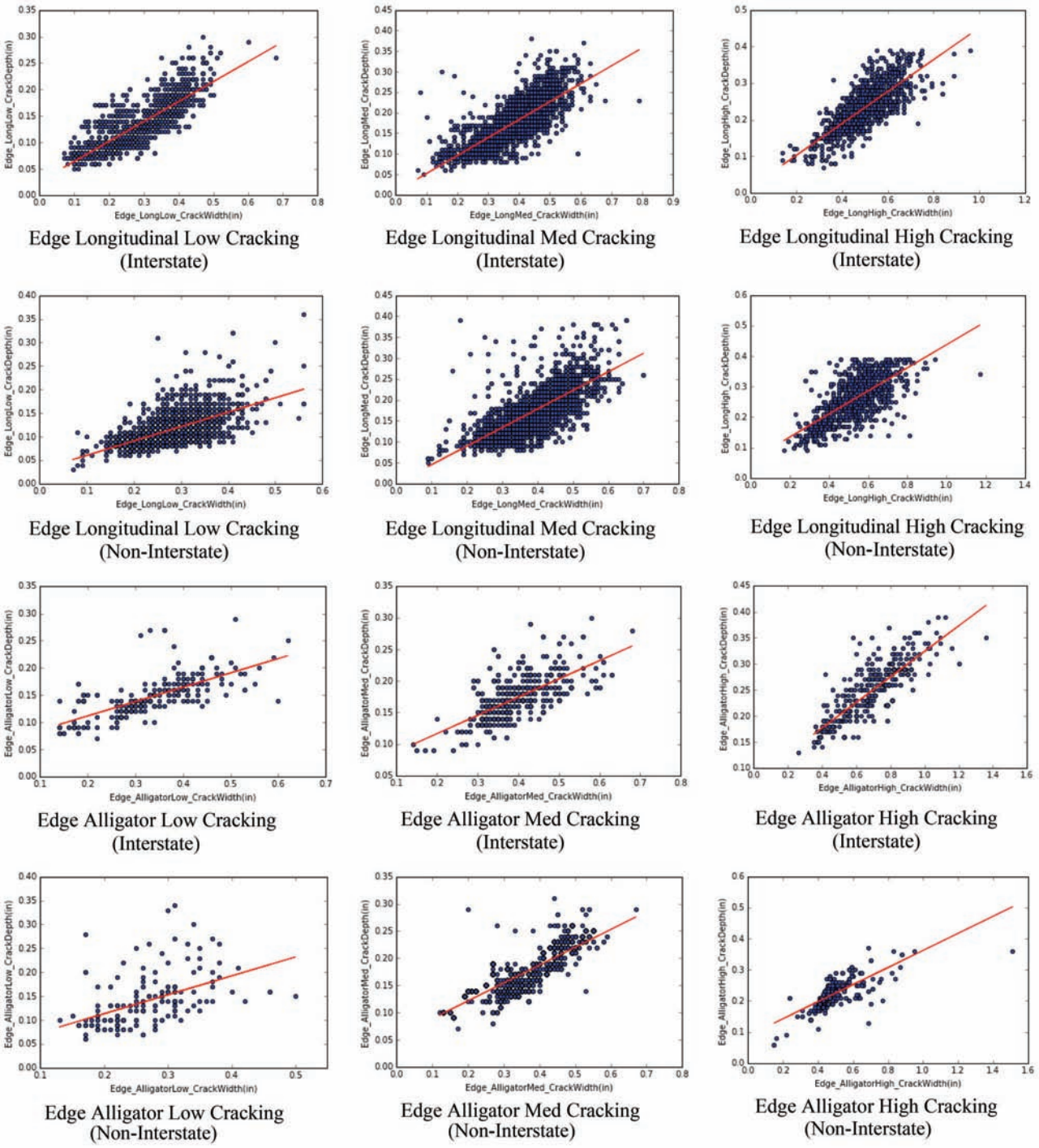

Figure 6.1 (Continued)

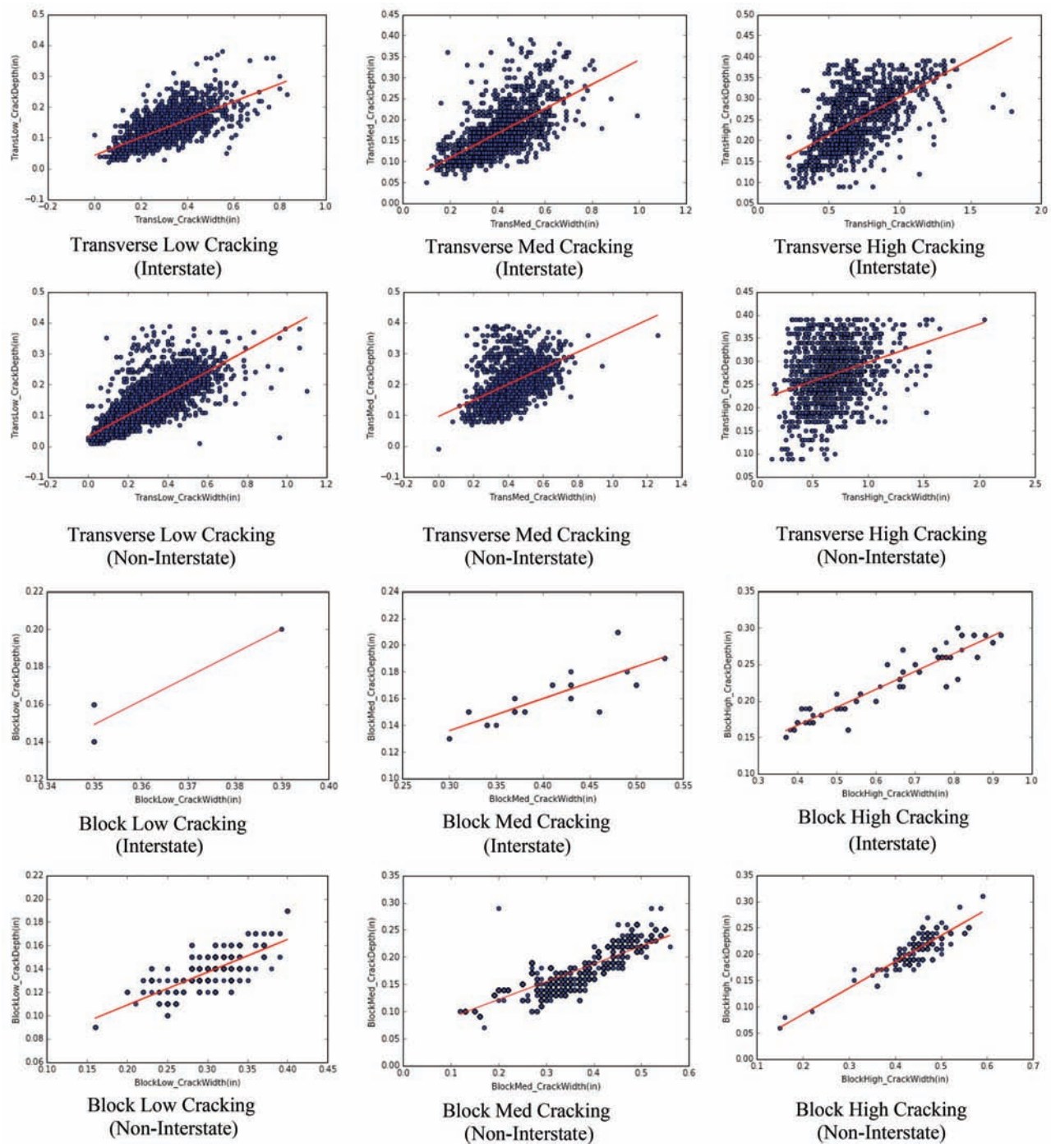

Figure 6.1 (Continued)

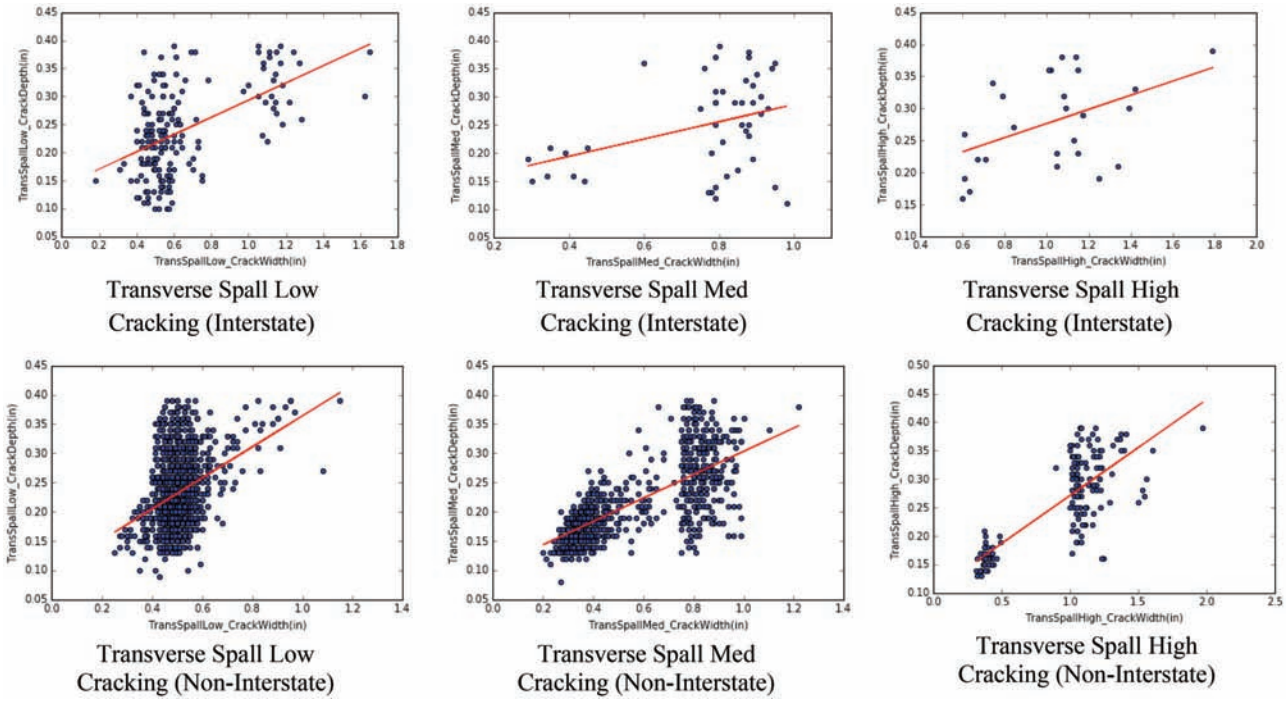

Figure 6.1 (Continued)

crack models are higher than 0.6, and only a few of the models have R^2 values below 0.5.

$$Crack\ Depth = a + b * Crack\ Width \qquad (6.1)$$

6.2 Correlation between Different Crack Types

In the initial analysis, we calculated the correlation coefficients between each pair of crack types that might be related to each other. For example, there might be some correlation between non-wheel path longitudinal cracks and non-wheel path alligator cracks. In the initial analysis, the correlation coefficient between the width and depth of the two variables was very small (for width: 0.087 at low severity, 0.086 at medium severity, 0.038 at high severity; for depth: 0.059 at low severity, 0.053 at medium severity, 0.022 at high severity).

However, if we remove the observations for which at least one of the two variables (non-wheel path longitudinal crack width/depth and non-wheel path alligator crack width/depth) is equal to zero, we find that some correlation does exist in the remaining observations between the two variables at some level of severity. Figures 6.2 and 6.3 illustrate that some relationships exist at the medium and high severity levels for crack width and at all three severity levels for crack depth. Although there is no relationship between the existence of two types of cracking, the crack width and crack depth of different types of cracking might be correlated to each other at some severity levels if the two cracking types occurred at the same location.

Therefore, focus was placed on the correlation between crack width and crack depth for two cracking types existing at the same location. Each pair of cracking types that are possibly correlated were analyzed. The results are summarized in the following sections, with only the models that have R^2 values (correlation coefficient between the widths/depths of two crack types) greater than 0.4 reported.

6.2.1 Non-Wheel Path Longitudinal Cracking versus Non-Wheel Path Alligator Cracking

The first pair of cracking types tested was non-wheel path longitudinal cracking and non-wheel path alligator cracking; the regression results are summarized in Table 6.2, and the correlations between the two types of cracking in terms of length and depth at three severity levels are shown in Figure 6.4. Some correlation (>0.4) was found between non-wheel path longitudinal cracking and non-wheel path alligator cracking except for low-severity crack depth. It was also found that the correlation coefficient is very high for high-severity crack depth, which means that when both non-wheel path longitudinal cracks and non-wheel path alligator cracks appear at the same location, the crack depths of the two cracking types are highly linearly correlated.

6.2.2 Wheel Path Longitudinal Cracking versus Wheel Path Alligator Cracking

Table 6.3 and Figure 6.5 show that a correlation (>0.4) only exists for crack width and crack depth at the high severity level, which means that in the intial

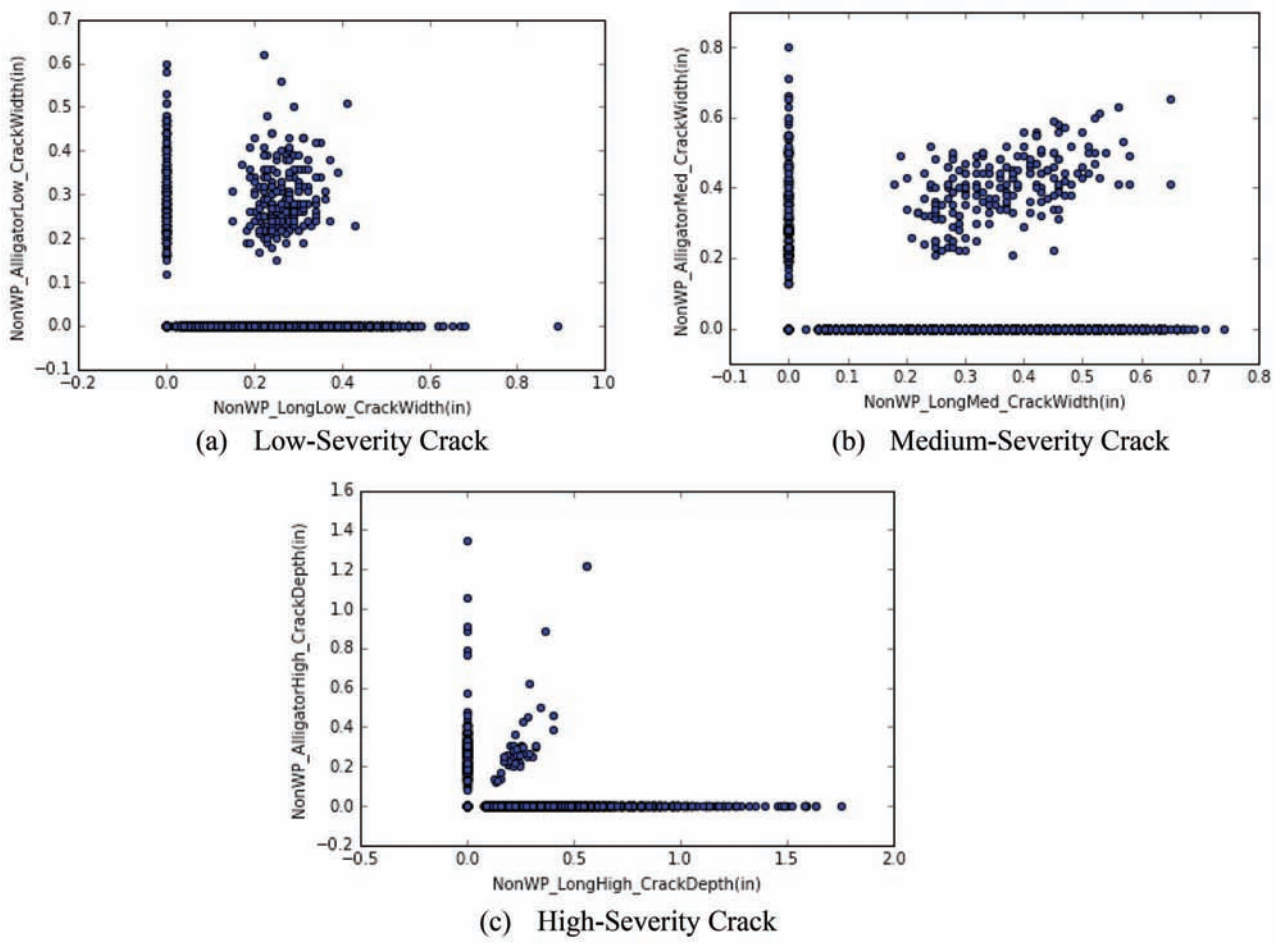

Figure 6.2 Scatter plots relating non-wheel path longitudinal crack width and non-wheel path alligator crack width.

stages (low and medium severity) the development of wheel path longitudinal cracking and wheel path alligator cracking are independent of each other. When the deterioration progresses into the high severity level, the development of the two cracking types starts to become increasingly related.

6.2.3 Edge Longitudinal Cracking versus Edge Alligator Cracking

Table 6.4 and Figure 6.6 show that edge longitudinal cracking and alligator cracking are only correlated at the low severity level, which means that the development of the two cracking types is related at the intial stage (low severity) but becomes increasingly uncorrelated as the cracks develop into the higher severity levels.

6.2.4 Shoulder Longitudinal Cracking versus Shoulder Alligator Cracking

As shown in Table 6.5 and Figure 6.7, shoulder longitudinal cracking and shoulder alligator cracking were found to be generally correlated at the low and high severity levels but uncorrelated at the medium severity level. It was also found that the correlation at the high severity level is very significant and much higher than the correlaiton at the low severity level. This means that at the intial stage of deterioration (low severity), the development of the two crack types is somewhat related and becomes less correlated when the cracks progress into the medium severity level. However, as the deterioration continues, the development of the two crack types starts to be highly correlated again at the high severity level.

6.2.5 Block Cracking versus Transverse Cracking

The correlation seen in Table 6.6 and Figure 6.8 is similar to that found for shoulder longitudinal cracking and shoulder alligator cracking. Block cracking and transverse cracking were found to be related to each other at the low and high severity levels but not at the medium severity level, and the correlation coefficient at high severity level is very high.

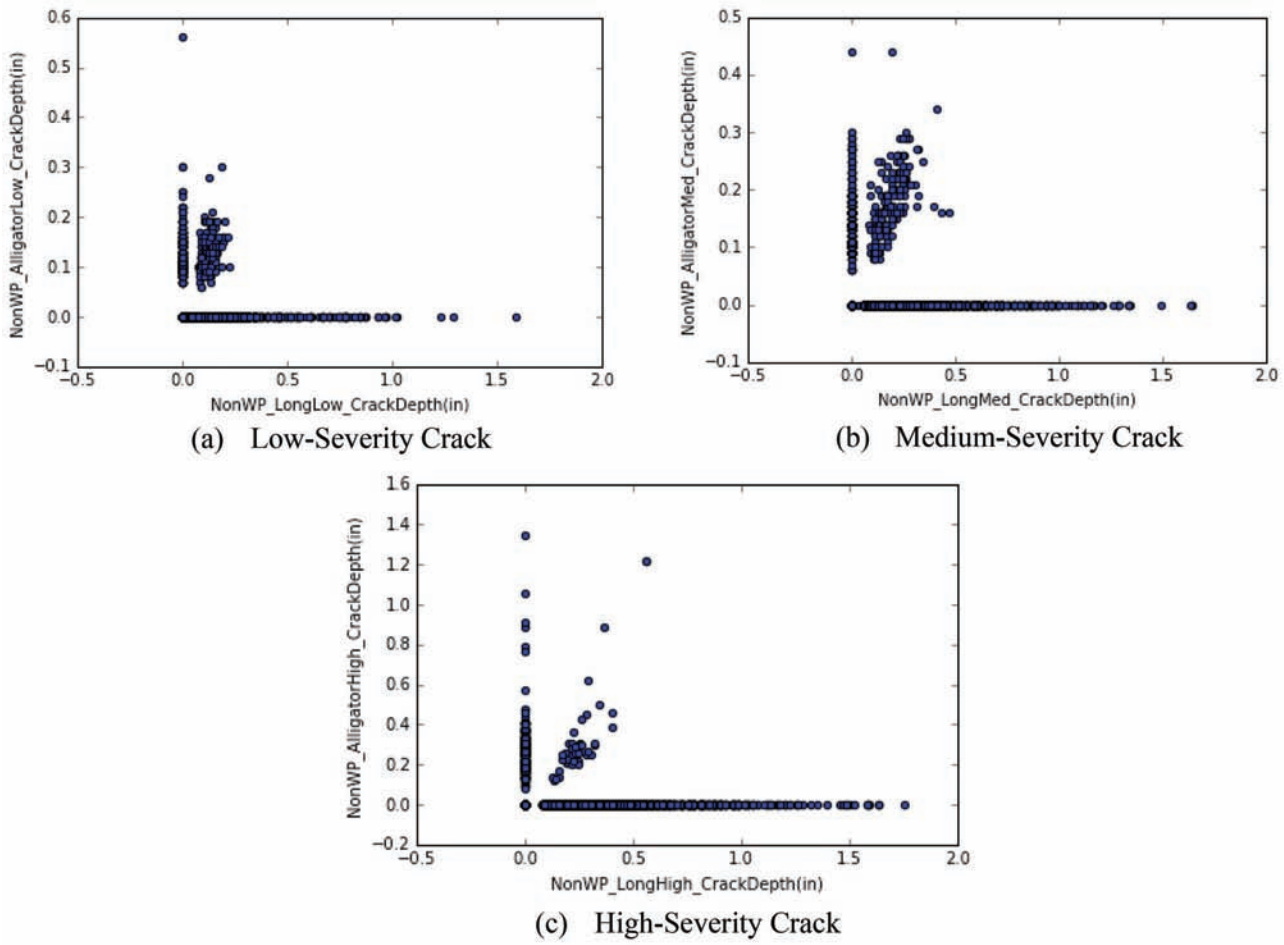

Figure 6.3 Scatter plots relating non-wheel path longitudinal crack depth and non-wheel path alligator crack depth.

TABLE 6.2
Regression Results between Non-Wheel Path longitudinal Cracking and Non-Wheel Path Alligator Cracking

X variable	Y variable	obs	a	b	R^2
Non-Wheel Path longitudinal Med Crack Width	Non-Wheel Path Alligator Med Crack Width	200	0.232	0.48	0.514
Non-Wheel Path longitudinal High Crack Width	Non-Wheel Path Alligator Med Crack High	47	0.34	0.717	0.494
Non-Wheel Path longitudinal Low Crack Depth	Non-Wheel Path Alligator Low Crack Depth	207	0.056	0.556	0.433
Non-Wheel Path longitudinal Med Crack Depth	Non-Wheel Path Alligator Med Crack Depth	200	0.078	0.534	0.62
Non-Wheel Path longitudinal High Crack Depth	Non-Wheel Path Alligator Med Crack Depth	47	-0.203	2.148	0.869

6.2.6 Block Cracking versus Non-Wheel Path and Wheel Path Longitudinal/Alligator Cracking

We also analyzed the correlations between block cracking and non-wheel path and wheel path longitudinal or alligator cracking. The results of significant pairs are summarized in Table 6.7 and Figures 6.9, 6.10, and 6.11.

6.2.7 Transverse Cracking versus Non-Wheel Path and Wheel Path Longitudinal/Alligator Cracking

Finally, the correlations between transverse cracking and non-wheel path and wheel path longitudinal or alligator cracking were analyzed. The results are summarized in Table 6.8 and Figures 6.12, 6.13, and 6.14.

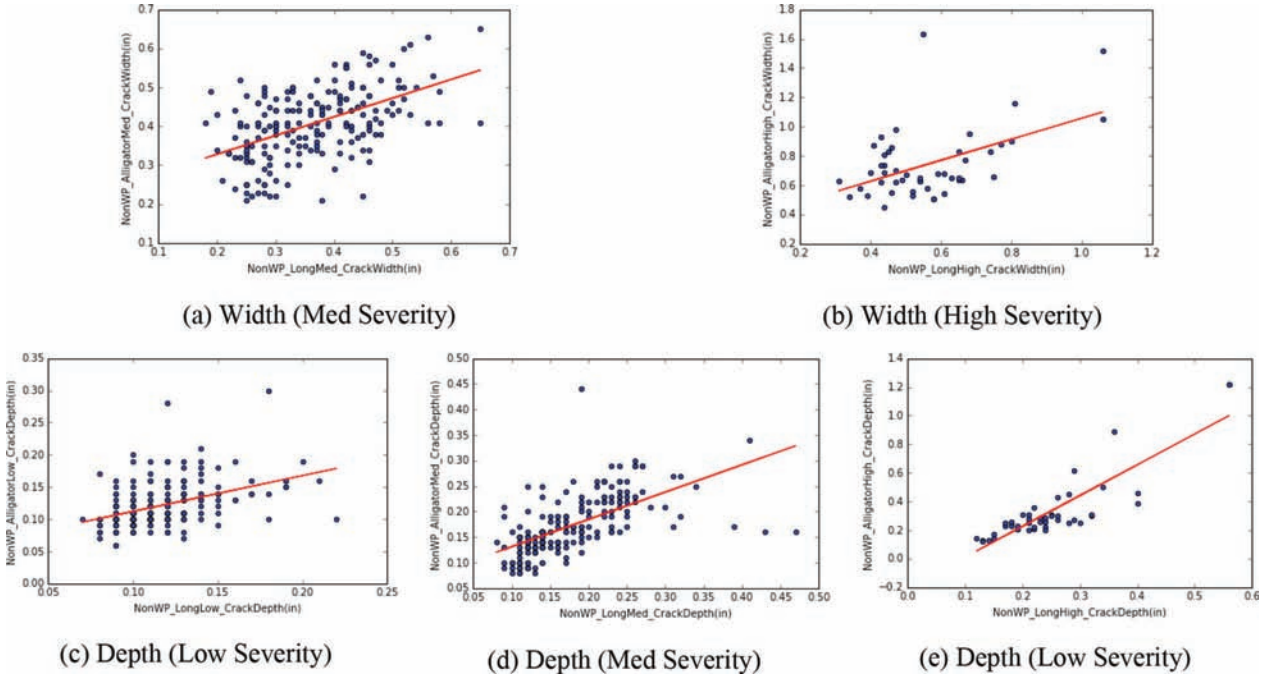

Figure 6.4 Correlation between non-wheel path longitudinal cracking and non-wheel path alligator cracking.

TABLE 6.3
Regression Results between Wheel Path longitudinal Cracking and Wheel Path Alligator Cracking

X variable	Y variable	obs	a	b	R^2
Shoulder longitudinal High Crack Width	Shoulder Alligator Med Crack High	109	0.308	0.48	0.405
Shoulder longitudinal High Crack Depth	Shoulder Alligator Med Crack Depth	109	0.151	0.437	0.301

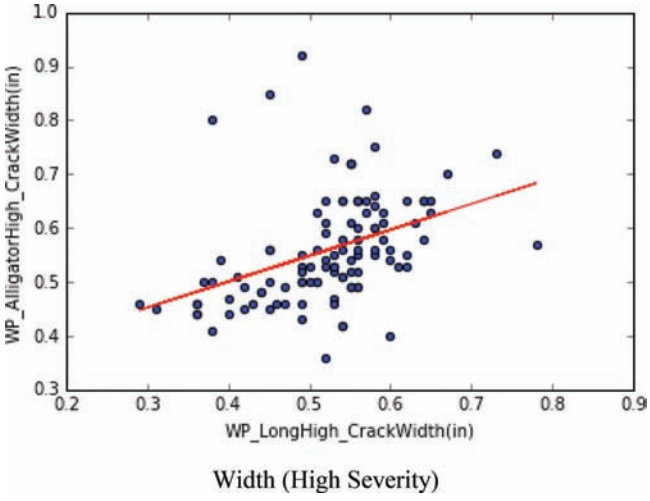

Figure 6.5 Correlation between wheel path longitudinal cracking and wheel path alligator cracking.

TABLE 6.4
Regression Results between Edge longitudinal Cracking and Edge Alligator Cracking

X variable	Y variable	obs	a	b	R^2 (corr)
Edge longitudinal Low Crack Width	Edge Alligator Low Crack High	153	0.069	0.578	0.467

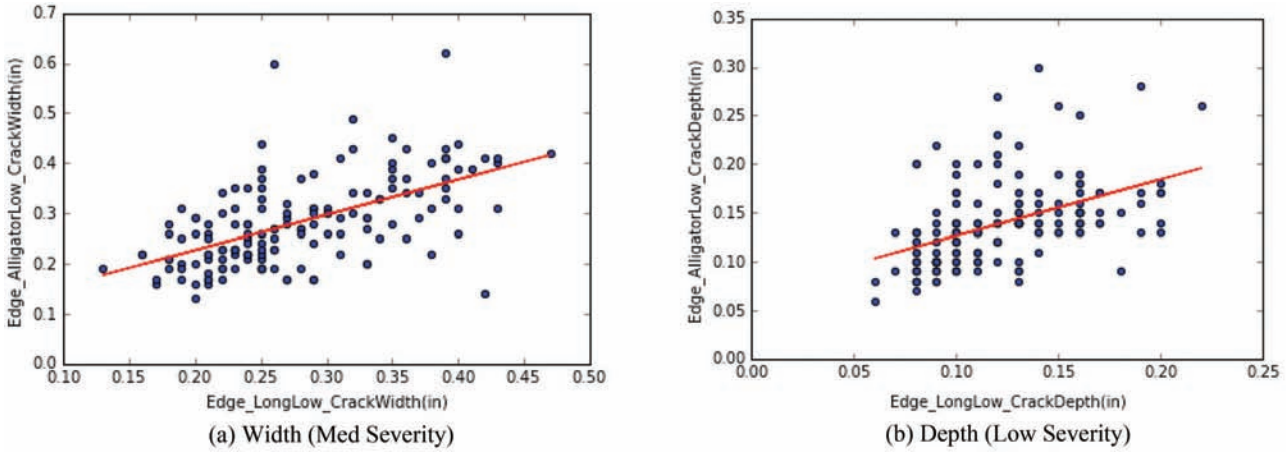

Figure 6.6 Correlation between edge longitudinal cracking and edge alligator cracking.

TABLE 6.5
Regression Results between Shoulder longitudinal Cracking and Shoulder Alligator Cracking

X variable	Y variable	obs	a	b	R^2 (corr)
Shoulder longitudinal Low Crack Width	Shoulder Alligator Low Crack Width	9	0.113	0.694	0.603
Shoulder longitudinal High Crack Width	Shoulder Alligator Med Crack High	14	0.231	0.789	0.758
Shoulder longitudinal High Crack Depth	Shoulder Alligator Med Crack Depth	14	-0.502	3.451	0.885

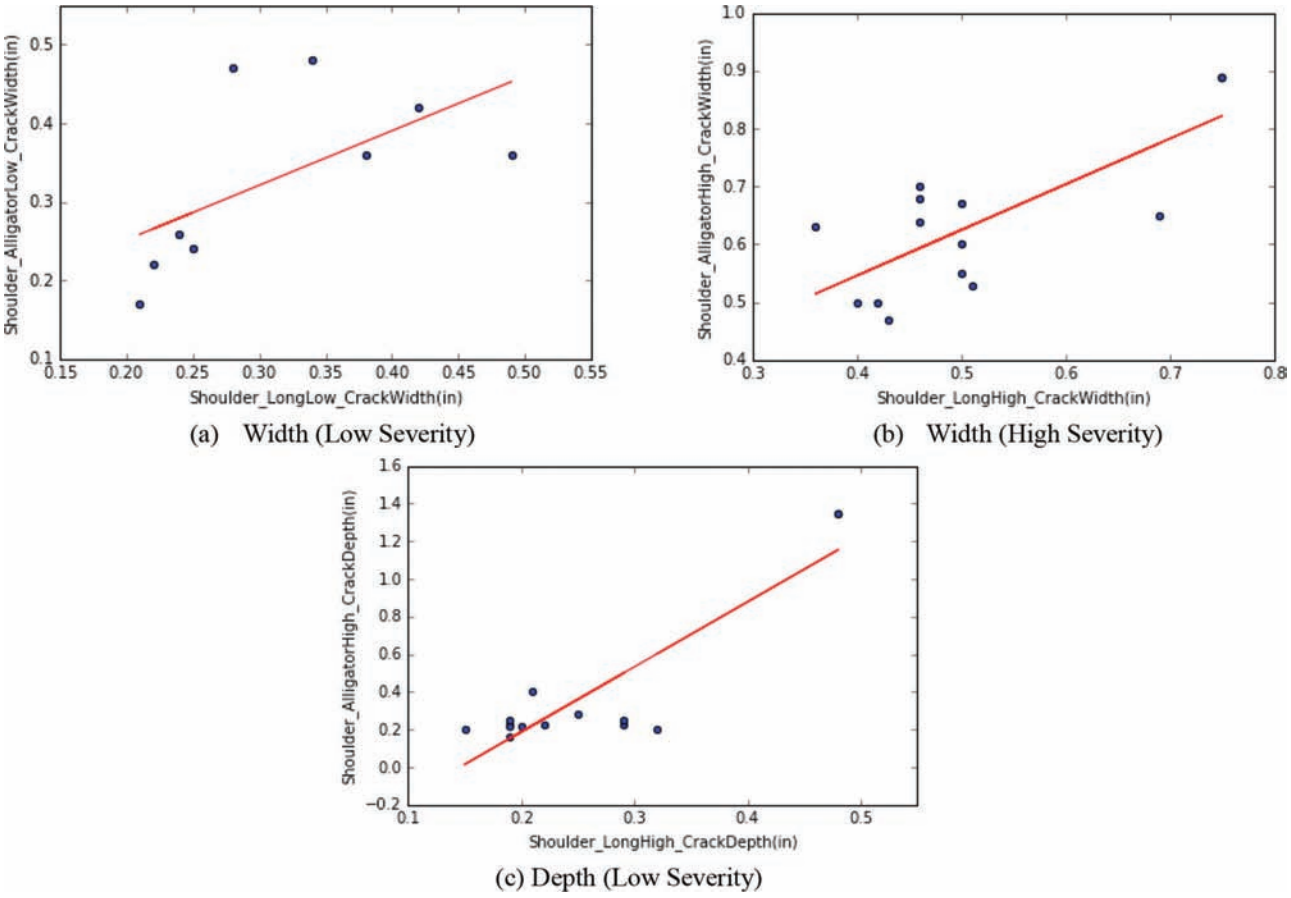

Figure 6.7 Correlation between shoulder longitudinal cracking and shoulder alligator cracking.

TABLE 6.6
Correlation between Block Cracking and Transverse Cracking

X variable	Y variable	obs	a	b	R^2 (corr)
Block Low Crack Width	Transverse Low Crack Width	50	0.124	0.648	0.451
Block High Crack Width	Transverse High Crack Width	16	0.294	0.746	0.659
Block High Crack Depth	Transverse High Crack Depth	16	0.053	0.837	0.612

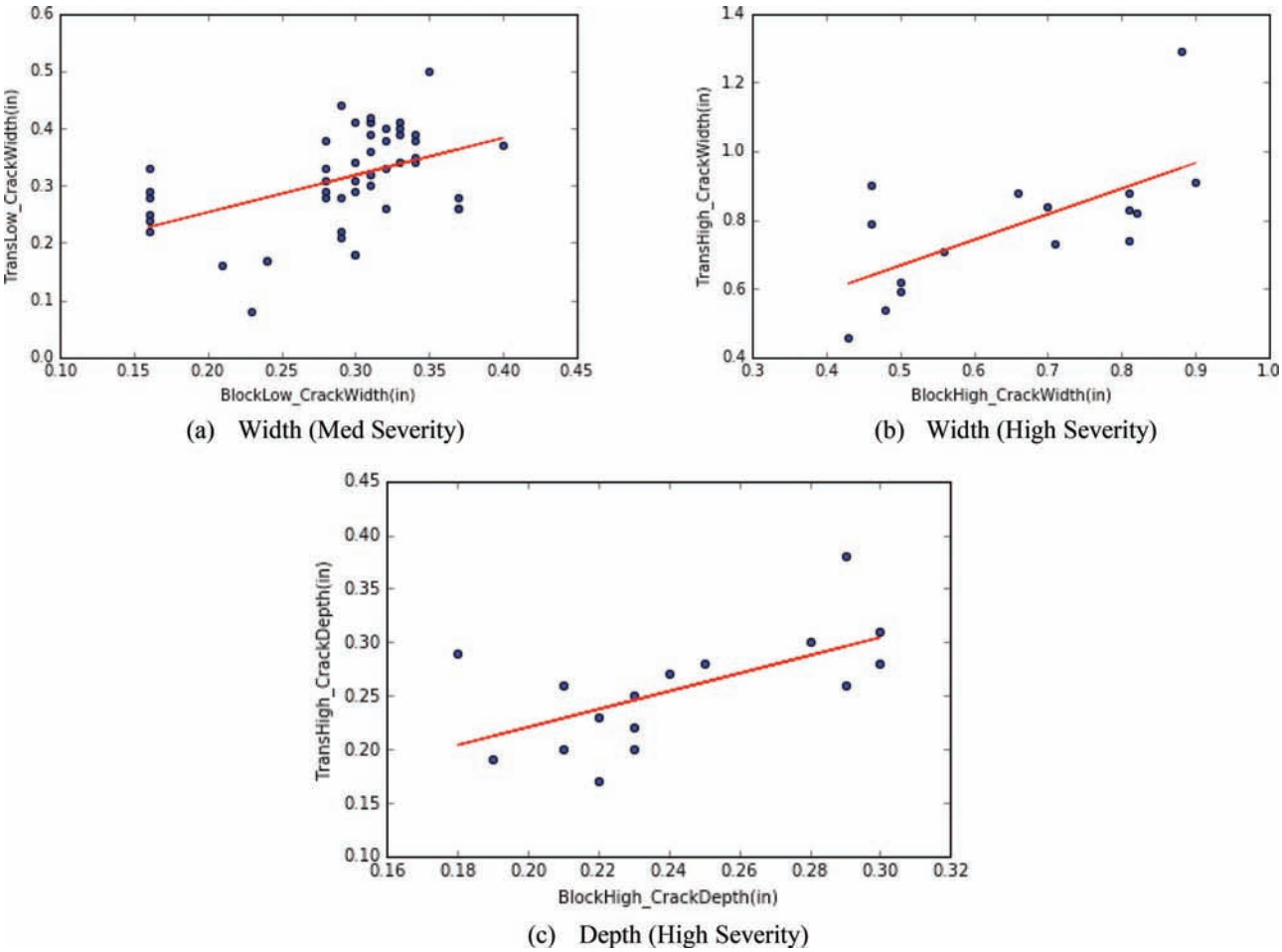

Figure 6.8 Correlation between block cracking and transverse cracking.

TABLE 6.7
Correlation between Block Cracking, Non-Wheel Path Longitudinal/Alligator Cracking, and Wheel Path Alligator Cracking

X variable	Y variable	obs	a	b	R^2 (corr)
Block High Crack Width	Wheel Path Alligator High Crack Width	87	0.012	1.226	0.611
Block High Crack Depth	Wheel Path Alligator High Crack Depth	100	0.026	1.244	0.559
Block Low Crack Width	Non-Wheel Path Alligator Low Crack Width	13	-0.152	1.436	0.808
Block High Crack Width	Non-Wheel Path Alligator High Crack Width	41	0.143	1.023	0.584
Block Low Crack Depth	Non-Wheel Path Alligator Low Crack Depth	13	0.017	0.803	0.451
Block High Crack Depth	Non-Wheel Path Alligator High Crack Depth	41	0.069	0.935	0.353
Block Med Crack Width	Non-Wheel Path longitudinal Low Crack Width	116	0.167	0.326	0.337
Block High Crack Width	Non-Wheel Path longitudinal High Crack Width	38	0.318	0.405	0.441
Block Med Crack Depth	Non-Wheel Path longitudinal Low Crack Depth	116	0.06	0.481	0.447
Block High Crack Depth	Non-Wheel Path longitudinal High Crack Depth	38	0.086	0.728	0.4

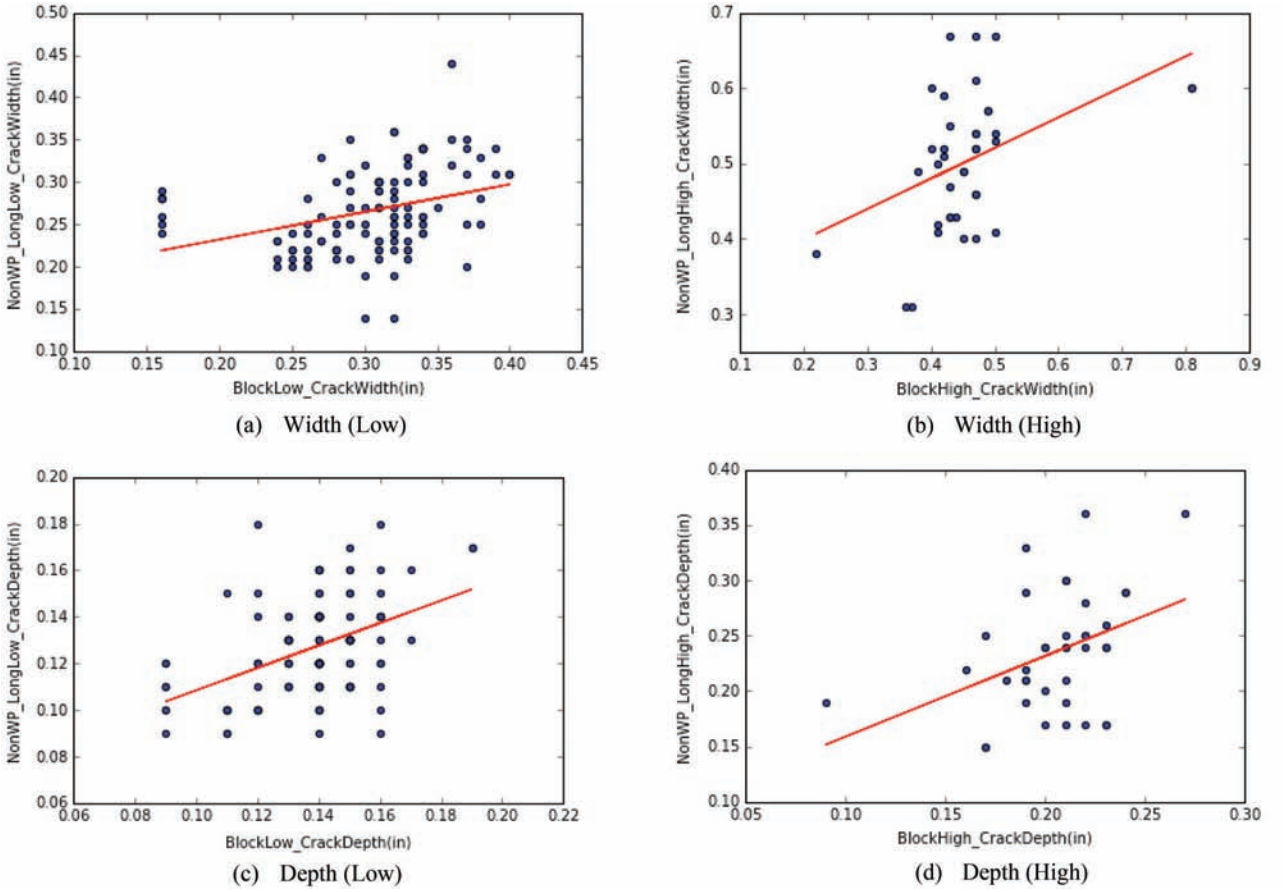

Figure 6.9 Correlation between block cracking and non-wheel path longitudinal cracking.

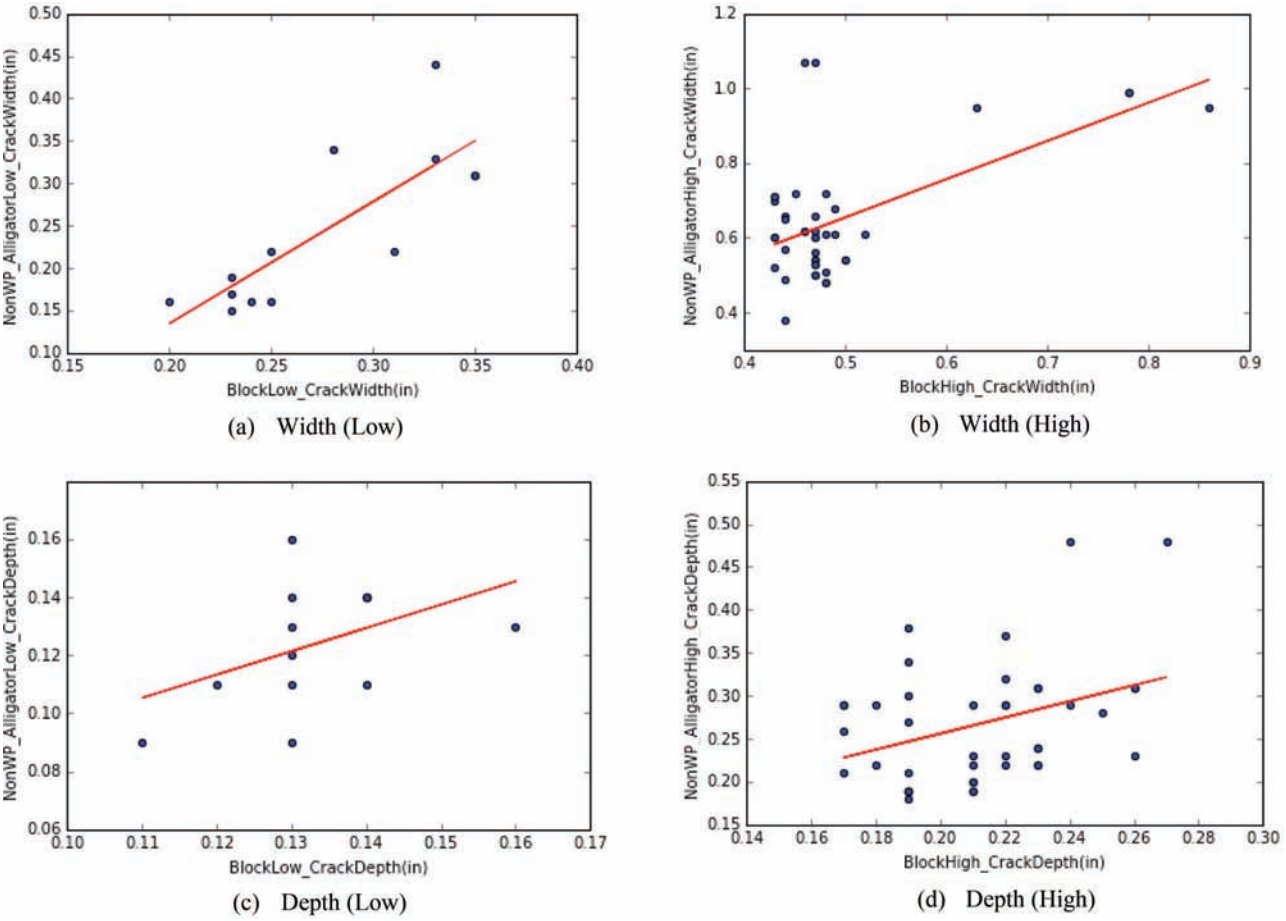

Figure 6.10 Correlation between block cracking and non-wheel path alligator cracking.

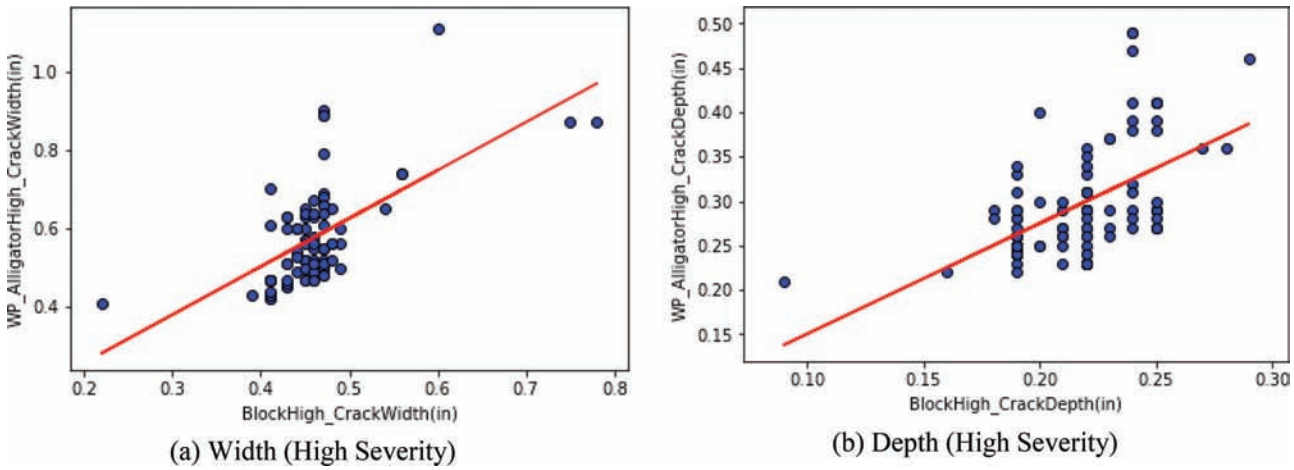

Figure 6.11 Correlation between block cracking and wheel path alligator cracking.

TABLE 6.8
Regression Results for Transverse Cracking, Wheel Path Longitudinal Cracking, and Wheel Path Longitudinal/Alligator Cracking

X variable	Y variable	obs	a	b	R^2
Transverse Low Crack Width	Non-Wheel Path Alligator Low Crack Width	214	0.161	0.44	0.473
Transverse Med Crack Width	Non-Wheel Path Alligator Med Crack Width	94	0.257	0.37	0.413
Transverse High Crack Width	Non-Wheel Path Alligator High Crack Width	97	0.343	0.527	0.555
Transverse High Crack Depth	Non-Wheel Path Alligator High Crack Depth	97	0.068	0.809	0.459
Transverse High Crack Width	Wheel Path Alligator High Crack Width	154	0.215	0.52	0.648
Transverse High Crack Depth	Wheel Path Alligator High Crack Depth	154	0.159	0.45	0.481
Transverse Low Crack Width	Wheel Path longitudinal Low Crack Width	1446	0.126	0.377	0.479
Transverse Med Crack Width	Wheel Path longitudinal Med Crack Width	854	0.242	0.321	0.422
Transverse Low Crack Depth	Wheel Path longitudinal Low Crack Depth	1446	0.055	0.495	0.554
Transverse Med Crack Depth	Wheel Path longitudinal Med Crack Depth	854	0.118	0.417	0.478

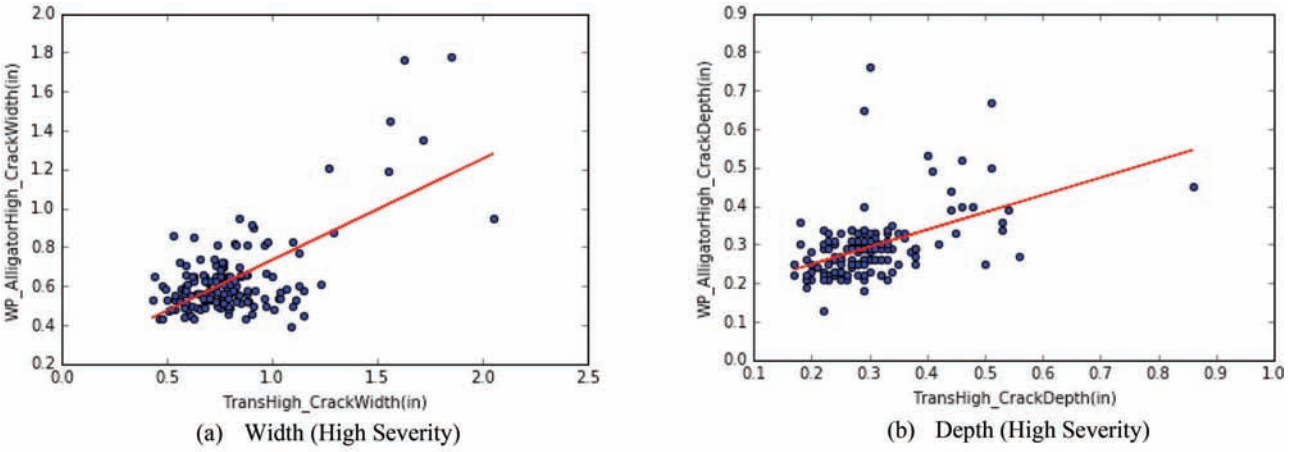

Figure 6.12 Correlation between transverse cracking and wheel path alligator cracking.

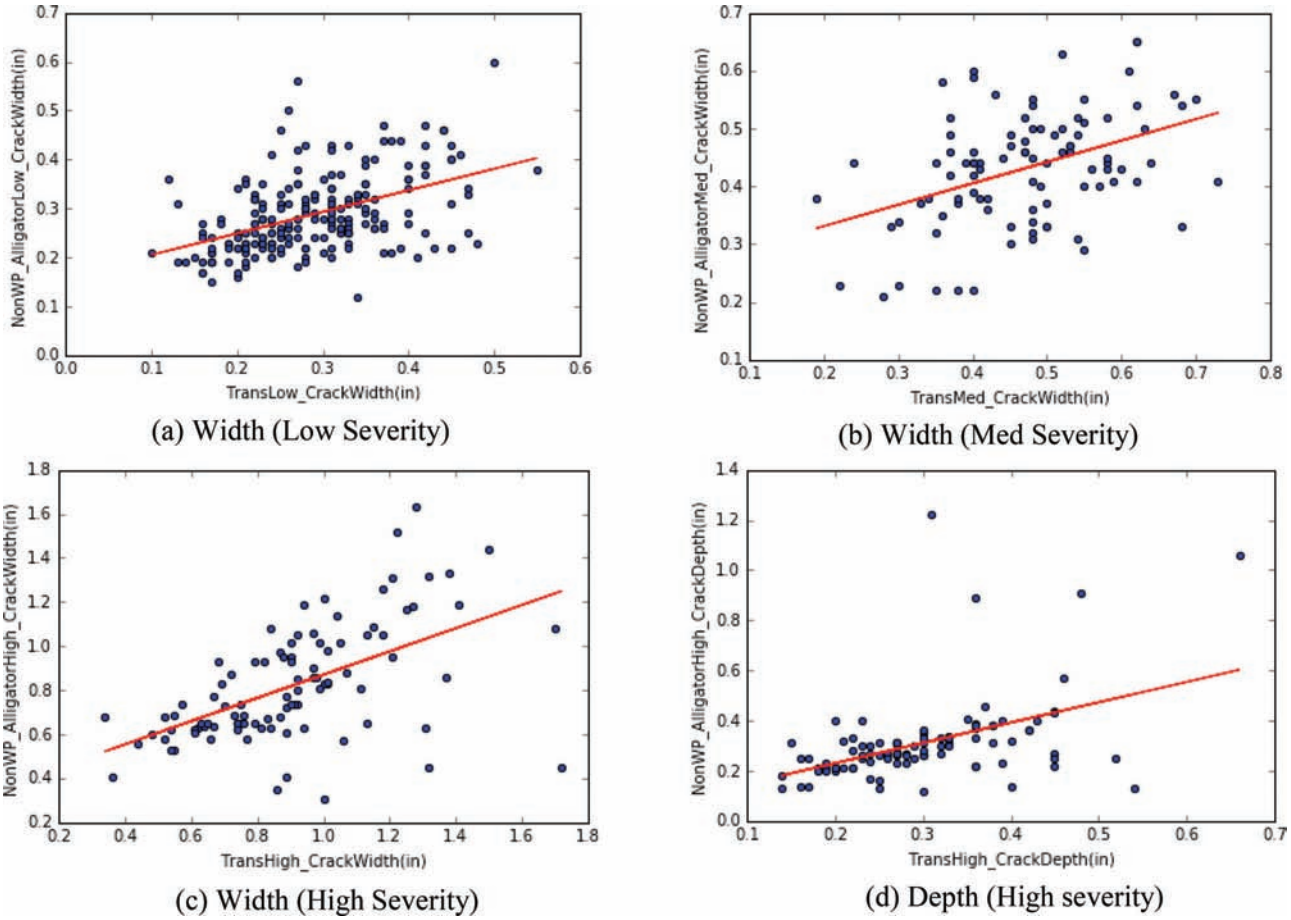

Figure 6.13 Correlation between transverse cracking and non-wheel path alligator cracking.

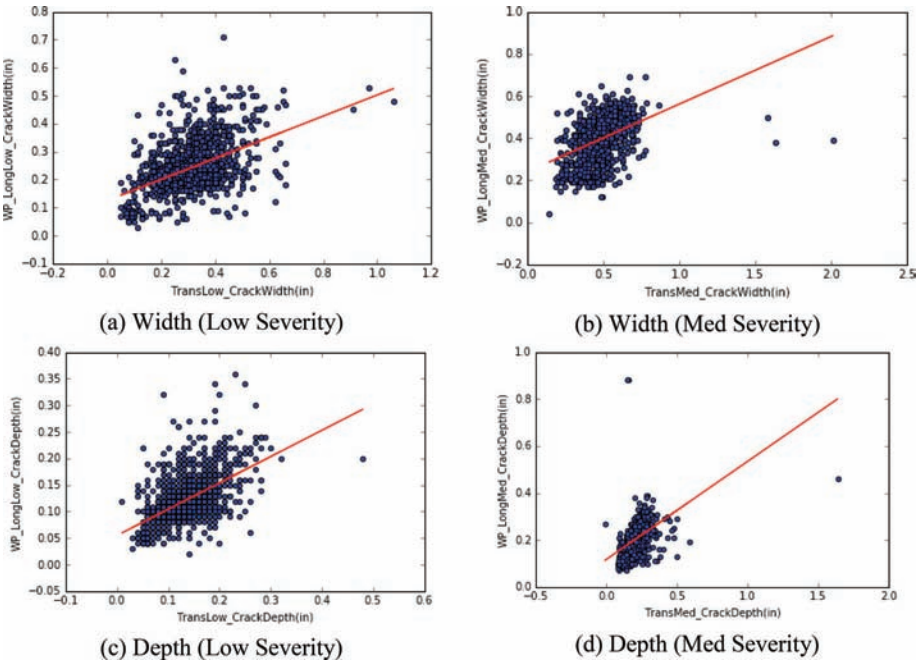

Figure 6.14 Correlation between transverse cracking and wheel path longitudinal cracking.

6.3 Relationship between IRI and Pavement Cracking

Collecting distress data is useful for highway management. The use of both IRI and specific distress types can provide a more justifiable set of prescriptions for a distressed pavement. However, distress data collection for an entire state network can be challenging. If it can be proven that IRI adequately reflects the pavement cracking conditions and that there is a strong relationship between IRI and certain pavement distresses, then the easily measurable IRI can serve as a valuable basis to estimate the distress levels for pavements on the state highway network. In this study, the relationship model between IRI and pavement cracking was developed in two ways: (1) building a probability model of the existence of certain types of pavement cracking with IRI as the independent variable and (2) predicting the IRI of a pavement segment given the data for other pavement distresses using machine learning methods.

6.3.1 Probability Model for the Existence of Cracking

Although no significant correlation was found between IRI and pavement cracking when the correlation coefficients between IRI and cracking width or depth for certain crack types were calculated directly, we found some relationships between IRI and the probability of the occurrence of pavement cracking at each severity level. This could be because pavement roughness (IRI) is typically higher for a pavement that has some cracks compared to those without cracks. However, IRI does not necessarily increase as cracking depth or width increases.

To calculate the probability of the occurrence of certain types of cracking for different IRI values, we count the number of pavement segments within a certain range of IRI values divided by the total number of pavement segments within the same range of IRI values. For example, if 50 pavement segments out of 1,000 total segments in an IRI range of 80 to 100 in/mi have low-severity longitudinal cracking in the wheel path, the probability of the occurrence of longitudinal cracking at a low level of severity is 0.05, given that the IRI is between 80 and 100 in/mi. The general form for calculating this probability is given in Equation 6.2.

$$P(x_{i,width} > 0 | I_1 < IRI \leqslant I_2) = \frac{N_{x_i, I_1 \leqslant IRI < I_2}}{N_{T, I_1 \leqslant IRI < I_2}} \quad (6.2)$$

where $x_{i,width}$ indicates the width of pavement cracking i, I_1 and I_2 are the lower and upper bounds of the given range of IRI, $N_{T,\, I_1 < IRI \leqslant I_2}$ is the total number of pavement segments within the IRI range of I_1 to I_2, $N_{x_i,\, I_1 < IRI \leqslant I_2}$, is the number of pavement segments that exhibit cracking type i and are in the IRI range of I_1 to I_2.

The IRI range (from I_1 to I_2) of 20 in/mi was chosen for this study. To avoid large variations and make the estimated probability distribution more reliable, we only keep the calculated probability of the occurrence of cracking within a certain IRI range if the number of observations (segments) within the given IRI range is greater than a preset lower bound value so that the variation can be controlled within a reasonable range. For example, assume there is only one pavement segment within a certain range of IRI. If the IRI of this segment is very high but there is no cracking on the pavement, then the probability of the existence of this type of cracking is 0 in the given range of IRI. This can lead to biased results because the sample is not large enough to represent the true population. The lower

bound value, which represents the minimum number of samples used in this study, is 30.

The proposed methodology was applied to all types of cracking at different severity levels. Figure 6.15 presents an example of the developed probability distribution for low-severity non-wheel path longitudinal cracking. It was observed that the probability of the existence of low-severity cracking increases sharply at the early stages as IRI increases, but the probability then decreases continuously after IRI reaches a certain value. The probability of medium-severity cracking follows a similar pattern, but the probability reaches its peak at a higher IRI value (around 220 in/mi) and has a slightly slower increase and significantly slower decrease rate. The probability of high-severity cracking increases continuously as IRI increases. The probability of no cracking continuously decreases as IRI increases. These patterns are expected because cracking usually starts at a low severity level and develops into medium and high severity levels at later stages. This pattern was found for most of the cracking types analyzed in this study. The probability distribution of each cracking type can be found in Figure 6.16.

Building regression models for the probability curves using Gaussian distribution. The probability curves developed in the previous section describe the actual data. However, without a generalized equation, it is difficult to use these distribution plots directly in practice. Moreover, we want to remove variations in the data by smoothing the curves. Therefore, in this section, we identify the most appropriate functional forms to fit these curves using the regression method.

To capture the characteristics of the probability curves described in the previous section, a skewed Gaussian distribution was used. The Gaussian equation is given in Equation 6.3:

$$P(x) = \beta_3 + \frac{\beta_2}{\beta_1 * \sqrt{2\pi}}\ exp(-\frac{(x-\beta_0)^2}{2{\beta_1}^2}) \qquad (6.3)$$

where x is the IRI; P(x) is the probability of a crack appearing in a pavement segment with certain x; β_0, β_1, β_2, β_3 are the parameters to be estimated.

Table 6.9 summarizes the regression results of curve fitting using the Gaussian equation. Because the distributions of the estimated probability are somewhat skewed, log-transformation was applied on the independent variable (IRI) before the regression modeling. The R^2 values for most models are very high (greater than 0.9), which means that the developed models fit the curves very well. The probability distributions for all cracking types as well as the curves fitting the regression

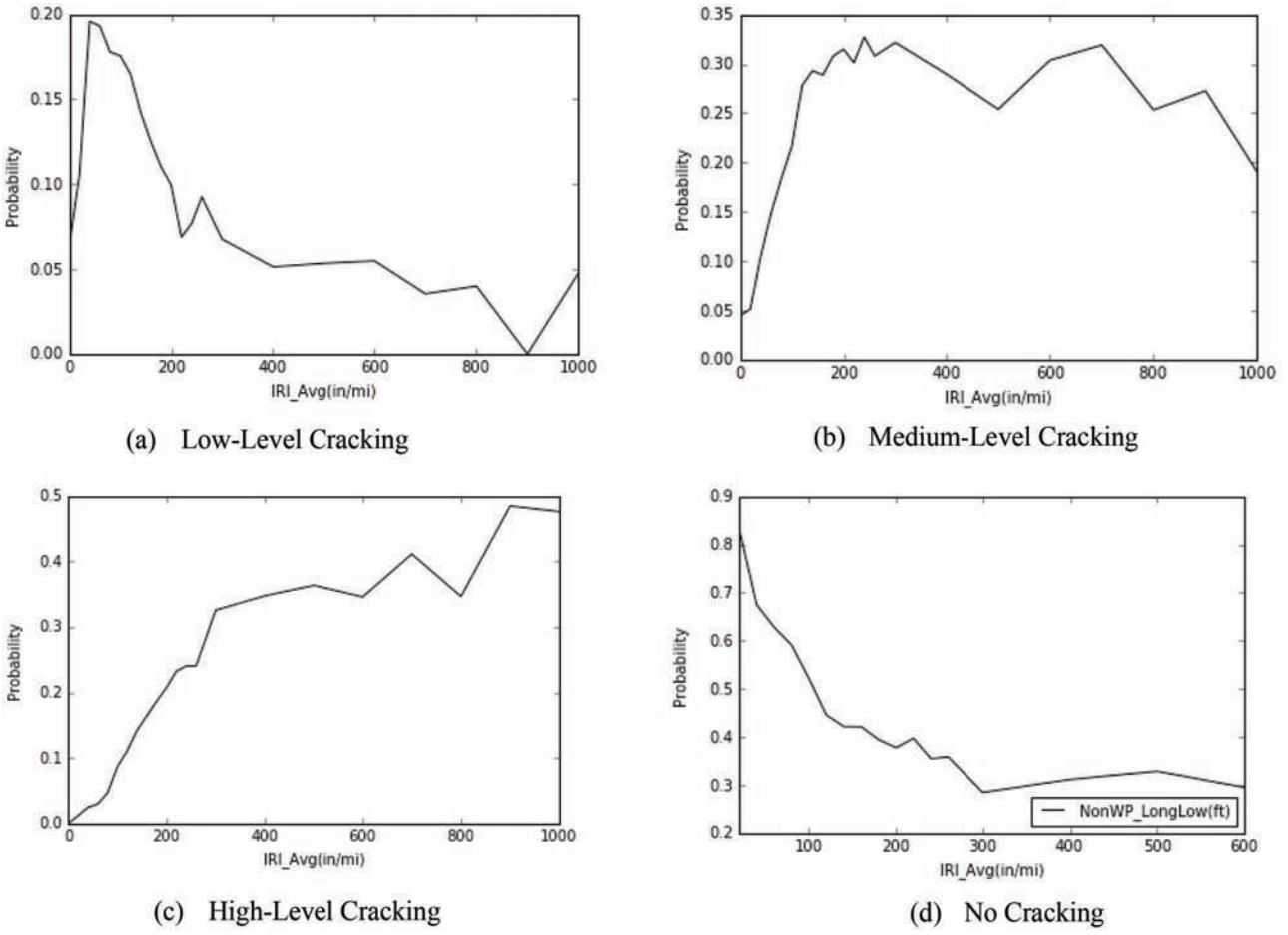

Figure 6.15 Probability distribution of non-wheel path cracking under different IRI values.

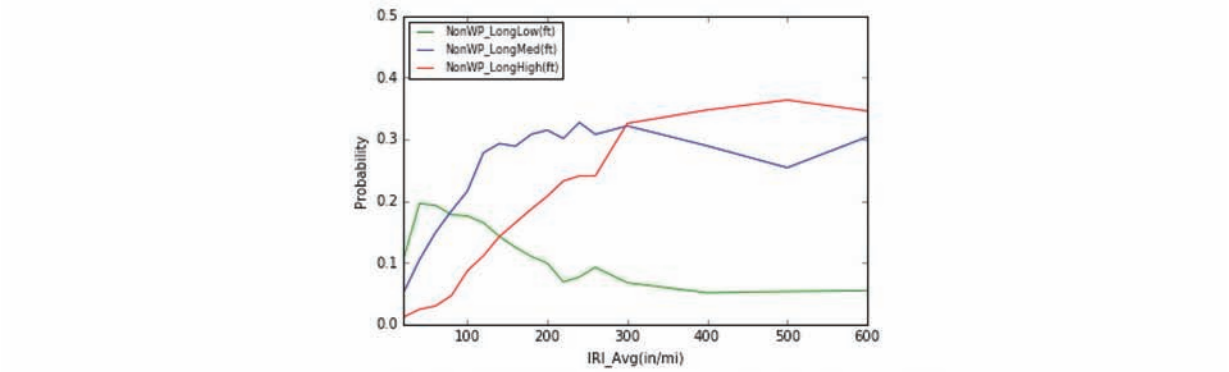

(a) Probability Distribution of Non-Wheel Path Longitudinal Cracking

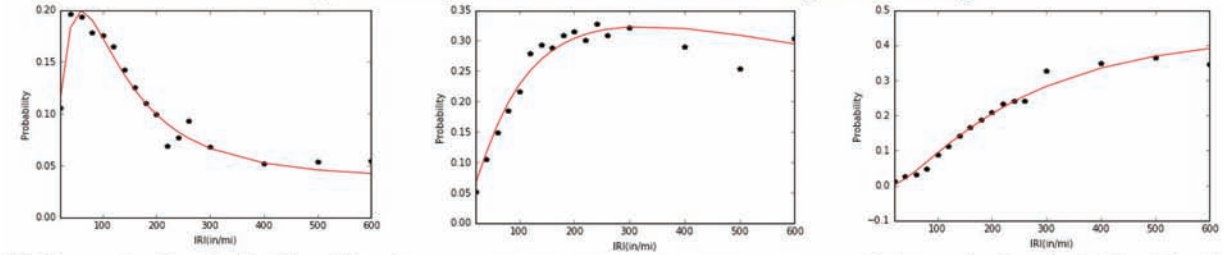

(b) Regression Results for Non-Wheel Path Longitudinal Low Cracking

(c) Regression Results for Non-Wheel Path Longitudinal Med Cracking

(d) Regression Results for Non-Wheel Path Longitudinal High Cracking

i. Modeling Results for Non-Wheel Path Longitudinal Cracking

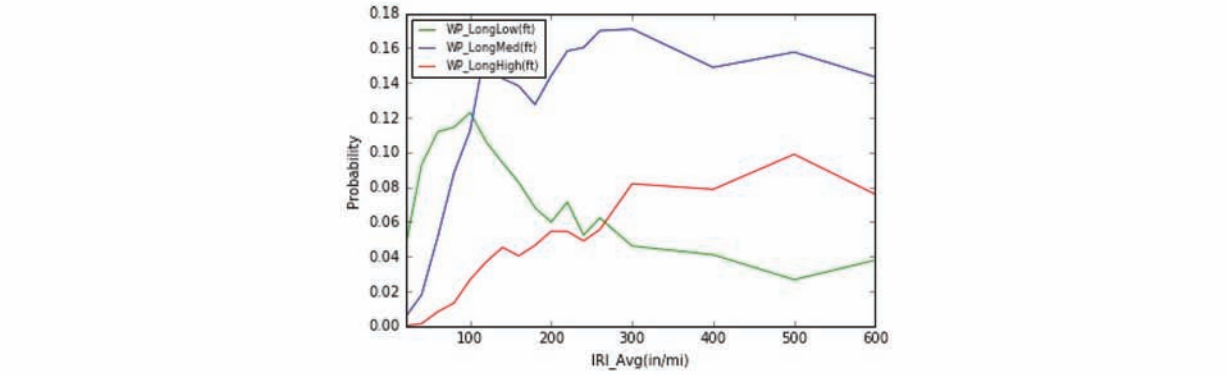

(a) Probability Distribution of Wheel Path Longitudinal Cracking

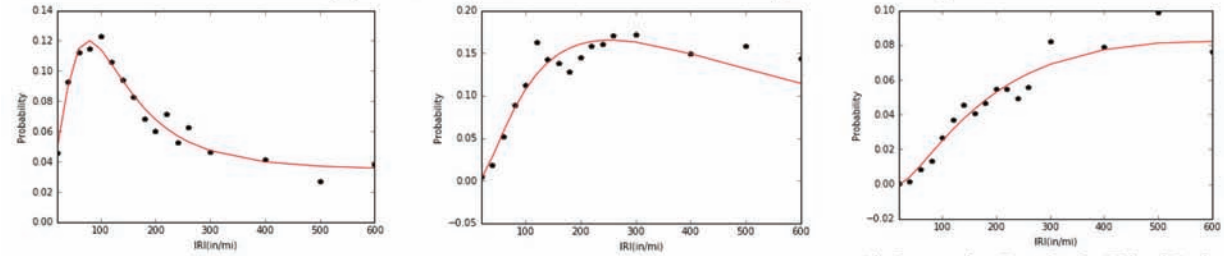

(b) Regression Results for Wheel Path Longitudinal Low Cracking

(c) Regression Results for Wheel Path Longitudinal Med Cracking

(d) Regression Results for Wheel Path Longitudinal High Cracking

ii. Modeling Results for Wheel Path Longitudinal Cracking

Figure 6.16 Probability distribution of pavement distresses for different IRI and curve fitting regression results. (*Figure continued on next page*)

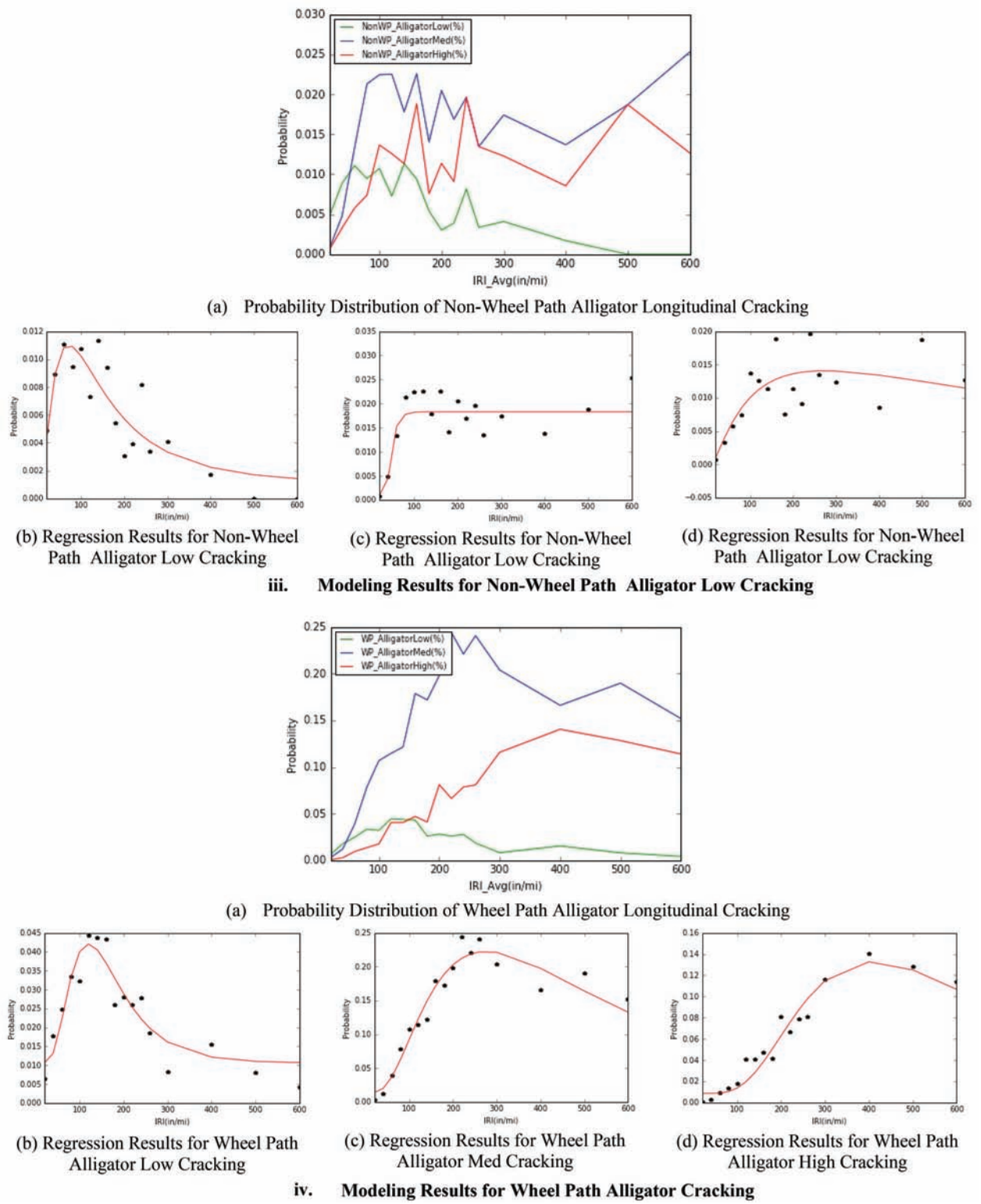

Figure 6.16 (Continued)

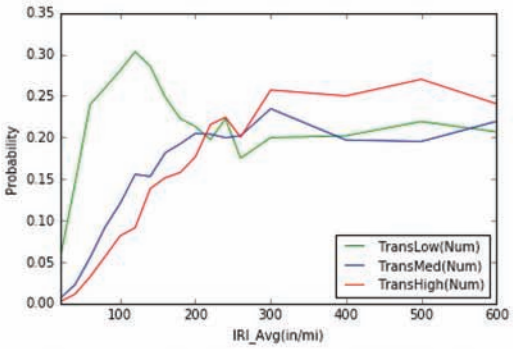

(a) Probability Distribution of Transverse Cracking

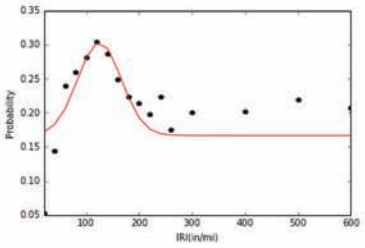

(b) Regression Results for Transverse Low Cracking

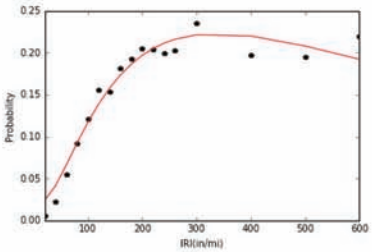

(c) Regression Results for Transverse Med Cracking

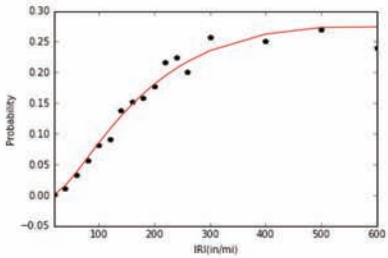

(d) Regression Results for Transverse High Cracking

v. **Modeling Results for Transverse Cracking**

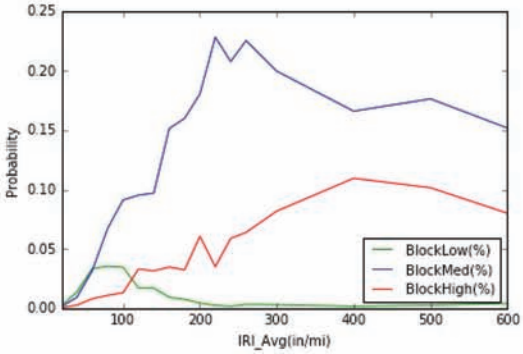

(a) Probability Distribution of Block Cracking

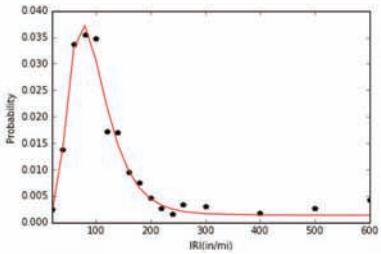

(b) Regression Results for Block Low Cracking

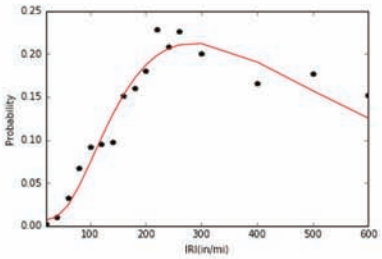

(c) Regression Results for Block Med Cracking

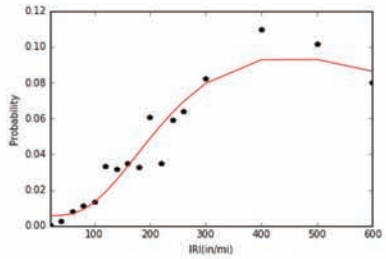

(d) Regression Results for Block High Cracking

vi. **Modeling Results for Block Cracking**

Figure 6.16 (Continued)

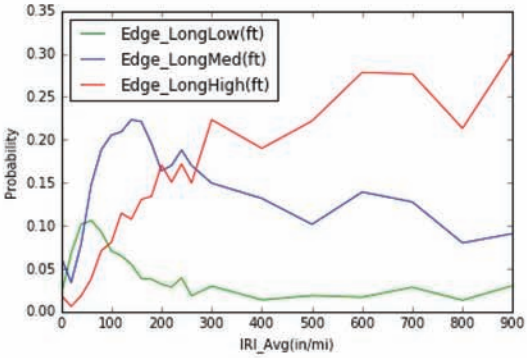

(a) Probability Distribution of Edge Longitude Cracking

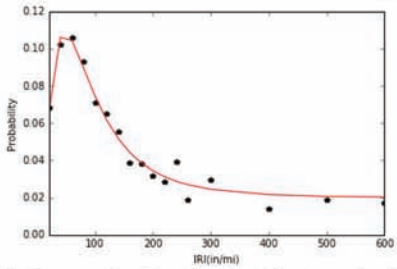

(b) Regression Results for Edge Longitude Low Cracking

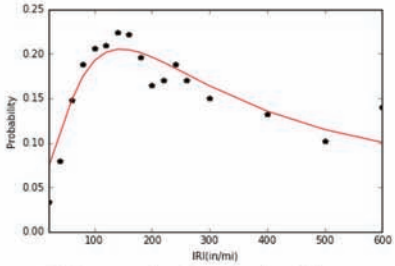

(c) Regression Results for Edge Longitude Med Cracking

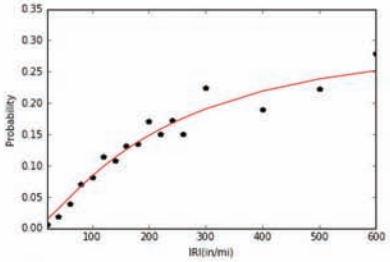

(d) Regression Results for Edge Longitude High Cracking

vii. Modeling Results for Edge Longitude Cracking

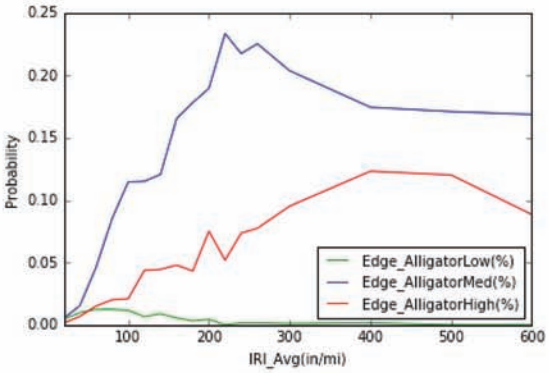

(a) Probability Distribution of Edge Alligator Cracking

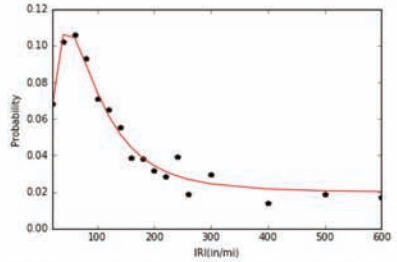

(b) Regression Results for Edge Alligator Low Cracking

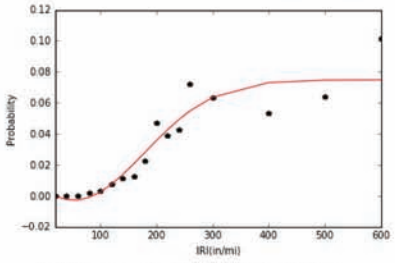

(c) Regression Results for Edge Alligator Med Cracking

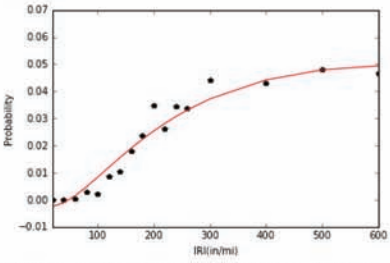

(d) Regression Results for Edge Alligator High Cracking

viii. Modeling Results for Edge Alligator Cracking

Figure 6.16 (Continued)

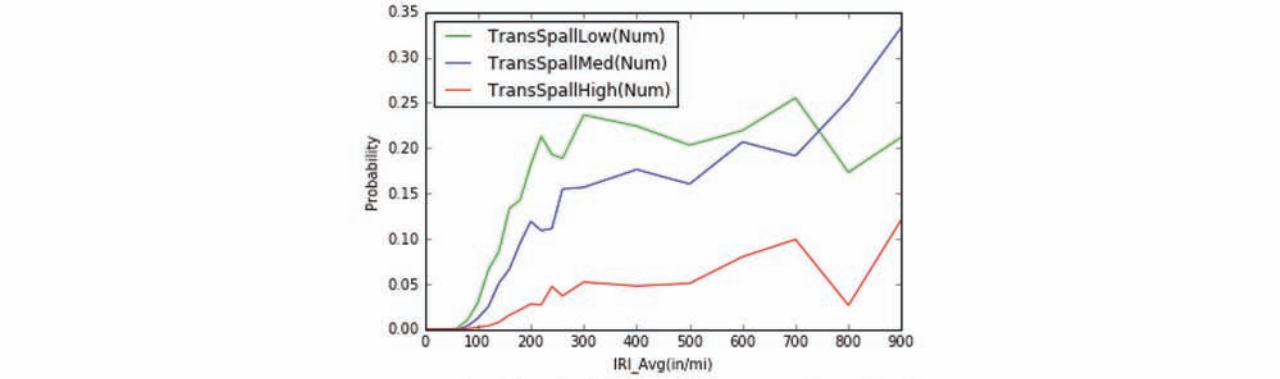

(a) Probability Distribution of Transverse Spall Cracking

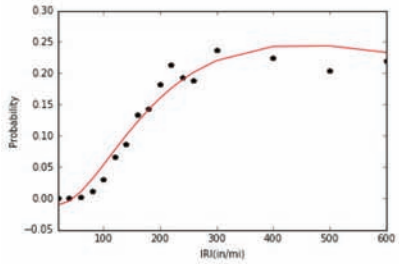

(b) Regression Results for Transverse Spall Low Cracking

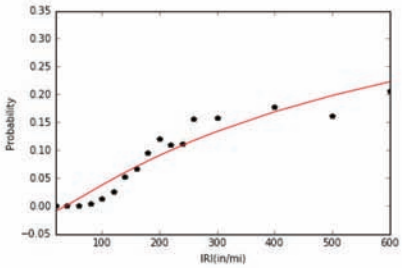

(c) Regression Results for Transverse Spall Med Cracking

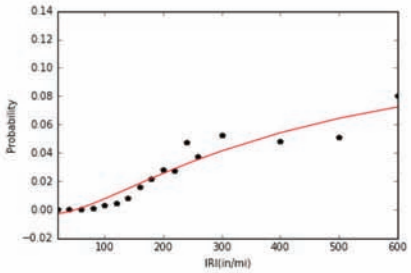

(d) Regression Results for Transverse Spall High Cracking

ix. Modeling Results for Transverse Spall Cracking

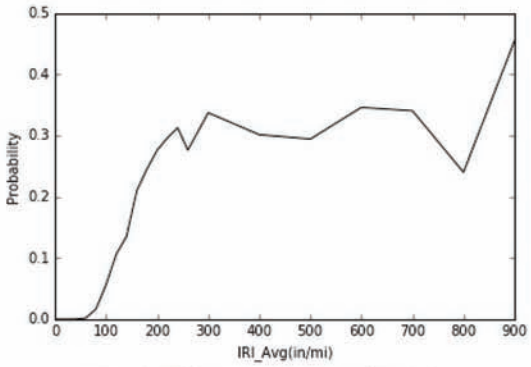

(a) Probability Distribution of Faulting

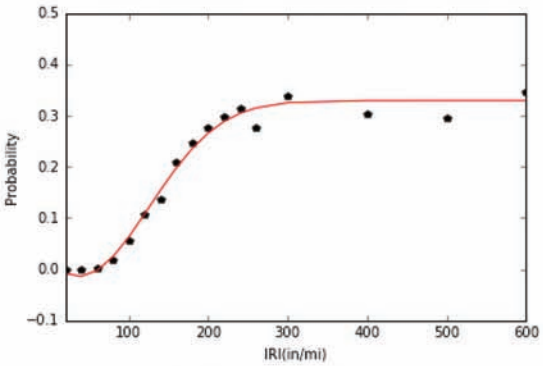

(b) Regression Results for Faulting

x. Modeling Results for Fatigue Cracking

Figure 6.16 (Continued)

TABLE 6.9
Regression Model Results

	Distress Level	Transformation	β_0	β_1	β_2	β_3	R^2
Longitudinal Cracking Non-Wheel Path	Low	$\log_e X$	4.0892	0.8702	0.353	0.0376	0.943
	Med	$\log_{10} X$	2.5159	0.5784	0.4236	0.0311	0.942
	High	$\log_{10} X$	2.9685	0.567	0.5942	-0.0044	0.966
Longitudinal Cracking Wheel Path	Low	$\log_e X$	4.3442	0.6939	0.1486	0.0347	0.932
	Med	$\log_{10} X$	2.4049	0.4444	0.1902	-0.0056	0.913
	High	$\log_{10} X$	2.7776	0.515	0.1087	-0.0021	0.911
Alligator Cracking Non-Wheel Path	Low	$\log_e X$	4.7858	0.4934	0.039	0.0105	0.74
	Med	$\log_{10} X$	1.4283	0.1737	-0.0099	0.0183	0.461
	High	$\log_{10} X$	2.4371	0.5492	0.0204	-0.0007	0.537
Alligator Cracking Wheel Path	Low	$\log_e X$	1.3908	0.7429	0.0588	0.0086	0.766
	Med	$\log_{10} X$	2.4421	0.3171	0.1661	0.0136	0.945
	High	$\log_e X$	6.014	-0.5574	-0.1735	0.0086	0.825
Transverse Cracking	Low	X/100	1.2511	0.4105	0.1408	0.1666	0.511
	Med	$\log_{10} X$	2.529	0.4362	0.2217	0.02	0.942
	High	$\log_{10} X$	2.7499	0.494	0.3436	-0.0029	0.978
Block Cracking	Low	$\log_{10} X$	1.8774	0.1913	0.0173	0.0014	0.975
	Med	$\log_{10} X$	2.4577	0.3056	0.1578	0.0064	0.951
	High	$\log_{10} X$	2.6529	0.294	0.0651	0.0056	0.714
Edge Longitudinal Cracking	Low	$\log_{10} X$	1.6777	0.3271	0.0725	0.02	0.963
	Med	$\log_{10} X$	2.1653	0.3794	0.1368	0.0613	0.86
	High	$\log_{10} X$	3.0574	0.6752	0.4557	0.0045	0.941
Edge Alligator Cracking	Low	$\log_{10} X$	1.7994	0.3044	0.0099	0	0.944
	Med	$\log_{10} X$	2.4362	0.3382	0.1772	0.0056	0.948
	High	$\log_{10} X$	2.5962	0.2382	0.0608	0.0123	0.803
Transverse Longitudinal Cracking	Low	X/100	0.3044	1.2813	-0.7133	0.2169	0.925
	Med	X/100	0.5315	1.2555	-0.2442	0.0748	0.895
	High	$\log_{10} X$	2.8182	0.4633	0.0608	-0.0027	0.887
Transverse Spall Cracking	Low	$\log_{10} X$	2.6562	0.3951	0.2545	-0.0119	0.946
	Med	$\log_{10} X$	3.5862	0.7841	0.7964	-0.0157	0.928
	High	$\log_{10} X$	3.1967	0.5703	0.142	-0.0036	0.764

results using the Gaussian function are presented in Figure 6.16 (i) to (x). We herein present models in this section for only some of the pavement distress types because for others, there were either insufficient observations for modeling (e.g., corner cracking) or lack of an identified relationship between the probability of the existence of the distress type (e.g., spalling) and IRI.

6.3.2 Predictive Models for IRI Using Machine Learning Methods

Naïve Bayes classifier. The feature set used in this analysis included the road functional class, pavement surface material type (asphalt, concrete, jointed concrete pavement, overlay), and the presence of longitudinal/traverse/aligator cracking, edge cracking, block cracking, faulting, and rutting (55 variables in all). The dependent variable is the pavement roughness measured in terms of IRI. The data set was divided into two: 80% was used as training data, and 20% was used as testing data.

As discussed in Section 4.2, the Naïve Bayes method assuming Gaussian distribution is suitable for continuous features. Therefore, for this analysis, we applied a Gaussian-type Naïve Bayes classifier to our training data and evaluated the model's performance in terms of its prediction accuracy using the testing data. Figure 6.17 presents the tesing results for the Naïve Bayes classifier using 100 randomly selected observations. The blue (dark) curve is the observed IRI, while the green (light) curve is the IRI predicted using the developed Naïve Bayes classifier.

It was found that the devloped model does not predict IRI very well when the IRI is extremely high. To address this problem, we could either use more highly aggregated data or identfy outliers (observations for which IRI exceeded a certain threshold) and remove such outliers.

Using more highly aggregated data. The data used in this study are highly disaggregated, in the sense that all the pavement distresses are measured for each section

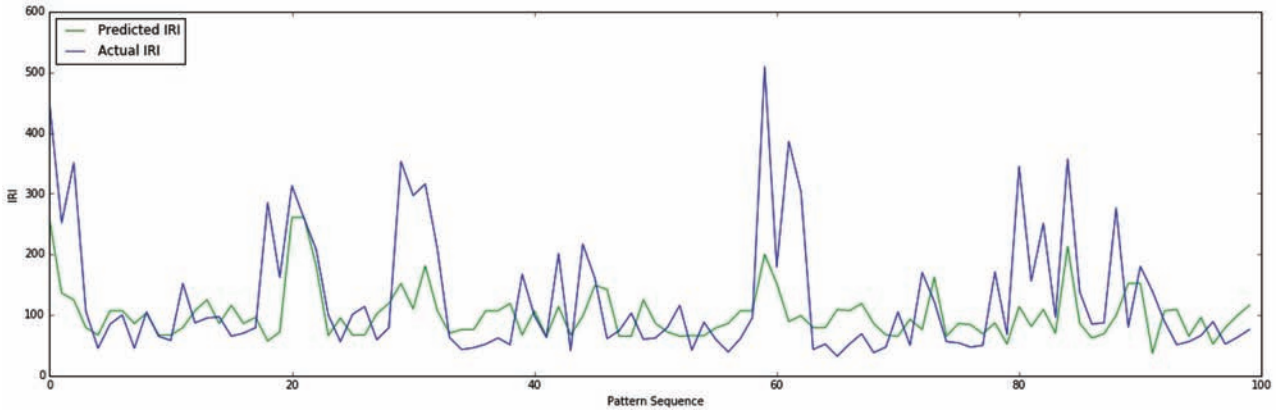

Figure 6.17 Testing results for Naïve Bayes classifier for 100 random observations.

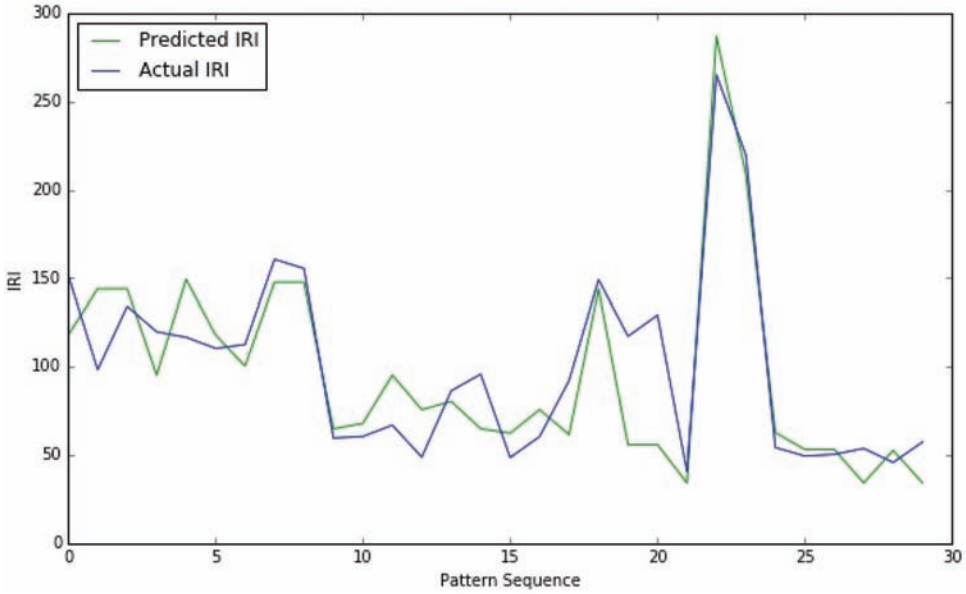

Figure 6.18 Testing results with aggregate data for 30 random observations.

of only a 0.005-mile pavement segment. This level of aggregation is beneficial when evaluating pavement distresses that do not continuously span a large area of the pavement surface or small distresses that only exist in a very short section; in these cases, using disaggregate data is much more accurate than using aggregate data. However, there are some reference misalignment issues in the current study that can significantly bias the results when one attempts to predict IRI using other distresses occurring at the same road section. This problem is exacerbated when the data are highly disaggregate.

To address this issue, we aggregated the data into 1-mile sections and trained the Naïve Bayes classifier again based on such aggregate data. The problem now was to predict the average IRI within 1 mile, given the averaged data of all the pavement distresses within the 1-mile section. Using the aggregate data, the analysis results are shown in Figure 6.18. It can be observed that the prediction accuracy increased significantly compared to the initial model.

Developing the model using data after extremely large IRI values are removed. As discussed, the initially developed classifier was unable to predict the actual IRI accurately. In addition to using more highly aggregated data, another way to address this problem is simply to remove the extremely high IRI values as outliers. Figure 6.19 presents the histogram of average IRI values, which indicates that most pavements have IRI values less than 100 in/mi and some pavement segments have IRI values ranging from 100 to 250 in/mi. Only few segments have IRI values greater than 300 in/mi. In this study, 300 in/mi was chosen as the upper bound for IRI: any segment with IRI values greater than 300 in/mi were removed. These outliers were very few. The testing results are presented in Figure 6.20 for disaggregate data and Figure 6.21 for aggregate data.

Performance comparison. In this section, we compare the performance of the models using the Naïve Bayes classifier trained with different training data, in terms

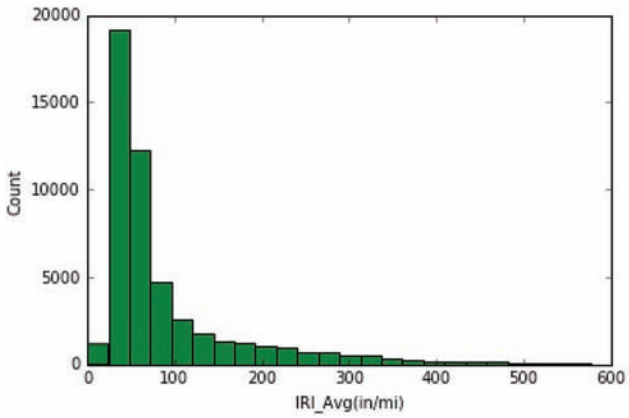

Figure 6.19 Histogram of average IRI values.

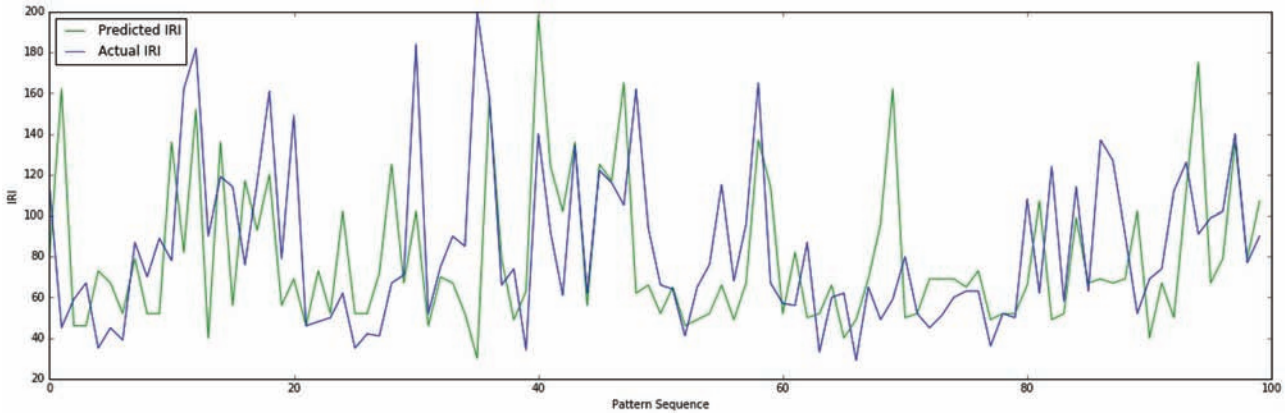

Figure 6.20 Testing results for Naïve Bayes classifier using disaggregate data with IRI values smaller than 300 in/mi for 100 random observations.

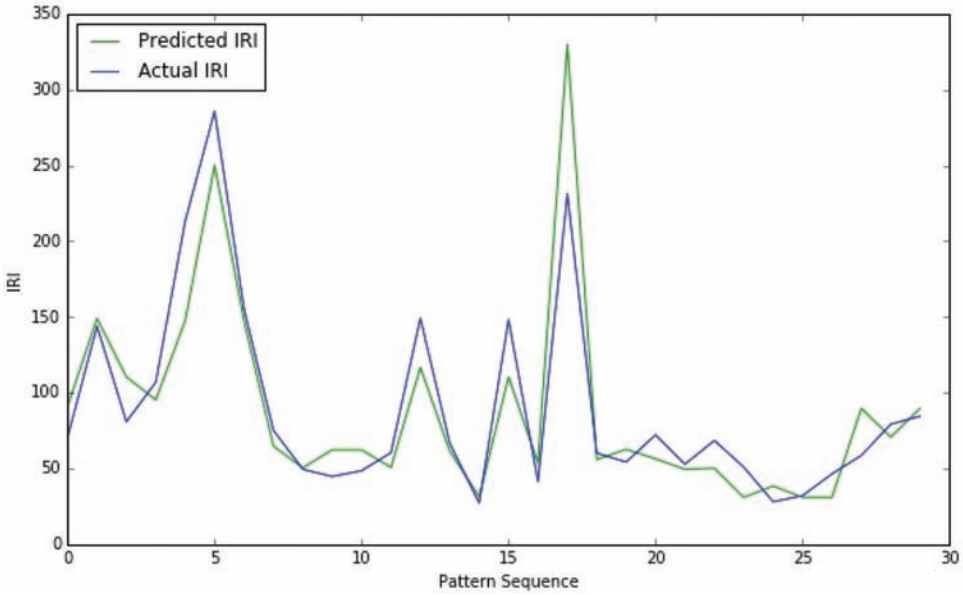

Figure 6.21 Testing results for Naïve Bayes classifier using aggregate data with IRI values smaller than 300 in/mi for 30 random observations.

of the model prediction accuracy under different error tolerances. We do this to show how aggregating data and removing outliers can help improve the model performance. The prediction accuracy under certain error tolerances is calculated using the following formula:

$$Ac_{toler=T} = \frac{N_{abs(predIRI-actIRI)<T}}{N_{Test}} \tag{6.4}$$

where $Ac_{toler=T}$ is the prediction accuracy under an error tolerance equal to T, N_{Test} is the total number of observations in the testing data, and $N_{predIRI\text{-}actIRI<T}$ is the number of observations in the testing data that meet the criteria that the difference between the predicted IRI and the actual IRI is less than T.

Table 6.10 and Figure 6.22 summarize the comparisons between the models using original disaggregate data, disaggregate data after removing extreme values, aggregate data without removing extreme values, and aggregate data after removing extreme values. A significant improvement in prediction accuracy was found due to data aggregation and the removal of extreme values. After the two processes, the prediction accuracy increased by 23% under the strict error tolerance scenario (20 in/mi error) and by 25% under the relaxed error tolerance scenario (50 in/mi error).

Support vector method. Next, we used the support vector method to carry out the same analysis on the aggregate data with the extreme IRI values removed.

TABLE 6.10
Performance Comparison of Models with Different Training Data

	Error Tolerance Prediction Accuracy		
Training Data	**20**	**30**	**50**
Original Disaggregate Data	0.55	0.67	0.77
Disaggregate Data (remove IRI >200)	0.62	0.83	0.88
Aggregate Data	0.60	0.72	0.88
Aggregate Data (remove IRI >200)	0.68	0.92	0.96

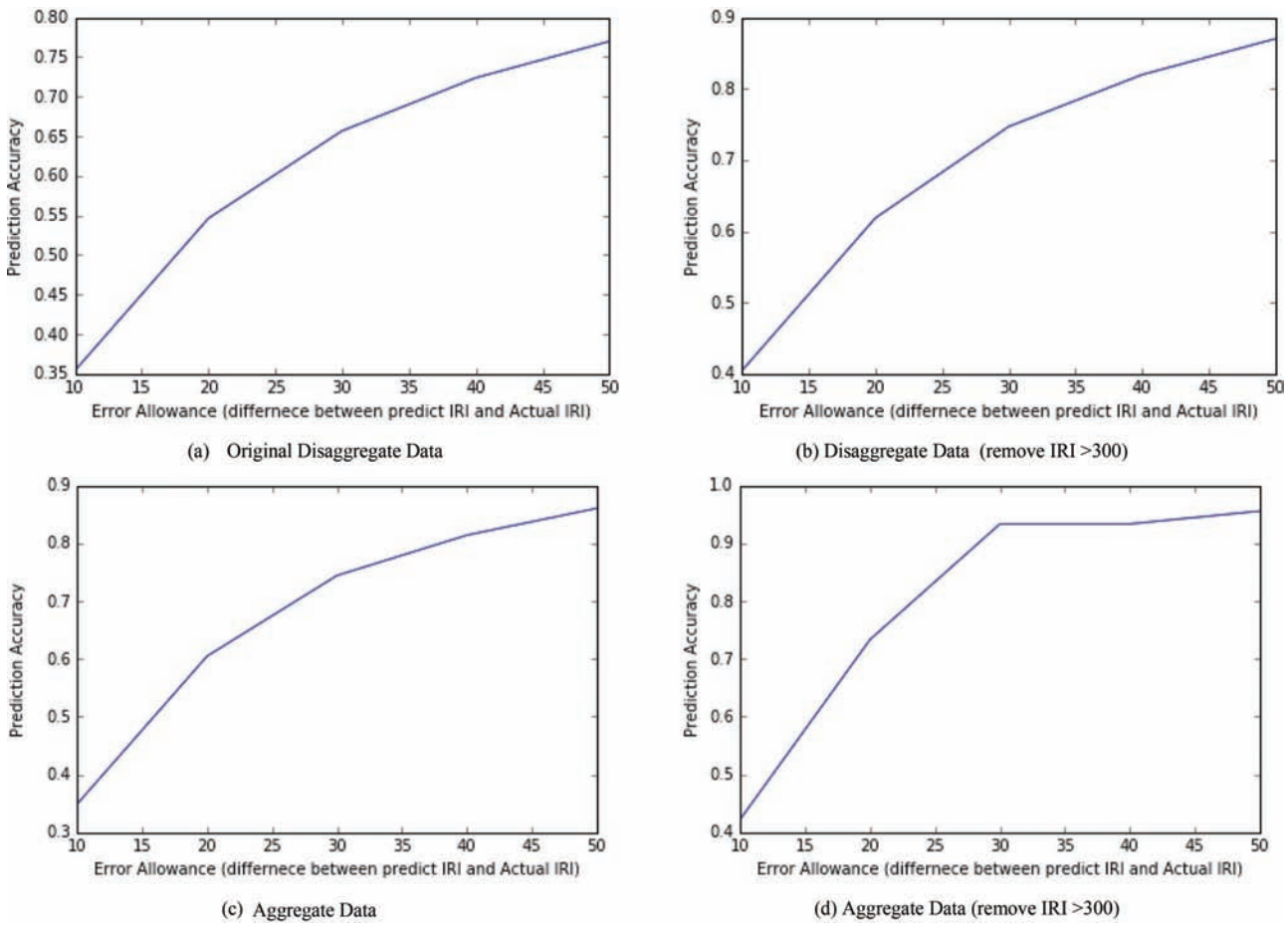

Figure 6.22 Performance comparison between models using different training data.

TABLE 6.11
Performance Comparison of SVM Models with Different Kernels

	Error Tolerance Prediction Accuracy		
Kernel	**20**	**30**	**50**
Linear	0.73	0.78	0.94
RBF	0.73	0.84	0.95
Polynomial	0.8	0.81	0.93

We applied three different kernels for the support vector method: linear, polynomial, and RBF. The results for the different kernels are shown in Table 6.11 and Figure 6.23. The comparison of prediction accuracy among different kernels is shown in Figure 6.24. Using the testing data, it was found that compared to the others, the RBF kernel performed slightly better overall.

Logistic regression classifier. Finally, we implemented a logistic regression method to conduct the analysis using the aggregate data with the extreme IRI values removed. The testing results and model performance are shown in Figures 6.25 and 6.26.

Comparison of model performance of different machine learning techniques. In this section, we compare the performance of the models described in the previous sections in terms of their prediction accuracies using the testing data. The results are summarized in Table 6.12 and Figure 6.27. It was found that the Naïve Bayes classifier has the best performance, followed by the SVM model. However, due to the limited number of observations in the testing data, the Naïve Bayes classifier might not consistently perform better than other models when another testing dataset is used. With more data becoming available in the future, the model development can be replicated to improve its predictive accuracy.

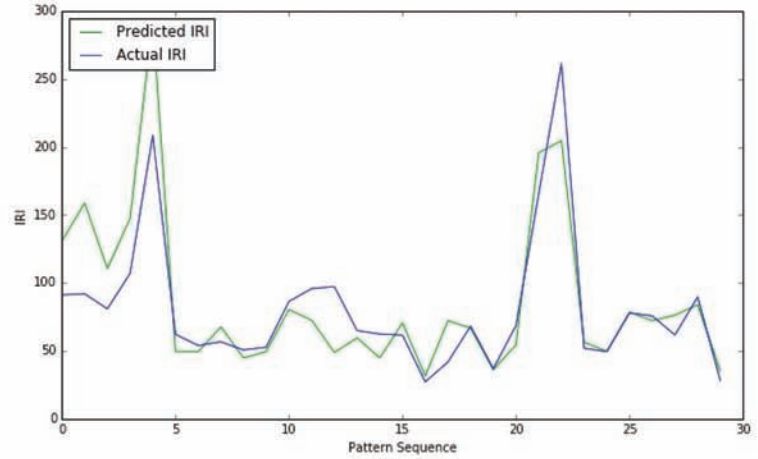

(a) Testing Results for Linear Kernel SVM for 30 Random Observations

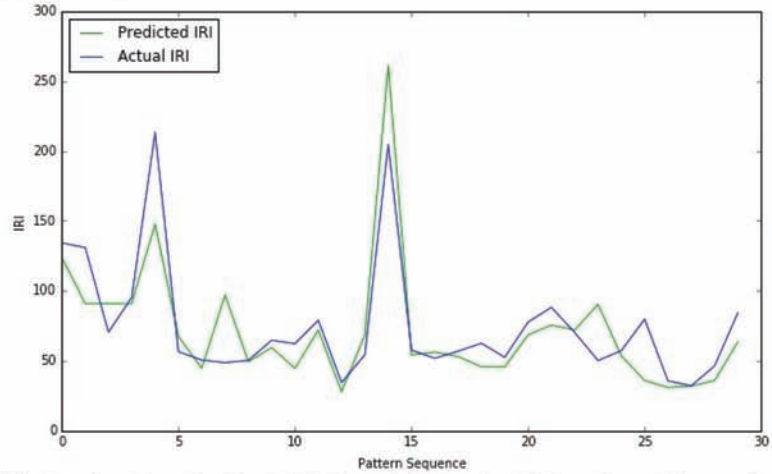

(b) Testing Results for RBF Kernel SVM for 30 Random Observations

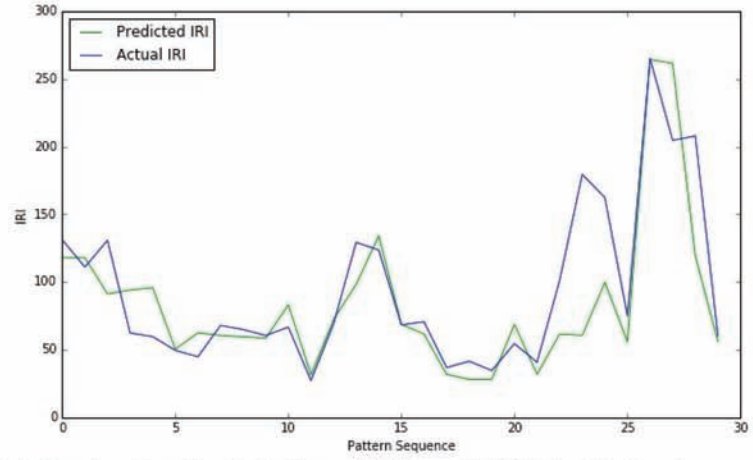

(c) Testing Results for Polynomial Kernel SVM for 30 Random Observation

Figure 6.23 Testing results for SVM models with different kernels.

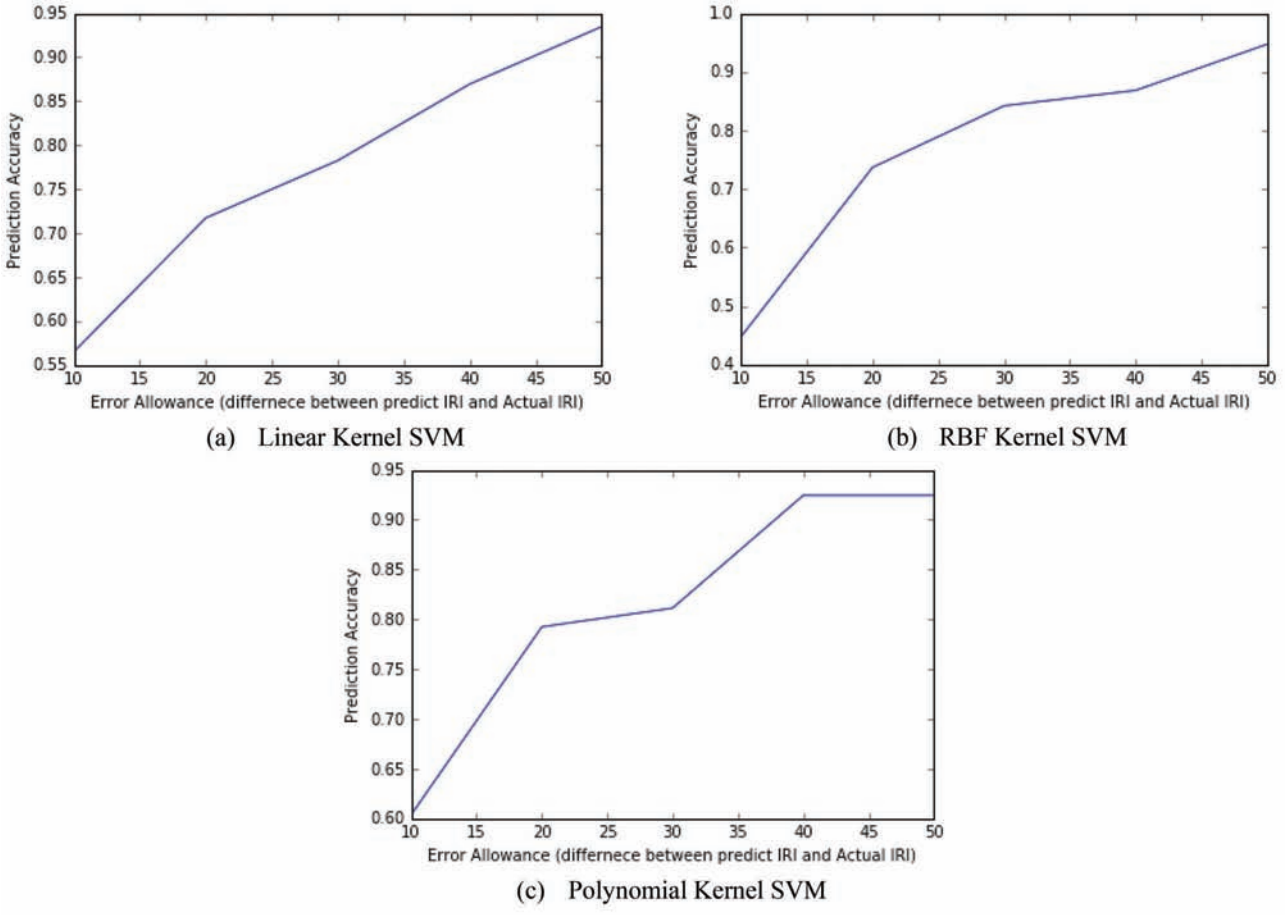

Figure 6.24 Performance comparison among SVM models with different kernels.

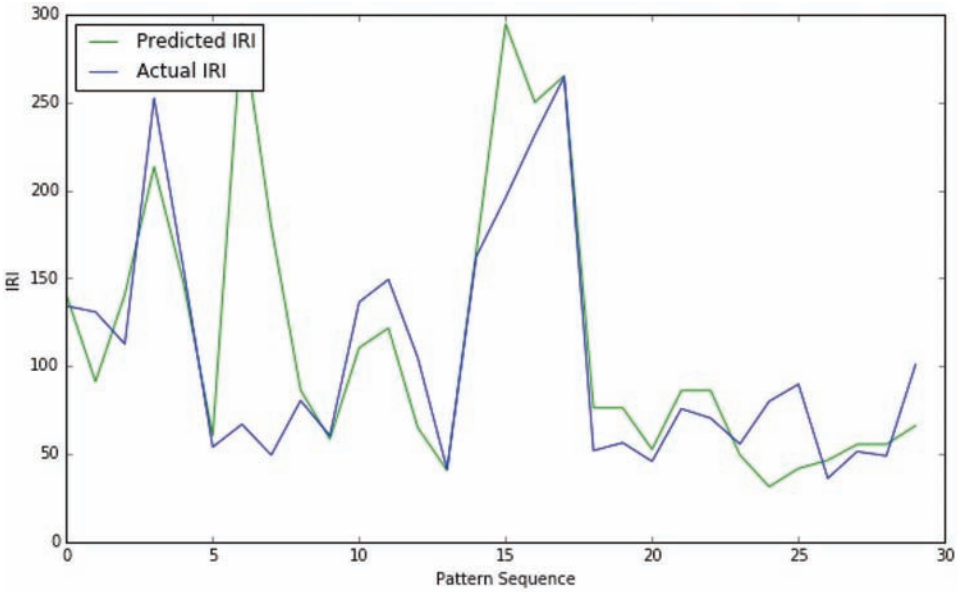

Figure 6.25 Testing results for logistic regression model (30 random observations).

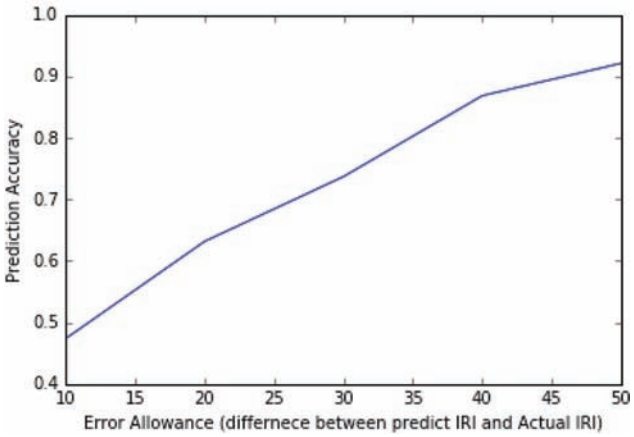

Figure 6.26 Model performance of logistic regression model for different error tolerances.

TABLE 6.12
Performance Comparison of SVM Models with Different Models

	Error Tolerance Prediction Accuracy		
Model	**20**	**30**	**50**
Naïve Bayes Classifier	0.68	0.92	0.96
SVM Model (RBF Kernel)	0.73	0.84	0.95
Logistic Regression Model	0.62	0.71	0.91

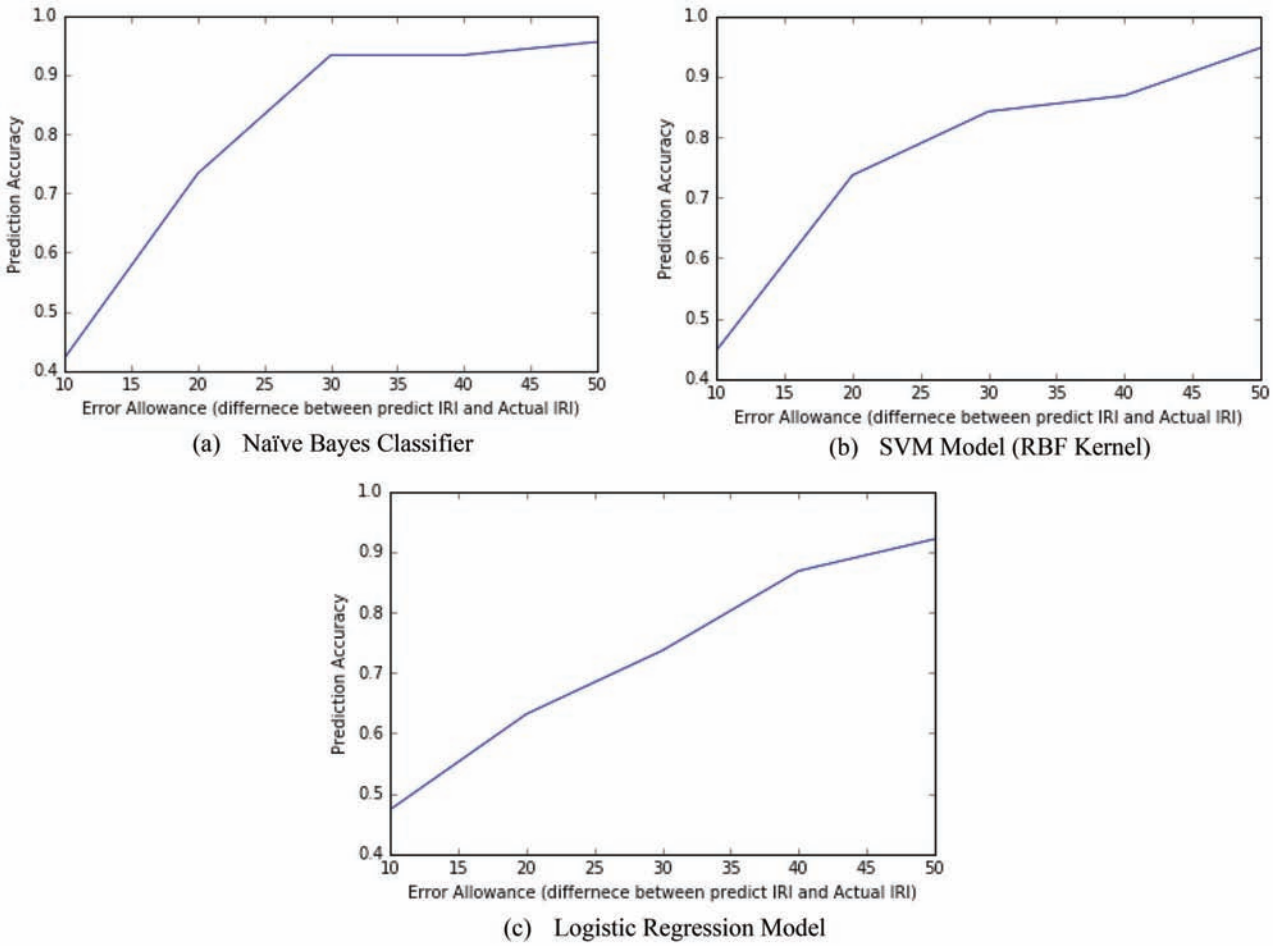

Figure 6.27 Performance comparison between different methods (with aggregate data and extreme IRI values removed).

6.4 Discussion and Conclusions

The correlation among pavement distresses was explored using several machine learning algorithms. INDOT provided detailed pavement condition data reported at 0.005-mile intervals at thousands of road sections along three corridors, over three consecutive years. The focus was on analyzing the relationships among cracking, rutting, faulting, and roughness. The analysis was divided into three parts: (1) building statistical regression models relating crack depth and crack width for each type of pavement cracking and at different highway functional classes (Section 6.1); (2) exploring the relationships among different types of cracking in terms of crack depth and crack width (Section 6.2); and (3) relating IRI to pavement cracking by modeling the probability of the existence of certain types of cracking for different IRI values and predicting IRI values given other pavement distress data (Sections 6.3 and 6.4).

Some interesting results were found in each of the three parts of the analysis. In Section 6.1, an almost linear relationship was found between crack depth and crack width for most types of pavement distresses in the data set. The linear regression models were built for all types of cracks at different severity levels (low, medium, and high) for the different functional classes (Interstate and non-Interstate). Very high R^2 values were obtained for most of the models.

In Section 6.2, the correlation of each pair of pavement distresses that is possibly correlated was analyzed, and a linear model was developed for each pair that was found to be somewhat correlated (correlation coefficient >0.4). Some distresses were found to be highly correlated, such as non-wheel path longitudinal cracking with non-wheel path alligator cracking and block cracking with wheel path alligator cracking. Other distress types were found to be correlated only at certain levels of severity and less correlated or uncorrelated at other levels of severity.

In Section 6.3, we analyzed the correlation between IRI and the probability of the existence of certain types of cracking. We developed models for predicting IRI based on other types of pavement distress using three different machine learning techniques. Two methods were applied to improve the models' performance: aggregate the data to 0.1 miles per section and remove extremely large IRI values as outliers. The prediction accuracy improved significantly when the two approaches were applied to the original data set. Among the three machine learning techniques, Naïve Bayes classifier yielded the highest accuracy when used with the aggregate data and when extreme IRI values were removed. The sample size of the aggregate data, however, was not large enough to make conclusions regarding the relative performance superiority across different models.

All of the models developed in this study can be improved or extended when additional pavement distress data become available in the future. When such data become available, the relationship between pavement distress and time, such as the occurrence order of the distresses and which distress causes another, can also be analyzed.

The results of the present study is in line with the basic principles of asset management. As more and more agencies automate their asset management processes, quick and cost-effective monitoring of infrastructure is becoming the target of most agencies. The infrastructure monitoring process, if automated, could lead to significant cost reduction and reliability enhancement. This is important if agencies are to establish reliable intervention programs for their infrastructure networks (Adey & Kielhauser, 2017). System-wide infrastructure tests such as IRI monitoring can help generate good data that are key for strategic infrastructure decisions (Moloney, McKenna, Fitzgibbon, & McKeogh, 2017; Taggart, Tachtsi, Lugg, & Davies, 2014). The role of reliable condition assessment in the life cycle management has been touted by Switzer and McNeil (2004). Kellick (2014) stated that this can help remove institutional inertia or barriers in the quest for increased funding for infrastructure repair.

REFERENCES

Adey, B., & Kielhauser, C. (2017). *A process to enable the automation of road asset management*. Paper presented at the 2nd International Symposium on Infrastructure Asset Management–SIAM 2017, June 29–30, Zurich, Switzerland.

Archondo-Callao, R. S., & Faiz, A. (1994). *Estimating vehicle operating costs* (Technical Paper 234). Washington, DC: World Bank.

Amarasiri, S., Gunaratne, M., & Sarkar, S. (2010). Modeling of crack depths in digital images of concrete pavements using optical reflection properties. *Journal of Transportation Engineering*, *136*(6), 489–499. https://doi.org/10.1061/(ASCE)TE.1943-5436.0000095

Caruana, R., & Niculescu-Mizil, A. (2006). An empirical comparison of supervised learning algorithms. In *ICML '06 Proceedings of the 23rd International Conference on Machine Learning* (pp. 161–168). New York, NY: Association for Computing Machinery. https://doi.org/10.1145/1143844.1143865

Chand, P., Aruna, A., Maqsood, A. M., & Rao, L. V. (2005). Novel mutation method for increased cellulase production. *Journal of Applied Microbiology*, *98*(2), 318–323. https://doi.org/10.1111/j.1365-2672.2004.02453.

Chesher, A., & Harrison, R. (1987). *Vehicle operating costs: Evidence from developing countries* (Publication No. PB-88-208574/XAB). Washington, DC: International Bank for Reconstruction and Development.

Cortes, C., & Vapnik, V. (1995). Support-vector networks. *Machine Learning*, *20*(3), 273–297. https://doi.org/10.1007/BF00994018

FHWA. (2002). *Status of the nation's highways, bridges, and transit: 2001 conditions and performance report*. Washington, DC: Federal Highway Administration, U.S. Department of Transportation. Retrieved from https://www.fhwa.dot.gov/policy/2002cpr/ch3b.cfm

FHWA. (2007). *Status of the nation's highways, bridges, and transit: 2006 conditions and performance report*. Washington, DC: U.S. Department of Transportation.

Furuya, K., Yokota, H., Komatsu, S., Hashimoto, K., & Kato, E. (2014). Prediction of extreme crack width of concrete coastal facilities based on extreme statistics. In *Proceedings of 4th International Symposium on Life-Cycle Civil Engi-*

neering, Tokyo, Japan: International Association for Life-Cycle Civil Engineering.

Haas, R. C. G., Hudson, W. R., & Zaniewski, J. P. (1994). *Modern pavement management*. Malabar, FL: Krieger Publishing Company.

Hall K. T., Correa, C. E., & Simpson, A. L. (2003). *LTPP data analysis: Effectiveness of maintenance and rehabilitation options* (NCHRP Web Document 47 (Project 20-50[3/4])). Washington, DC: Transportation Research Board.

Hand, D. J., & Yu, K. (2001). Idiot's Bayes: Not so stupid after all? *International Statistical Review*, *69*(3), 385–399. https://doi.org/10.2307/1403452

INDOT. (2001). *Pavement surface report*. Indianapolis, IN: Indiana Department of Transportation, Pavement Management Unit.

Irfan, M., Khurshid, M. B., & Labi S. (2009). Service life of thin HMA overlay using different performance indicators. *Transportation Research Record*, *2108*, 37–45. https://doi.org/10.3141/2108-04

John, G. H., & Langley, P. (1995). Estimating continuous distributions in Bayesian classifiers. In *Proceedings of the Eleventh Conference on Uncertainty in Artificial Intelligence* 338–345, P. Besnard & S. Hanks (Eds.). San Mateo, CA: Morgan Kaufmann Publishers.

Kellick, P. (2014). Leadership, the essential ingredient in asset management, Infrastructure Asset Management 2014 1:3, 75–80.

Khurshid, M. B. (2010). *A framework for establishing optimal performance thresholds for highway asset interventions* (Doctoral dissertation). West Lafayette, IN: Purdue University.

Labi, S., Lamptey, G., Konduri, S., & Sinha, K. (2005). Part 1: Pavement management: Analysis of long-term effectiveness of thin hot-mix asphaltic concrete overlay treatments. *Transportation Research Record*, 1940, 1–12. https://doi.org/10.3141/1940-01

McGhee, K. H. (2004). *Automated pavement distress collection techniques* (NCHRP Synthesis 334). Washington, DC: Transportation Research Board.

Miller, J. S., & Bellinger, W. Y. (2003). *Distress identification manual for the long-term pavement performance program* (Publication No. FHWA-RD-03-031). McLean, VA: Federal Highway Administration.

Moloney, M., McKenna, T., Fitzgibbon, K., & McKeogh, E. (2017). Quality data for strategic infrastructure decisions in Ireland. *Infrastructure Asset Management*, *4*(2), 40–49. https://doi.org/10.1680/jinam.16.00011

McCallum, A., & Nigam, K. (1998). A comparison of event models for naive Bayes text classification. In M. Sahami (Ed.), *Learning for Text Categorization: Papers from the 1998 AAAI Workshop*. Palo Alto, CA: AAAI Press.

Metsis, V., Androutsopoulos, I., & Paliouras, G. (2006). *Spam filtering with naive Bayes—which naive Bayes?* Paper presented at the Third Conference on Email and Anti-Spam, July 27–28, Mountain View, CA.

Murty, M. N., & Devi, V. S. (2011). *Pattern recognition: An algorithmic approach*. London, UK: Springer-Verlag.

Niculescu-Mizil, A., & Caruana, R. (2005). Predicting good probabilities with supervised learning. In *ICML '05 Proceedings of the 22nd International Conference on Machine Learning* (pp. 625–632). New York, NY: Association for Computing Machinery. https://doi.org/10.1145/1102351.1102430

Nigam, K., McCallum, A., Thrun, S., & Mitchell, T. (2000). Learning to classify text from labeled and unlabeled documents using EM. *Machine Learning*, *39*(2–3), 103–134. https://doi.org/10.1023/A:1007692713085

Park, K., Thomas, N. E., & Wayne Lee, K. (2007). Applicability of the international roughness index as a predictor of asphalt pavement condition. *Journal of Transportation Engineering*, *133*(12), 706–709. https://doi.org/10.1061/(ASCE)0733-947X(2007)133:12(706)

Paterson, W. D. (1987). *Road deterioration and maintenance effects: Models for planning and management*. Baltimore, MD: The Johns Hopkins University Press.

Pavement Interactive. (2016). Pavement management. Retrieved 10/10/16 from http://www.pavementinteractive.org/category/pavement-management

Prakash, A. (2014). Course notes from CE 5614, Big-Data Management Systems. Blacksburg, VA: Virginia Polytechnic Institute and State University.

Rennie, J. D., Shih, L., Teevan, J., & Karger, D. R. (2003). Tackling the poor assumptions of naive Bayes classifiers. In T. Fawcett & N. Mishra (Eds.), *ICML '03 Proceedings of the Twentieth International Conference on Machine Learning* (pp. 616–623). Palo Alto, CA: AAAI Press.

Rish, I. (2001). An empirical study of the naive Bayes classifier. In N. Lavrač, D. Gamberger, H. Blockeel, & L. Todorovski (Eds.), *Machine Learning: ECML 2003* (pp. 444–455). Berlin, Germany: Spinger Berlin Heidelberg. https://doi.org/10.1007/978-3-540-39857-8_40

Russell, S., & Norvig, P. (2003) *Artificial intelligence: A modern approach* (2nd ed.). Upper Saddle River, NJ: Prentice Hall.

Sayers, M. W., Gillespie, T. D., & Paterson, W. O. (1986). *Guidelines for conducting and calibrating road roughness measurements* (Technical Paper 46). Washington, DC: World Bank.

Sinha, K. C., & Labi, S. (2007). *Transportation decision making: Principles of project evaluation and programming*. New York, NY: John Wiley & Sons.

Switzer, A., & McNeil, S. (2004). Developing a road map for transportation asset management research. *Public Works Management and Policy*, *8*(3), 162–175. https://doi.org/10.1177/1087724X03259475

Taggart, A., Tachtsi, L., Lugg, M., & Davies, H. (2014). UKRLG framework for highway infrastructure asset management. *Infrastructure Asset Management*, *1*(1), 10–19. https://doi.org/10.1680/iasma.13.00012

Teede Tehnokeskus. (2016). Rut Depth Measurements. Retrieved from http://www.teed.ee/en/services/testing-and-measurement/measurements/rut-depth-measurements/

University of Michigan Transportation Research Institute (UMTRI). (1998). International roughness index [Web page from the Road Roughness home page]. Accessed October 6, 2016, at http://www.umtri.umich.edu/erd/roughness/iri.html

Xing, E., & Bar-Joseph, Z. (2015). Course notes from Introduction to Machine Learning. Pittsburgh, PA: Carnegie Mellon University. Retrieved from http://www.cs.cmu.edu/~epxing/Class/10701/lecture.html

Yang, M., Yin, Z., Zhong, Z., Wang, S., Chen, P., & Xu, Y. (2007). A contourlet-based method for handwritten signature verification. In *2007 IEEE International Conference on Automation and Logistics* (pp. 1561–1566). New York, NY: IEEE. https://doi.org/10.1109/ICAL.2007.4338820

Zhang, H. (2004). The optimality of naive Bayes. In V. Barr & Z. Markov (Eds.), *Proceedings of the Seventeenth International Florida Artificial Intelligence Research Society Conference* (FLAIRS 2004). Palo Alto, CA: AAAI Press.

Zhang, Y., Oussena, S., Clark, T., & Hyensook, K. (2010). Using data mining to improve student retention in higher education, In *ICEIS 12th International Conference on Enterprise Information Systems*, June 8–12, Portugal.

Zhefu, Y., & Chuanying, J. (2008). Applying SVM to pavement evaluation. In *China Transportation Development Forum, Sciencemeeting Online*. Retrieved from http://www.meeting.edu.cn/meeting/paper!detail1.action?id=22699

About the Joint Transportation Research Program (JTRP)

On March 11, 1937, the Indiana Legislature passed an act which authorized the Indiana State Highway Commission to cooperate with and assist Purdue University in developing the best methods of improving and maintaining the highways of the state and the respective counties thereof. That collaborative effort was called the Joint Highway Research Project (JHRP). In 1997 the collaborative venture was renamed as the Joint Transportation Research Program (JTRP) to reflect the state and national efforts to integrate the management and operation of various transportation modes.

The first studies of JHRP were concerned with Test Road No. 1—evaluation of the weathering characteristics of stabilized materials. After World War II, the JHRP program grew substantially and was regularly producing technical reports. Over 1,600 technical reports are now available, published as part of the JHRP and subsequently JTRP collaborative venture between Purdue University and what is now the Indiana Department of Transportation.

Free online access to all reports is provided through a unique collaboration between JTRP and Purdue Libraries. These are available at: http://docs.lib.purdue.edu/jtrp

Further information about JTRP and its current research program is available at: http://www.purdue.edu/jtrp

About This Report

An open access version of this publication is available online. This can be most easily located using the Digital Object Identifier (doi) listed below. Pre-2011 publications that include color illustrations are available online in color but are printed only in grayscale.

The recommended citation for this publication is:

Alinizzi, M., Qiao, J. Y., Kandil, A., Cai, H., & Labi, S. (2017). *Integration and evaluation of automated pavement distress data in INDOT's pavement management system* (Joint Transportation Research Program Publication No. FHWA/IN/JTRP-2017/07). West Lafayette, IN: Purdue University. https://doi.org/10.5703/1288284316507